UiT The Arctic University of Norway

Faculty of Science and Technology – Department of Geosciences

Stratigraphy, neo-tectonics and mass wasting of deep water drifts in the Fram Strait

Bjarte Selsaas

Master's thesis in Geology - GEO-3900 - May 2020

Abstract

The primary goal for this thesis was the reprocessing and interpretation of 2D seismic lines in the Fram Strait and West Svalbard Margin (WSM). Seismic data quality was significantly improved through the implementation of new processing steps that had previously not been applied, incl. e.g. burst removal and a more advanced type of migration. The reprocessed lines were acquired by CAGE over multiple years prior to 2016 and were integrated in a seismic database with a number of seismic surveys in the study area to comprise a regional database. This database, together with bathymetric data collected in the area, made up the basis of interpretations, which focused on stratigraphic development of the deep-water area of the West Svalbard Margin and Fram Strait in relation to contourite drift development, neotectonic setting and processes of submarine landslides in the area. Notable features in this deep-water setting were several smaller and larger drift deposits, among which the Vestnesa Ridge is well-known and well-studied for its active fluid flow system.

The seismic database allowed extending stratigraphic correlations of the 1.5 Ma and 2.78 Ma horizons from ODP sites and existing stratigraphy on the Yermak Plateu further south and into the deep-water area. This facilitated studying the differences in sedimentation rates on the WSM and revealed high sedimentation rates at Vestnesa Ridge as well as slightly thicker sediment packages south on WSM than north. Two main seismic facies were identified in the data and were characterized by 1) Parallel and horizontal and 2) subparallel and wavy reflection patterns. Parallel and horizontal reflection patterns were observed along the gentler sloped areas east on the WSM and are related to hemipelagic settling and sheeted drift structures. Subparallel and wavy reflection patterns were interpreted to be related to drift deposits with moat-levee structures and were observed exclusively on the deeper and steeper parts of the western slope along the WSM, indicating strong bottom currents along the Molloy Ridge.

Landslides were observed on the western slope of WSM and are related to the development of drift deposits on the steeper slopes, which have contributed to slope instability. Combined with toe erosion of the slope by normal faults related to the Knipovich and Molloy Ridges and earthquakes these conditions may have triggered the landslides observed.

Table of Contents

List of Tables

List of Figures

Acknowledgements

Firstly, I would like to thank my advisor Stefan Bünz for an interesting and challenging thesis. His assistance and great insight along the way was extremely helpful, especially towards the end. A great thanks is also owed to Kate Alyse Waghorn who helped me with the seismic processing and countless other problems encountered over the past year.

A special thanks also goes to Tor Geir Ødegård Garpestad who proved to be a great roommate and fellow master student during the special time over last two months. You made working from home very enjoyable. I would also like to thank Mathea Fennefoss Johnsgård, who helped me stay motivated with her constant support, kind words and positive energy. It would not have been the same without you. Thanks to my family back home for their support and good talks along the way.

This last year proved to be the most challenging of my 5 year education within geology and marks the end of a great journey. Thanks to all fellow students and friends, in Sogndal and in Tromsø, for this great time. I am forever grateful for the experience.

1 Introduction

The main objective of this thesis was to reprocess and interpret already acquired 2D seismic lines from West Svalbard Margin and the Fram Strait. Several lines have been acquired in the area, but few have been processed with today's standard of seismic processing and fewer integrated into a regional study. The main data that was included in the database for this thesis, was Multi-channel 2D seismic data acquired with R/V Helmer Hanssen during cruises over the last 7-8 years combined with existing regional 2D seismic lines from the previous decade. The goal was to bring different 2D seismic surveys collected in the area (Figure 1), reprocess them and interpret over larger areas and multiple surveys to get a better understanding of the regional sedimentary and tectonic processes affecting the areas surrounding the Fram Strait. Combining the seismic lines with ODP drilling data and available bathymetry data, the aim of this thesis was to (1) achieve a better stratigraphic delineation of the large sediment drifts in the Fram Strait, (2) a better understanding of neotectonics in this setting and (3) a better understanding of mass wasting in relation to stratigraphy and tectonic activity.

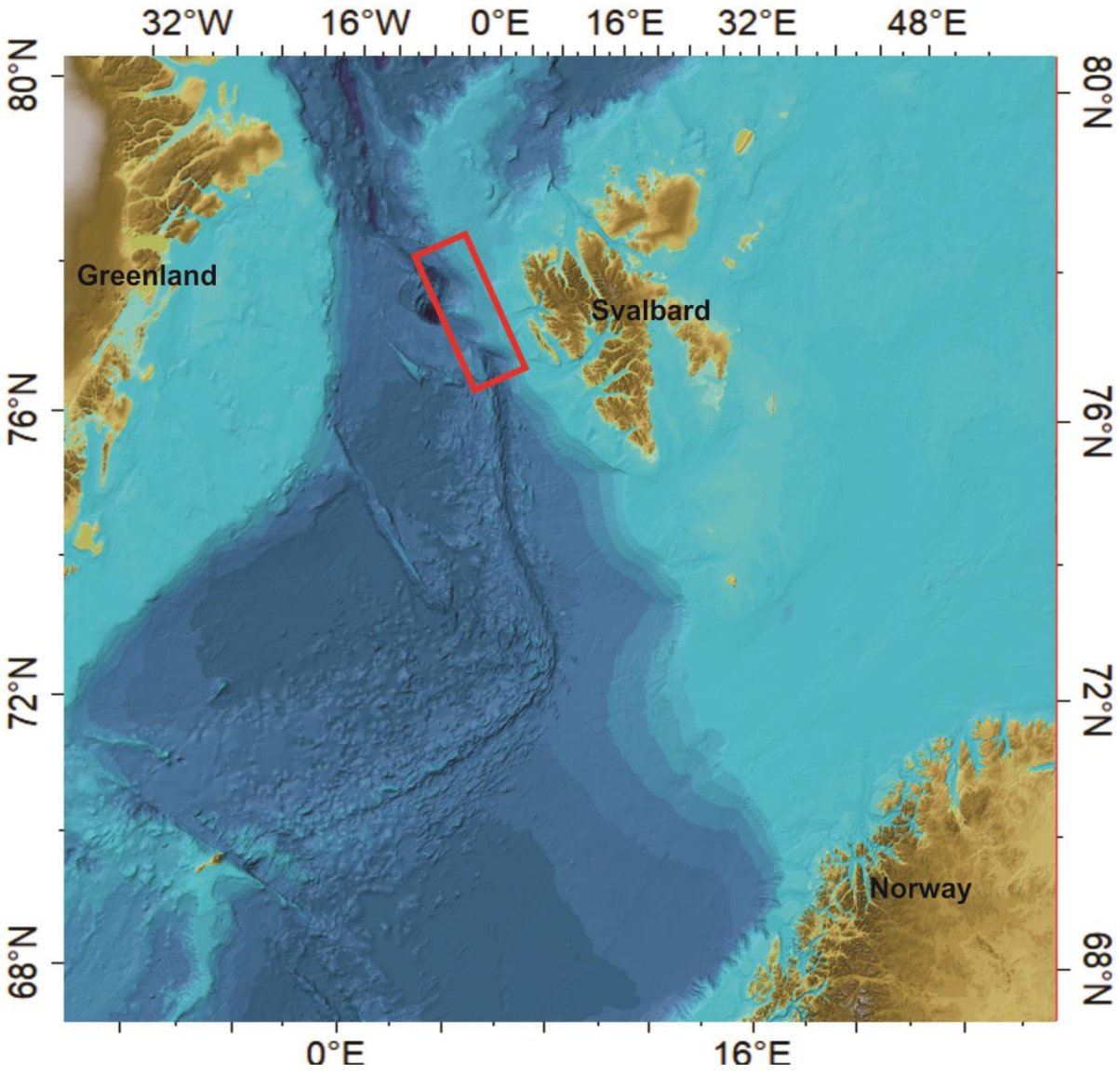

Figure 1 Study area (red square) on the West Svalbard Margin. IBCAO V3 bathymetry.

1.1 Sedimentology

In deep sea environments there are several sedimentary processes that occur. Grains are entrained into the water column by oceanic currents when the velocity is sufficient to lift the particle. All grain sizes have a velocity threshold whereby the current is flowing fast enough to lift, and where the current velocity is reduced sufficiently to deposit a particle. Generally clays and large clasts require higher velocities to become entrained than sand sized grains and mud, while the deposition velocity threshold is a function of grain size (Hjulstrom, 1935). Settling of pelagic and hemipelagic particles through the water column by gravity is the dominant processes in abyssal plain settings. Pelagic and hemipelagic materials are very fine

particles that have a much lower transport velocity than larger grain sizes, so they tend to be the last grains to fall out, typically in exceedingly low velocities over the deep ocean basins.

In deep marine settings a number of depositional processes are from currents that transports sediments either along slope or down slope. Currents that are produced by the different temperatures and salt contents in the ocean are called Thermohaline currents, which is what drives the thermohaline circulation, also known as the global conveyor belt. This process can carry and deposit sediments and can be contourites, contourite deposits or contourite drifts. (see chapter 1.1.1)

Another process carries sediments down slope from the shelf, fluvial systems or land to the deep sea by turbidity currents and mass wasting processes (Dott Jr, 1963; Rebesco et al., 2014). Turbidity currents are caused by suspended sediments in a mixture of water, which will have a higher density than surrounding water and will flow downwards by gravity. Turbidty currents are often caused by other events, such as earthquakes and debris flows which consequently leads to suspended sediments in water. They produce erosional and depostional features such as channels, levees and sediment waves (Meiburg & Kneller, 2010).

The Western Svalbard Margin (WSM) forms the North-West corner of the Barents Sea and the Eurasian Continental plate, bordering the Fram Strait to the west and Arctic Ocean to the north. The opening of the Fram Strait enabled the circulation of water masses between the Arctic Ocean, the Norwegian-Greenland Sea and the rest of the world's oceans (Eiken & Hinz, 1993).

The last 2.5 My glacial/interglacial changes in periods of 100 ky have had a major effect on high latitude areas including the WSM. And can probably be corresponded to changes in the circulation system and sedimentation rates in the area (Eiken & Hinz, 1993).

1.1.1 Contourites

Sediments substantially reworked or deposited by ocean bottom currents are defined as contourites and cover large parts of ocean floors and continental margins (Rebesco et al., 2014). These bottom currents flow in response to major thermohaline and wind driven circulations and can accumulate large amounts of sediments in the deep sea. They can occur in most marine settings from abyssal ocean floors to upper slope settings typically below

300m water depth (J. C. Faugères & Stow, 2008). Contourites cover a large amount of present day sea floor, building up large contourite mounds or drifts over millions of years - often adjacent to regions of erosion as a contour current will deposit and erode depending on its velocity. (Stow et al., 2008). Contourites often occur interbedded close to other deep-water facies and vary in grain size from very fine-grained to relatively coarse-grained materials with siliclastic, bioclastic, volcaniclastic and chemogenic compositional varieties, although are typically composed of a well-sorted homogeneous grain size (Stow et al., 2008).

Rebesco and Stow (2001) present seven types of large-scale drift geometries recognized in contourites (Figure 2). These geometries typically represent the velocity field of the oceanic current in the region. Contour currents/oceanic currents can be divided into confined and unconfined, whereby the velocity variations across the current will alter more or less rapidly. Confined currents, such as those flowing along slope, or being channeled through some obstacle (seamounts or tectonic features) have a varying velocity field as some areas flow faster in response to the confinement. Depending on the initial current velocity this can result in preferential erosion in the faster moving areas and preferential deposition in the slower – resulting in geometries (3-7). Unconfined currents tend to maintain a relatively static velocity field, resulting in geometries (1-2). Features such as channels or moats, or features that appear to incise into the surrounding sediment are typically erosional features representing current velocities at or above entrainment velocity while depositional features such as mounds are representative of current velocities at or below deposition velocity.

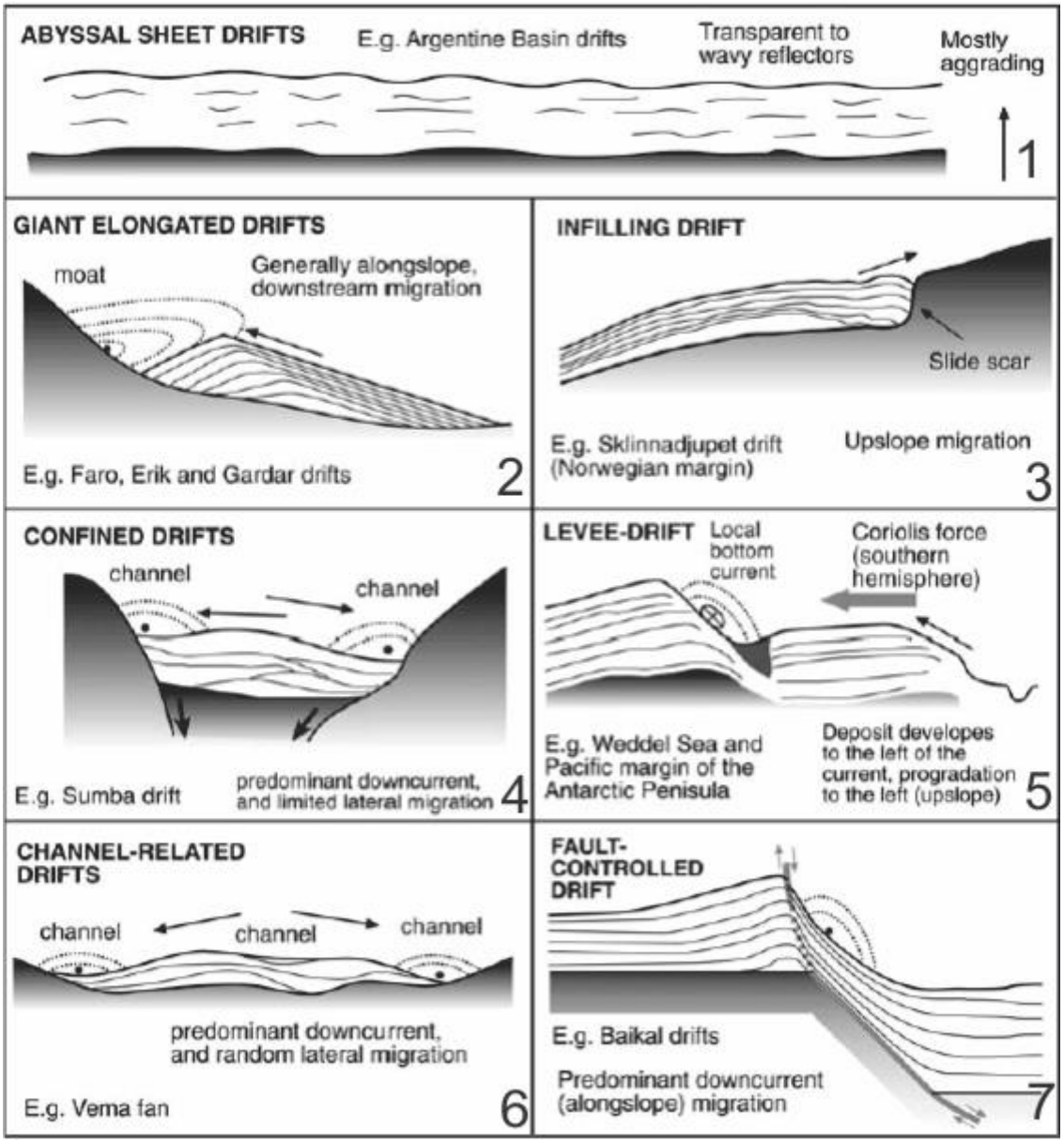

Figure 2 Seven different styles of contourite development. Figure modified from Rebesco and Stow (2001)

1.1.2 Seismic characteristics of contourites

As previously stated there are three sedimentary processes that influence deep water environments. Hemipelagic settling, along slope and down slope processes. These processes often play interactive roles in sedimentation and are often found interbedded with each other (J.-C. Faugères et al., 1999). Both down slope and along slope processes are considered critical in the construction and shaping of continental margins. Along slope currents form contourite drifts and share similar dimensions and associated facies with deep sea fans constructed by downslope processes, in particular turbidites (J.-C. Faugères et al., 1999).

Turbidites and contourites share in result much of the same seismic characteristics and can be quite hard to differentiate on a seismic profile, especially in regions where both types are deposited closely to one another. Contourite fans and separated drifts are developed primarily along one flank and show erosional features such as channels or moats with elongated mounds or drifts. These types of deposition have similar seismic facies as a turbidite-levee system from a sub marine fan, slope apron and basin plain settings.

The seismic facies of these two systems are characterized with chaotic to strong reflections in the channel or moat with parallel to wavy reflections on the levee or mound (J.-C. Faugères et al., 1999). Even though these are highly similar, their progradation direction in relation to the overall trend of the margin and flow direction are not. Both turbiditic levees and contourites tend to migrate down current. As they are products of different types of currents, contourites will migrate along slope and turbidites will migrate downslope (J.-C. Faugères et al., 1999).

Seismic facies found in contourite drifts have also been recognized in turbidite systems. However, distinctions can be made as turbidite systems have certain seismic facies that are more typical of, and even excluded to, turbidite systems. Well stratified, horizontal parallel and high amplitude reflections that are related to ponded turbidites in basin plains are not found in contourite deposits. Along with other high amplitude reflections and strong prolonged bottom reflections peculiar to turbidite channels with infilled coarse-grained material (J.-C. Faugères et al., 1999). Other patterns that suggest a turbidite system over a contourite one is general turbidite channel behavior, such as channel switching, channel-levee migration and two clear levees on the flanks of channel systems. Chaotic reflection patterns and erosive scars are indicative of mass wasting processes such as slides, slumps and debris flows (J.-C. Faugères et al., 1999).

1.1.3 Trough mouth fans

A significant influence in the sedimentary processes on the West Svalbard Margin comes from glacial input. Since 3.5 Ma the margin have experienced strong influence from intensification of glaciations. Though mouth fan (TMF) complexes are common features at high latitude continental margins and are built up by glacigenic debris flow up to 200 km long, less than 50 m thick and 1-40 km wide which are only deposited during shelf edge glaciations (Amundsen et al., 2011). These types of fans are deposited in front of larger scale

troughs that are caused by ice streams. TMF develop under conditions like the West Barents Sea continental shelf and the West Svalbard Margin with wide continental shelf that have easily erodible sediments – high sediment supply to the shelf edge and a low slope gradient (Cofaigh et al., 2003). The seismic character of TMFs are characterized by chaotic reflection pattern on the upper fan and have a mounded seismic facie further downslope that represent large submarine debris flow deposits. During interstadials and interglacials, sedimentation rates are reduced because of no glacial sediment input (Laberg & Vorren, 1996).

1.1.4 Gas hydrated sediments

In deep-water settings where temperatures are low and pressure is high the formation of gas hydrates occur with the presence of water and natural gas (Makogon, 1981). Gas hydrates are solid and is a physical compound of gas occluded in crystalline cells consisting of water molecules. Gas hydrates are only stable at certain temperature and pressure conditions. 97% of gas hydrates are found offshore while the last 3% are found in permafrost (Makogon, 1981). Offshore they are usually found under the seafloor at outer continental margins under conditions were bottom water temperature, geothermal gradient, seabed pressure, composition of gas and porewater salinity support the formation and stability of gas hydrates. This zone is also called gas hydrate stability zone (GHSZ) and the base of this zone follows the topography of the seafloor (Kvenvolden & McMenamin, 1980). As hydrates form in the sediments they create an impermeable layer where free gas and fluids get trapped under. In a seismic section this will create a strong reflection, which will follow the base of the GHSZ and simulate the seafloor. This reflection is called a Bottom Simulating Reflector (BSR) and will stand out in a seismic section, as it is a response to the GHSZ and not the subsurface geology, and will cut across other reflections (Figure 3)(Kvenvolden & McMenamin, 1980).

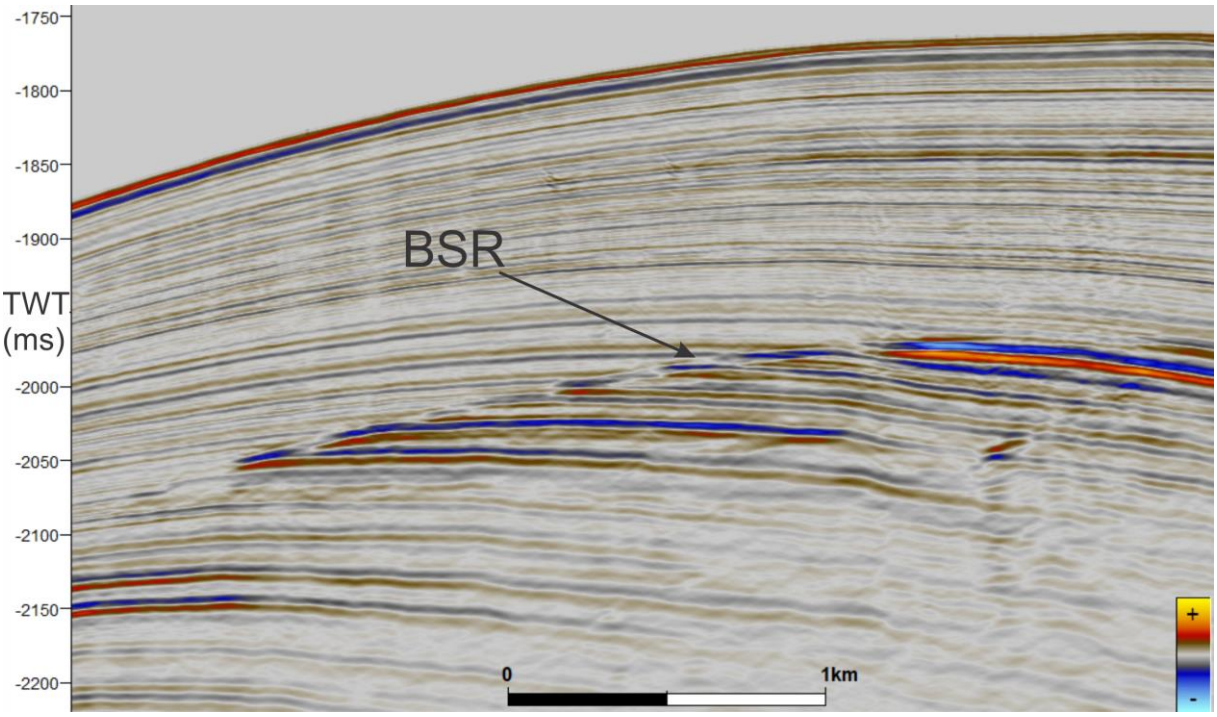

Figure 3 Bottom Simulating Reflector located in parallel sediments. High amplitude reflections below the BSR.

1.1.5 Submarine landslides at high latitudes

Submarine landslides are commonly observed along arctic continental margins and many factors are influencing slope failures in such settings. The development of contourite drifts along slopes may lead to over steepening and toe erosion effecting the slope stability (Elger et al., 2017). Contourite drifts are made up of very fine grained materials and are usually well sorted if the current is constant (Rebesco & Camerlenghi, 2008). This gives the drift deposition the ability to contain a high amount of water and are often underconsolidated because of high sedimentation rates, resulting in low shear strength. At high latitude margins where glacigenic sediments are deposited on top of contourites, it may develop excess pore pressure in the contourite sediments. Gas hydrate dissociation may also give excess pore pressure in contourite sediments as free gas will migrate into the sediments, which already have a high water content. These factors makes a slope prone to failure and may trigger landslides if earthquakes cause liquefaction of the sediments (Laberg & Camerlenghi, 2008).

1.2 Tectonic

The earth's outer shell and surface (lithosphere) is built up by rigid plates that move relative to one another on top of the earth's hotter mantle. The theory of plate tectonics describes how plates are formed and how their boundaries behave (Condie, 2013). The boundaries of plates

can take three different forms. First boundary is ocean ridges also called constructive plate margins where plates are diverging. Magma and mantle is pushed up at the boundary of the plates and creates new oceanic crust and gives rise to sea floor spreading. The spreading of seafloor from ocean ridges usually happens perpendicular to the plates boundary (Kearey et al., 2009). The second form a plate boundary can take is as a trench, which is where two plates are converging in a destructive matter as one plate is thrust under the other and is resorbed by the sub-lithospheric mantle. Since the earth is not expanding the amount of crust that is made from ocean ridges must be equal to the crust that is destructed by converging plates (Kearey et al., 2009). The last form a plate boundary can take is neither a destructive or constructive process. It is marked by tangential movements where adjacent plates are bounded by a transform fault. The plates movement usually are parallel to the fault but in some cases they move in a sinuous trace where on the bends of the faults, small regions of extension and compression are created (Kearey et al., 2009).

1.3 Study Area

The Fram Strait is located between Greenland and Svalbard, representing the northernmost extent of the North Atlantic ocean and the circulation passage between the North Atlantic and Arctic Oceans (Engen et al., 2008). This link features an interesting and important tectonic history in relation to the rifting and sea floor spreading of the North Atlantic that eventually separated the Greenland continental shelf with the Barents Sea Continental Shelf. With the opening of Lena Through north west of Svalbard, the first deep water passage was established between the Arctic and the Atlantic ocean in the Fram Strait and subsequently deep water currents eroding, transporting and depositing sediments along the Fram Strait (Eiken & Hinz, 1993).

1.3.1 Tectonic setting

The Fram Strait represents the northernmost part of the Northern Mid Atlantic Ridge, which starts at 60 degrees North and ends at circa 85 degrees North. It includes Reykjanes Ridge, the Iceland hotspot and The Kolbeinsey Ridge in the south and Mohns, Knipovich, Molloy Ridges and the Lena Through in the North (Kandilarov et al., 2010). The generation of new oceanic crust along Reykjanes, Aegir and Mohns Ridges marked the first stage of the generation of the North Atlantic Ocean in the early Eocene (54.6 Ma ago). Stage two was initiated 33 Ma ago when the relative spreading direction changed from NNW-SSE to NW-SE

as the Labrador Sea stopped spreading in the earliest Oligocene and the Greenland Plate became a part of the North American Plate. This 30 degree counter clockwise rotation of the spreading direction can be defined from the difference in trend between the East and West Jan Mayen Fracture Zones (Lundin & Doré, 2002). This induced the spreading center to shift from the Aegir ridge to the Kolbeinsy Ridge 20 Ma ago, making the Aegir Spreading Ridge extinct. Further North the active Mohns Ridge extends into the oblique-transform ridge system of the Knipovich Ridge caused by propagation of the spreading ridges into the Spitsbergen Shear Zone (Figure 4). Spreading started along the Molloy Ridges ca. 23 Ma ago and eventually circa 10.3 Ma ago along the Fram Strait connecting the Northern Mid Atlantic Ridges to the Mid Arctic Ridges (Kandilarov et al., 2010).

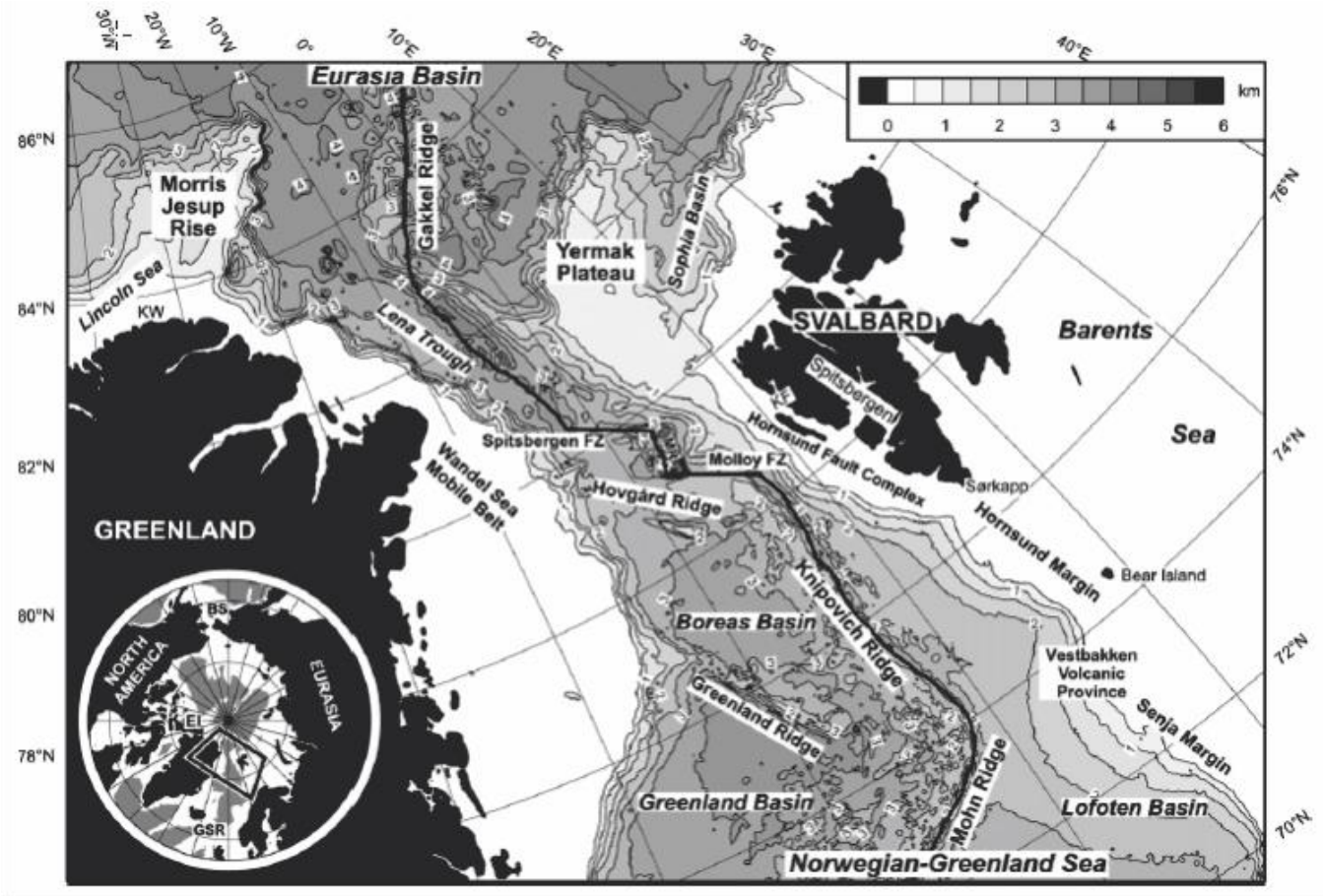

Figure 4 Northern part of the Mid Atlantic Ridge. Displaying the development of the ridges from Mohn Ridge in the south to Gakkel ridge in the north. Figure from Engen et al. (2008)

The opening of the mid-ocean ridge in the North Atlantic has been predominantly characterized by ultra slow spreading rates from the Northern Knipovich Ridge to the Lena Trough. Therefore, while the Mohns Ridge, Southern Knipovich Ridge and Gakkel Ridge

were opening faster, the section of the Fram Strait took longer (Engen et al., 2008). In part, the thermal anomaly under the Fram Strait, principally responsible for weakening the crust, appears to have not been particularly effective. The Mohns Ridge is striking relatively oblique to the Knipovich Ridge, which is believed to be due to the strength of the crust vs. the magnitude of thermal anomaly. North Atlantic spreading from Reykjanes Ridge to Kolbeinsey Ridge and into Mohns Ridge would have likely presumed this relative NE-SW strike if the strong crust of the Barents sea had not been encountered. Instead, the spreading center deviated to a N-S strike along what is thought to be a Caledonian-Inherited structural weakness (Crane et al., 1991).

The stress fields genereated in the study area by the oblique spreading of Molloy and Knipovich Ridge have been modeled for upper crustal tectonic stress fields and their orientation (Plaza-Faverola & Keiding, 2019). The model predicted tensile stress regimes near both Molloy Ridge and Knipovich Ridge and strike-slip stress regimes at larger distances from the ridges (Figure 5). The tensile stress regime of Knipovich Ridge extends northwards into the eastern part of Vestnesa Ridge. A faulting pattern is observed on the seafloor extending form the Knipovich ridge northwards into the eastern part of Vestnesa related to the northward extended tensile stress regime of Knipovich Ridge (Crane et al., 2001) (Plaza-Faverola & Keiding, 2019).

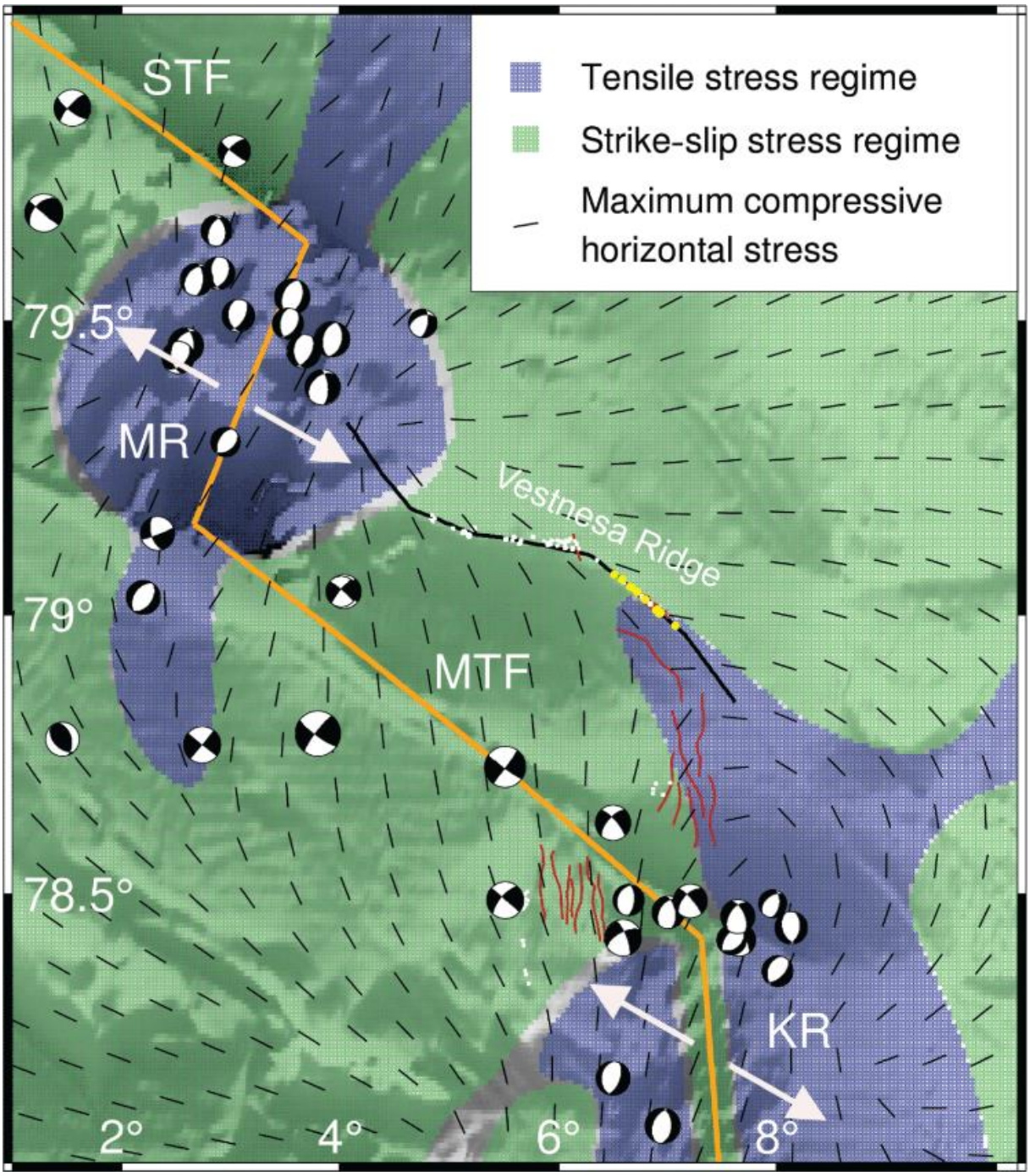

Figure 5 Stress regimes related to Molloy Ridge (MR) and Knipovich Ridge (KR). Faults observed are marked with red south of Vestnesa. Figure taken from Plaza-Faverola and Keiding (2019).

1.3.2 Sedimentary setting

From south to north the West Spitsbergen Current (WCS) transports warm water and sediments from the North Atlantic into the Arctic Ocean (Figure 6)(Beszczynska-Möller et al., 2012). It extends from the sea surface down to approximately 1000m and is measured to have an one-year average current of 8.2 cm/s 25 m above the bottom of the current and a

maximum velocity of 40 cm/s which is sufficient to erode seafloor sediments (Eiken & Hinz, 1993). The WCS and its eddying have influenced the sedimentation on the West Svalbard margin and the Fram Strait at least since the Late Miocene. Although it is uncertain when the opening of the deep-water gateway between The Arctic Ocean and The North Atlantic Ocean happened, Engen et al. (2008) have inferred ages of the oldest contourites depositions in the Fram strait to 19 Ma.

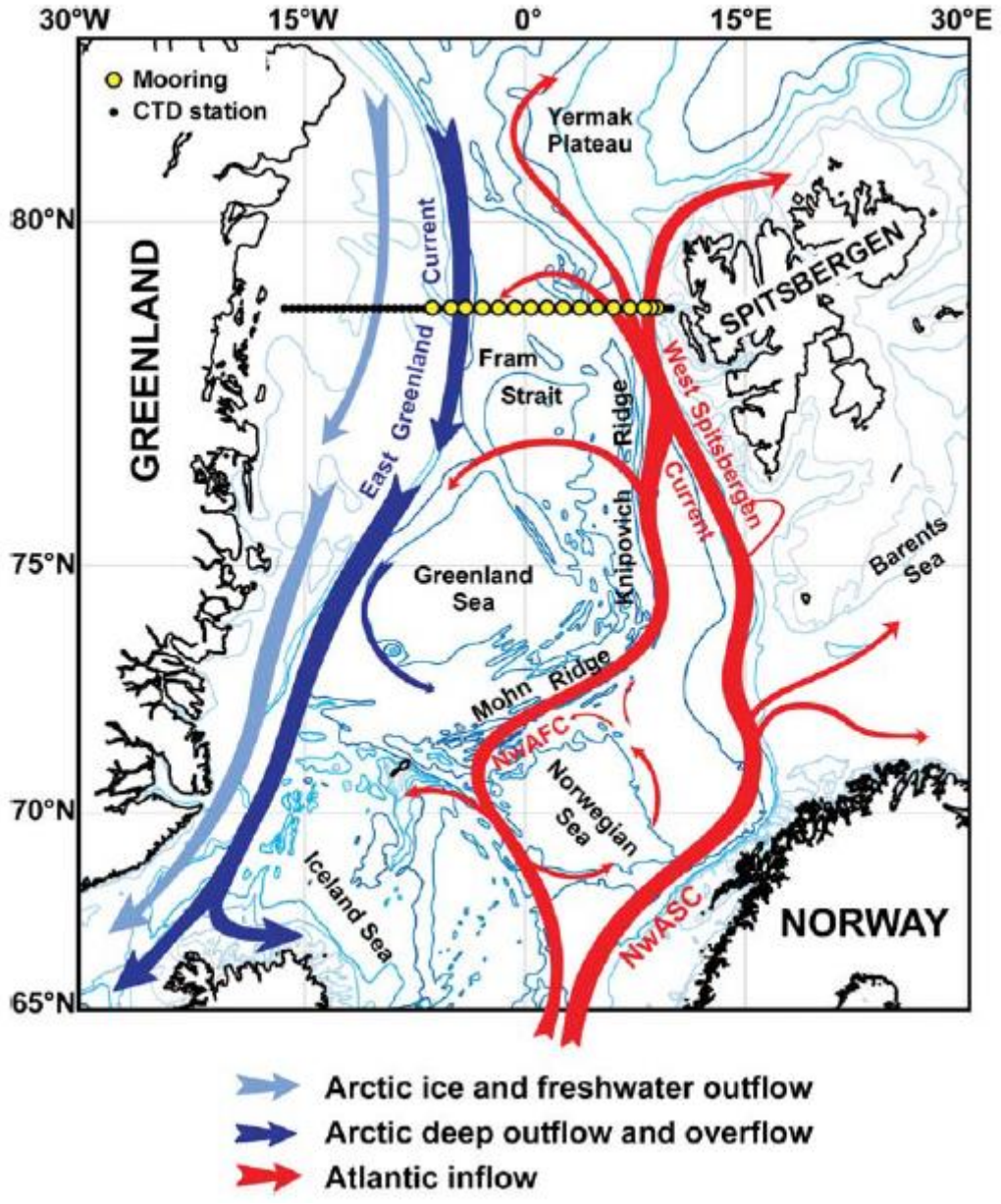

Figure 6 Major oceanic circulations in the North Atlantic and Fram Strait. Figure from Beszczynska-Möller et al. (2012)

From the ODP leg 151 sites 908 -912 a sedimentary framework was made with units YP-1 trough YP-3 (Eiken & Hinz, 1993; Thiede et al., 1995). The framework is based on sedimentary sequences recognized on Vestnesa and the Yermak Plateu. Vestnesa compromises more than 2km thick sedimentary strata with minor unconformities. Sedimentary sequence YP-3 is the youngest sequence and is characterized by its depocenters at the outer shelf and at Vestnesa. Between the depocenters the sequence is thin, which indicates the importance of along slope transport and contourite deposition. It extends north where moats have been observed on the banks of southeastern Yermak Plateu, which have been explained by locally increased currents. The sequence can be characterized with continuous and sub-parallel reflections, but cannot be attributed to a depositional facie (Eiken & Hinz, 1993).

Sequence YP-2's depocenter strikes parallel to the Svalbard Margin and extends all the way to the southwestern Yermak Plateu. The sequence show westward migration by westward thickening wedges which downlaps to the west. YP-2 is thickest just east of the Molloy Transform fault, the northernmost Knipovich rift-valley and the northeast of Hayes Deep where it is characterized by layers truncated at the seafloor (Eiken & Hinz, 1993). These characteristics are also to be found in contourites. Based on these characteristics Eiken and Hinz (1993) suggests that sequences YP-3 and YP-2 are have been dominated by bottom currents. The boundary between the YP-3 and YP-2 have been estimated to 2.7 Ma and is the base of glacial deposits as YP-3 have been correlated with glacial-marine sediments with high incidences of dropstones (Geissler & Jokat, 2004; Knies et al., 2009). YP-1 sequence have not been imaged much by seismic and was only identified in one profile by Eiken and Hinz (1993) due to its depth. The sequence showed sub-parallel reflection patterns in syn-rift and post-rift sediments deposited on top of oceanic crust (Eiken & Hinz, 1993).

1.3.3 Stratigraphic framework

A new 6 My stratigraphic framework for the Yermak Plateu and North West Svalbard was established by Mattingsdal et al. (2014). Based on paleomagnetic and biostratigraphic sampling and correlation between high resolution seismic data and Ocean Drilling Program (ODP) holes 911A, 910C and 912A. Figure 7 display the stratigraphy developed from the study with age, depth in meters and time (ms) and sedimentation rate for each of the ODP holes. The oldest penetrated reflections had an estimated age of 11 Ma implied that

contourites deposition had been present since at least 11 Ma. 2.78 Ma marks the boundary between YP-2 And YP-3 and at all three ODP sites the sedimentation rate has been lower prior to 2.7 Ma at circa 3-10 cm/ka and circa 9-19 cm/ka after 2.7 Ma. This is probably related to the increase in glacial erosion as the glaciation in the Northern Hemisphere intensified. This is observed with an increase in the presence of dropstones and ice-rafted debris in ODP sites 910C and 911A at ca 2.7 Ma (Mattingsdal et al., 2014). Between 2.7 Ma and 1.5 Ma continuous parallel seismic reflection patterns is observed demonstrating the continued deposition of contourites. From 1.5 Ma toward present day a more chaotic reflection pattern is observed in the shallowest seismic data. Underneath the chaotic pattern the continuous seismic pattern are truncated and is interpreted as erosional truncations against the assumed unconformity caused by extensive glacial erosion on the Yermak Plateu at ca. 1.5 Ma (Mattingsdal et al., 2014).

The framework based on the seismic data and ODP sites identifies three different depositional environments on Yermak Plateu. From at least 11 Ma to 2.7 Ma the deposition was mainly dominated by along slope currents and contourites deposition by the West Spitsbergen Current. From 2.7 Ma to 1.5 Ma the contourite deposition continued with influence by glaciation. After 1.5 Ma Glacially influenced contourite deposition continued, but with glacial erosional influence from the east (Mattingsdal et al., 2014).

Age (Ma)	912 Z* (mbsf)	912 TWT† (ms)	912 sed. rate§ (cm/kyr)	910 Z* (mbsf)	910 TWT† (ms)	910 sed. rate§ (cm/kyr)	911 Z* (mbsf)	911 TWT† (ms)	911 sed. rate§ (cm/kyr)	911 v_{int}# (m/s)
0	0	1411.5		0	750		0	1227		
			3.2			2.5			9.2	1565
0.78	24.6	1443		19.5	n.a.**		72.0	1319		
			4.1			1.0			10.0	1611
1.07	36.5	1458		22.2	n.a.**		101.0	1355		
			13.4			0.7			19.0††	1698§§
1.20	53.8	1479		23.1	n.a.**		n.a.**	n.a.**		
			9.2			8.7††			19.0††	1698§§
1.78	107.1	1542		n.a.**	n.a.**		236.0	1514		
			8.7			8.7††			19.2	1730
1.95	121.6	1559		88.0	853		268.0	1551		
			11.5			16.2			14.7	1824
2.58	194.0	1638		190.0	968		361.3	1653		
			9.0			16.6			15.4	1979
2.78	212.0	1657		223.0	1009		391.9	1686		
			2.3			10.1			6.8	1930
3.60	231.0	1677		305.0	1094		447.0	1743		
			3.4			9.5			3.2	1915
5.0	278.0	1726		438.0	1236		492.4	1790		
			6.5			15.8			6.6	2000
5.2	291.0	1739		470.0	1269		505.8	1804		
			7.0			6.2			3.2	1900
5.8	333.0	1783		507.4	1312		525.0	1824		

Note: Numbers in rectangles are from depths in ODP holes and TWT from seismic data. Other numbers are calculated. Row colors correspond to colors of seismic reflectors in Fig. 2A.
* Z = meters below seafloor (mbsf).
† TWT = two-way travel-time.
§ sed. rate = sedimentation rate.
# v_{int} = interval velocity.
** n.a. = not available.
†† Derived from depths above and below n.a. values.
§§ Derived from twt above and below n.a. value.

Figure 7 The stratigraphic framework from Mattingsdal et al. (2014) correlated with boreholes 910, 911 and 912.

1.3.4 Extent of gas hydrates and fluid flow

Several indications of fluid flow and gas hydrates formed along the WSM have been observed (Dumke et al., 2016). Along the crest of Vestnesa Ridge several pockmarks have been observed related to gas chimneys and fluid migration (Vogt et al., 1994) (Bünz et al., 2012). A BSR have been observed under the crest of Vestnesa Ridge with high amplitude reflections over a depth range of approximately 150 m under the BSR indicating a significant amount of free gas under the base of the GHSZ. Fluid flow features are only found at the crest of the ridge, while the BSR extend over the entire Vestnesa Ridge (Bünz et al., 2012). A BSR have been observed over several areas along the WSM, including Vestnesa, south of Vestnesa down to the Knipovich Ridge and north east of the Molloy Ridge at the western slope of WSM (Figure 8).

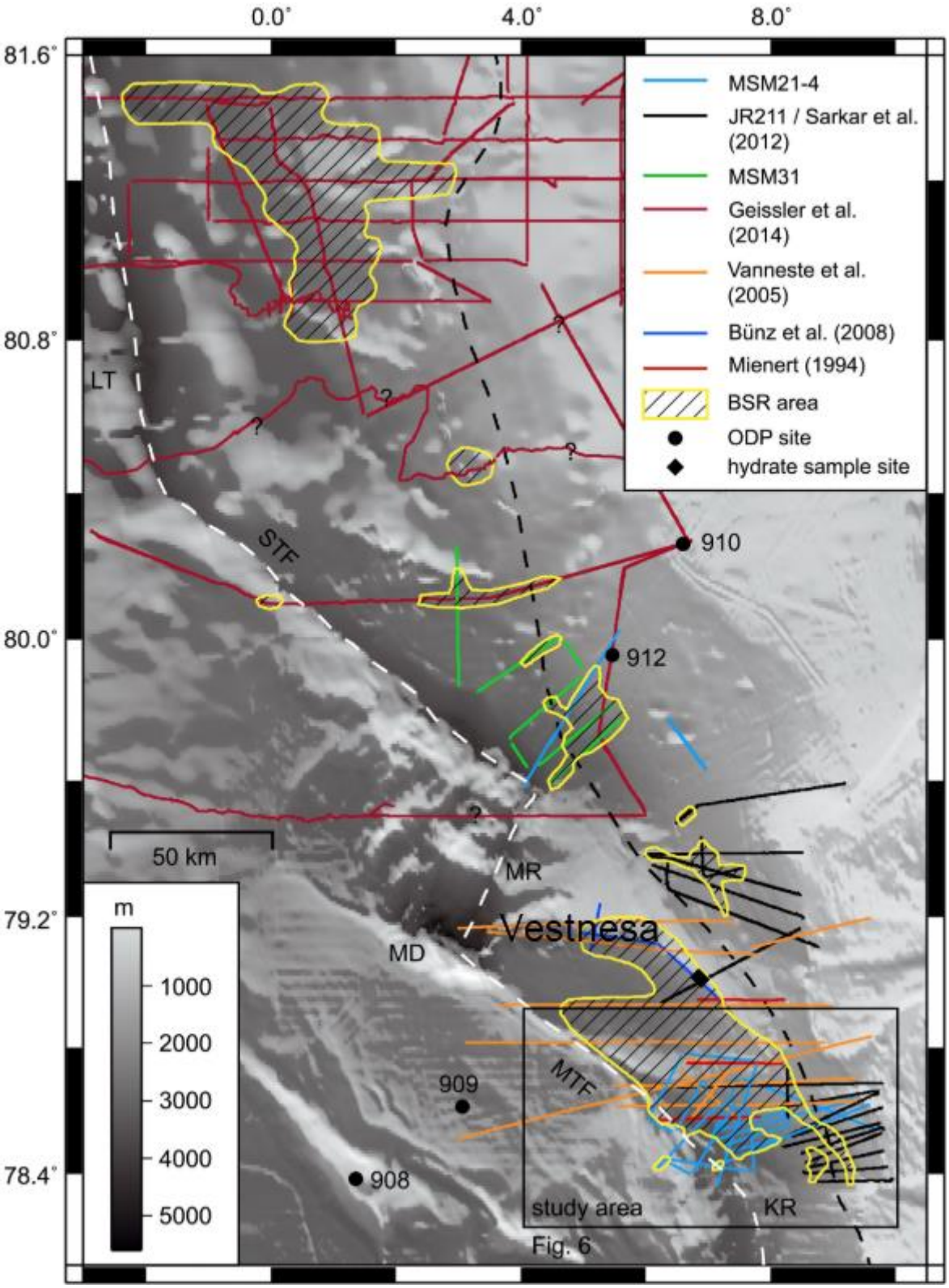

Figure 8 Extent of BSR based on 2-D seismic data from different surveys along the WSM and Yermak Plateu. Figure from Dumke et al. (2016)

1.3.5 Submarine landslides

The West Svalbard Margin have been subject to landslide events, which have been observed and investigated. The most significant landslide in the study area is the Fram Slide Complex, which is located east of the Molloy Ridge and north of Vestnesa in an area built of contourite drifts (Elger et al., 2017). The development of slope instability in this area is proposed to be influenced by the onset of contourite drifts in the form of sediment waves at the deeper parts of the slope (Osti et al., 2019). The wavy patterns of sediment wave formation allowed for the formation of shear planes along surfaces of sedimentary successions. This area is located close to Molloy Ridge which is seismically active and several earthquakes have been reported in the area over the last century (Läderach et al., 2011) which may have triggered the unstable slope failure.

2 Seismic data and processing

2.1 Seismic reflections

Seismic reflections appear in the data when there is an acoustic impedance contrast between two materials. Acoustic impedance is the product of density and seismic velocity in a material and the contrast is determined by the difference in acoustic impedance between materials. Higher contrast gives stronger reflection. When an acoustic wave travels in a material and crosses the interface of a material with a different acoustic impedance, the wave will reflect at the interface and make it travel back in a direction depending on the angle of the incident wave to the interface. This makes up the principles of seismic reflection and can help us identify different acoustic impedance contrasts in the subsurface made by changes in the geology (Kearey et al., 2013)

2.1.1 Vertical and Horizontal Resolution

An important aspect of seismic reflections is the resolution of seismic data. The resolution of the data is determined by the frequency, velocity and wavelength of the particular seismic survey (Brown, 2011). One of the main problems with seismic acquisition is interference between closely spaced interfaces of acoustic impedance contrasts, which is the concept of vertical resolution in seismic data; how closely can two acoustic impedance contrasts interfaces be to one another and still be visible on the seismic data? The time thickness between two interfaces must be equal to or greater than half the wavelength of the seismic

wavelet (Brown, 2011). If it is less, the reflections of the two interfaces will interfere destructively with each other and be inseparable. The vertical resolution can be found by looking at the relationship between frequency, velocity and wavelength, which is given by:

$$Wavelength\ (\lambda) = \frac{velocity\ (V)}{frequency\ (f)}$$

The velocity in the subsurface usually increases with depth due to overburden pressure resulting in higher densities. Consequently, the wavelength will increase and the resolution of the data will be poorer. In terms of frequencies, the higher the frequency the better the resolution.

A wavefront does not only reflect energy from a single point laterally on the reflector, but a circular zone. The circular zone that are reflecting back energy from a reflector that constructively sums up to produce a reflection is called the Fresnel Zone (Brown, 2011). The Fresnel Zone is the definition of horizontal resolution as a unit of the size ½ the Fresnel Zone cannot be distinguished from a diffraction hyperbolae produced by a point reflector. The radius of the Fresnel Zone is given by:

$$rf = \frac{V}{2} * \frac{t^{1/2}}{f}$$

Where rf is the radius of Fresnel Zone, *V* is the average velocity, *t* is two way time and *f* is the dominant frequency (Brown, 2011). The equation concludes that the Fresnel Zone will increase, as the horizontal resolution will decrease with depth, higher velocities and lower frequencies, as it does with vertical resolution.

2.1.2 Attenuation

Reduction of amplitude and loss of seismic energy with depth is called attenuation. Attenuation of seismic energy is caused by several factors. The most critical factor is geometric divergence or geometric spreading (Kearey et al., 2013). A single shot is thought to be a point source, which generates a spherical wavefront. As it propagates, the spherical wave will increase its radius causing its energy density to decrease. Wave amplitude is proportional to the square root of energy density and decreases accordingly (Kearey et al., 2013).

Some of the seismic energy also get absorbed by the rocks and are converted into heat. When seismic energy reflects, refracts and are converted into other modes (P-S wave conversions) amplitude decreases. The frequency of the initial wave shot from the source changes as it propagates. Higher frequencies are absorbed quicker than low frequencies (Kearey et al., 2013). Which means the lower the frequency, the greater the penetration depth. As the previous subchapter stated that lower frequencies would also have lower resolution. High frequencies will have high resolution, but lower penetration depth. Low frequency will have low resolution, but deeper penetration depth.

2.2 2D seismic acquisition

Most of the data that are processed in this thesis are acquired by a P-cable system that utilizes a high-resolution acquisition set-up to acquire 3D, and if configured, 2D seismic data with relative cost and work efficiency. The set-up for 2D acquisition are four streamers of 25 meters set together with a receiver interval of typically 3.125 meters. The four streamers add up to a total streamer length of 100m with 32 receivers (depending on acquisition set-up). This multichannel system utilizes source guns which typically are 15/30 in^3 mini airguns firing at 160-170 bar with a fire rate depending on water depth.

2.3 2D Seismic data processing

The main goal of seismic processing is to project the data with the least amount of noise and as much signal as possible, often referred to as the signal to noise ratio (S/N). The higher the S/N ratio the better the data. By applying different filters and processes to the data it will, if implemented correctly, preserve and enhance the primary signal, while reducing and removing noise and unwanted data. Effectively increasing the signal to noise ratio. The following sub chapters will go through each step of the processing done on the seismic lines in this thesis as represented in Figure 9.

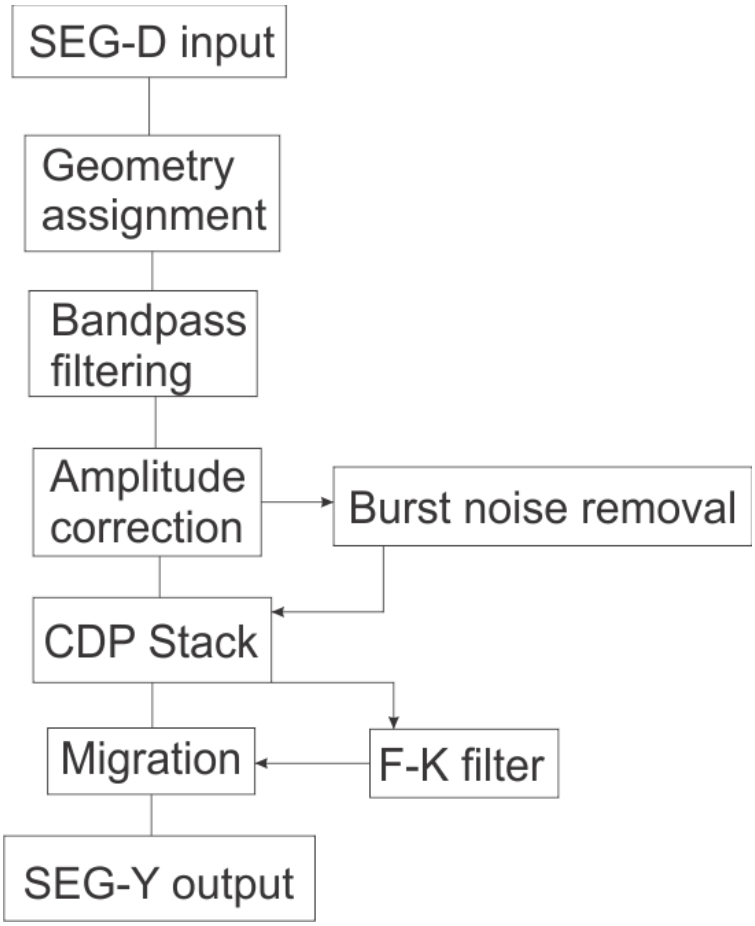

Figure 9 Overviwes of processing flow used in this thesis, implemented with RadExPro 2019.1

2.3.1 Import of data

Raw data collected in a survey is stored as SEG-D files and are imported into a processing software, such as RadExPro, to be processed and outputted as finished SEG-Y files, which further can be imported to an interpretation software for interpretation. SEG-D files are imported line by line until the whole survey is uploaded and processing of each line can begin. First flow after input of data is geometry assignment.

2.3.2 Assigning geometry

Assigning geometry is important for further processing and interpretation as it influences CDP gathering of the recorded traces and could ultimately affect the stacking of the data (Chapter 2.3.5). The geometry and coordinates for the survey and recorded traces were already processed and found in the ship log of the particular cruise. UTM coordinates together with time (in hour, minute and second) for each shot were assigned to the SEG-D data, together with the set parameters for the P-Cable setup (Figure 10).

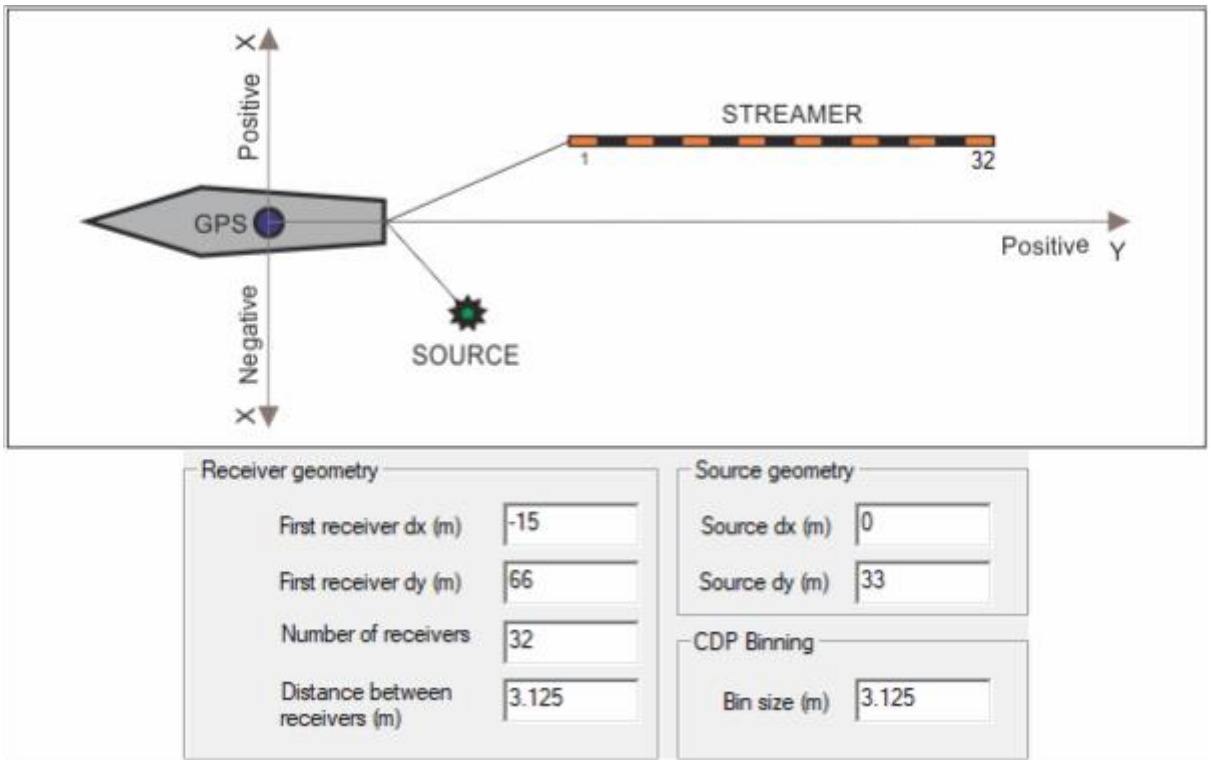

Figure 10 P-cable set-up illustrating the receiver and source geometry in relation to the ship's GPS coordinates.

2.3.3 Bandpass filtering

Band-pass filtering is a commonly used form of frequency filtering which reduces noise while preserving the seismic signal. A seismic trace, especially in a marine survey, contains many low frequencies such as swell noise and high frequency ambient noise. A band is a range of frequencies, which you can either reject or pass while filtering. A band-pass filter sets up limits for which frequencies that shall be preserved (Yilmaz, 2001). The range of frequencies is commonly defined by a low cut and a high cut ramp where you define the interval of which frequencies are passed. For example, you can set the low cut ramp to reject low swell noise or hydrostatic pressure noise, which is common in a marine survey. Similarly, the high cut ramp is set to exclude any high frequency noise that is not part of your main signal (Yilmaz, 2001). The result is the band pass of the wanted signal and a band reject of the determined low and high noise frequencies. As displayed in Figure 11a noise is covering the data, low frequency noise is dominating the amplitude percentage and is interfering with the signal. Figure 11b display the result after applying a bandpass filter. The low frequency noise is removed from the data and the signal is displayed more accurately.

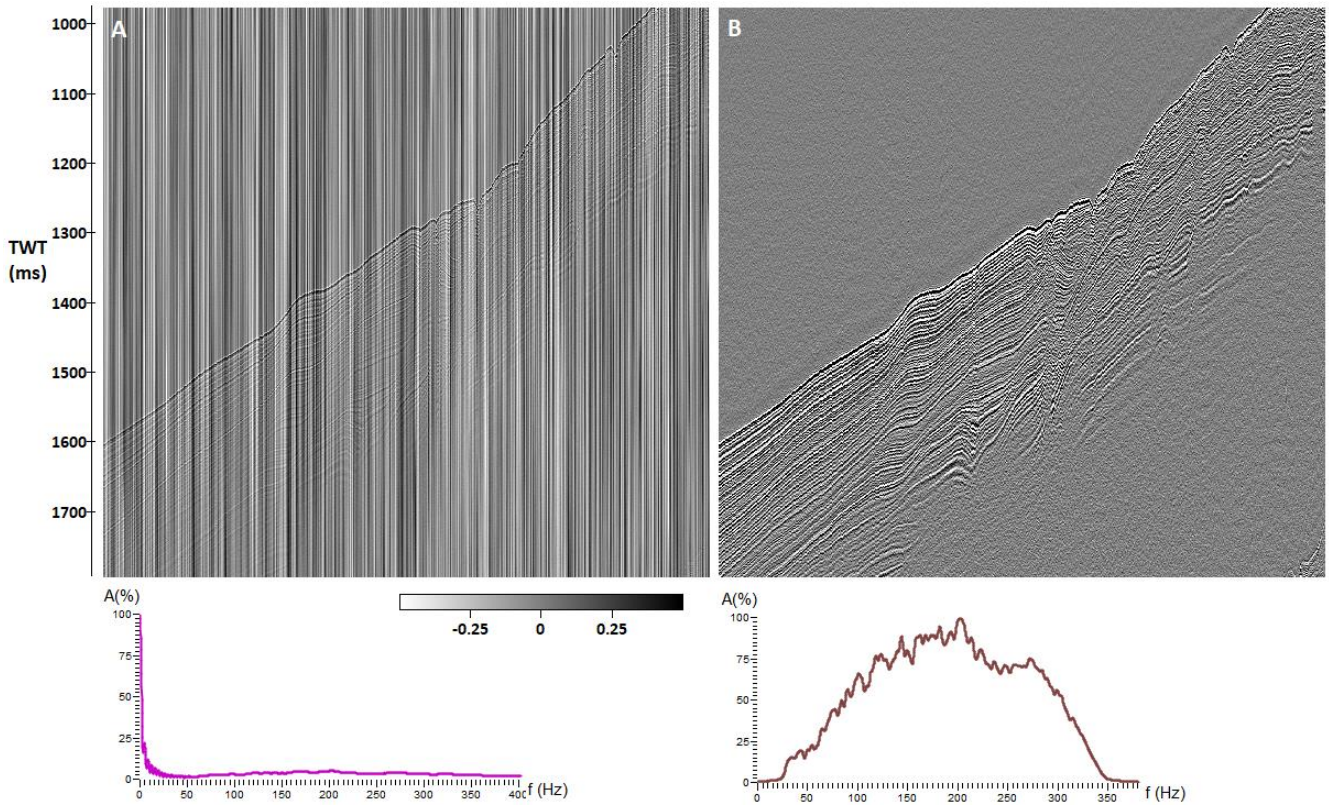

Figure 11 A) Seismic section before bandpass filtering were used. Graph show the dominating frequencies are in the lower end of the spectrum <20 Hz. B) Seismic section where bandpass filter have removed any low or high frequency noise

2.3.4 BNR

In the CAGE 14-5 survey some lines was affected by high amplitude bursts that affect the signal significantly that removing them was necessary. Especially some channels had high appearance of bursts. The filter Burst Noise Removal (BNR) can be applied to either the entirety of the seismic line or isolated channels. Bursts are in characteristic very high amplitude wavelets that appear in short periods of time on the traces, most likely caused by electrical interference and technical problems with the streamers such as leakage. The filter averages out the amplitude of a preset number of traces and removes the highest amplitudes in the data (DECO, 2019). This is optimal as the noise bursts are of so much higher amplitude than the signal that the amplitude "cut" can be set to remove almost all the bursts without removing any of the signal, improving the signal to noise ratio significantly.

Two different set of parameters were used for the survey, one aggressive and one passive. The aggressive one were only used for lines were only a few channels experienced severe amounts of bursts, while the passive set of parameters were used for larger parts of or the whole line

where bursts were present in smaller numbers. The reason for the two sets of parameters is to ensure that no signal is unnecessary lost as the aggressive filter may remove some signal if its applied to channels without bursts.

Figure 12a displays a channel with high amounts of bursts in the data. By applying the burst noise removal filter most of the high amplitude bursts are removed from the data and the results are significantly improved as seen in Figure 12b. Figure 12c show the data that has been removed and little to none of the signal have been affected by the filter.

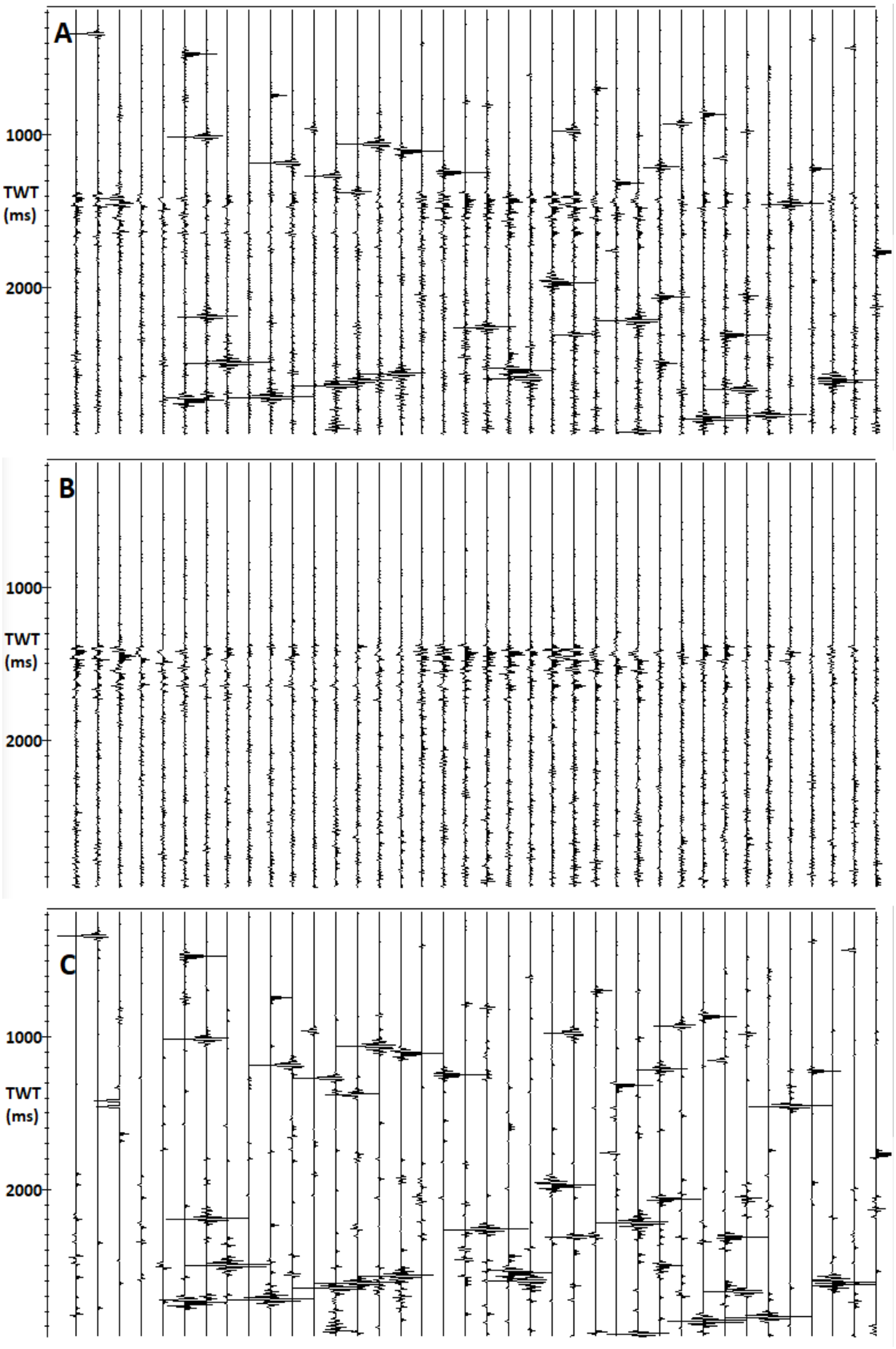
A
1000
TWT
(ms)
2000
B
1000
TWT
(ms)
2000
C
1000
TWT
(ms)
2000

Figure 12 Seismic section displayed in wiggle mode. A) Original seismic section with high amount of bursts. B) Seismic section after BNR has been implemented. Bursts have been successfully been removed. C) The filtered seismic section subtracted from the original seismic section reveal the noise that have been removed by the BNR filter.

2.3.5 Stacking

After basic noise removal has been applied to the line, the next step in processing is to stack the traces together to improve the signal to noise ratio and get a clear image of the subsurface. Stacking is done by CDP gathers (Figure 13). A CDP gather includes all traces that are thought to have the same Common Depth Point i.e. they display the same point independent of which channel and shot it is.

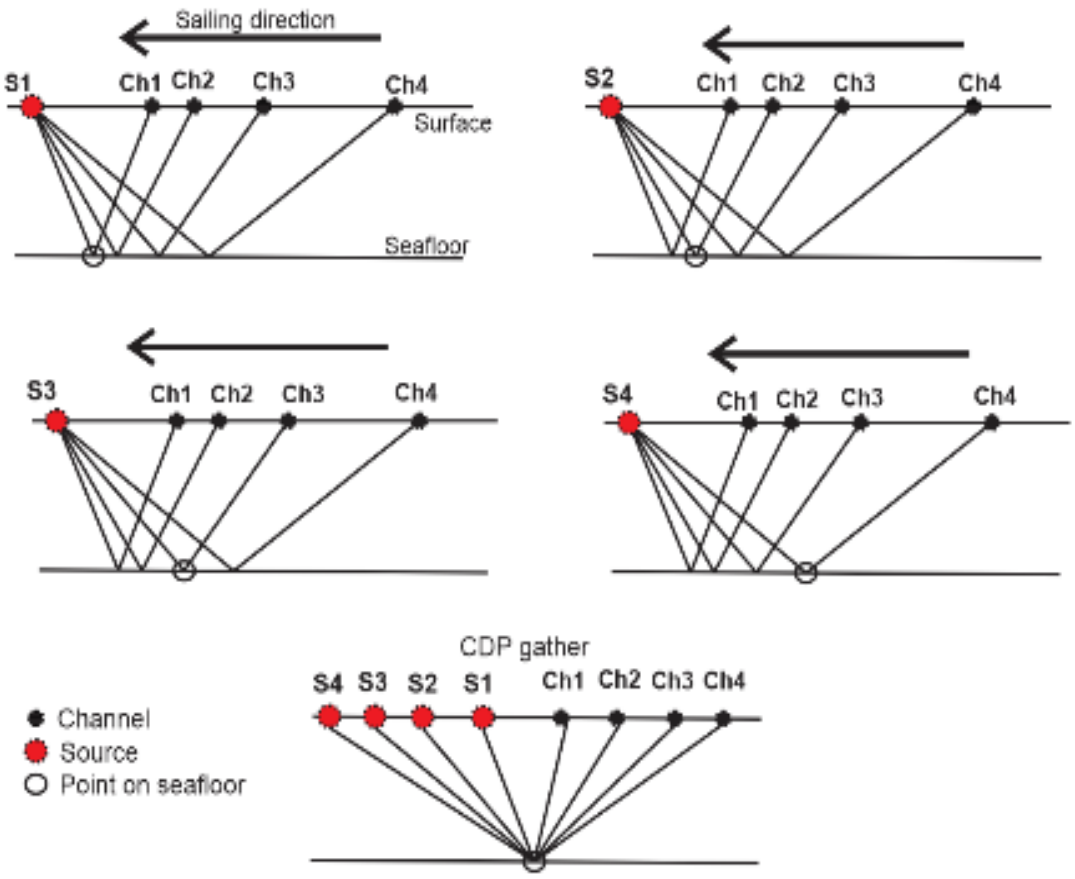

Figure 13 Illustration of a CDP gather made up of traces from different shots and channels with the same perceived CDP.

The traces that have the same CDP are then summed together in a stack attenuating all noise that do not add together, and amplifying the signal that are coherent in the traces (Figure 14).

Stacking significantly improves the S/N ratio by an estimate of $(N)^{1/2}$, where N is the number of traces in one CDP gather (Alsadi, 2017).

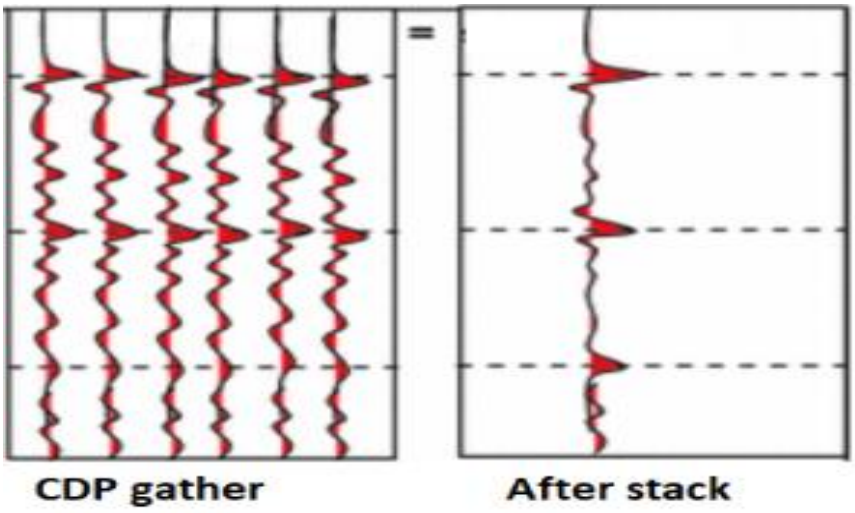

Figure 14 Example of a stacked CDP gather and how the coherent energy are stacked while noise is significantly reduced.

2.3.6 F-K filtering

By transferring seismic data into other domains by applying mathematical algorithms to the traces, it is possible to do two-dimensional filtering to suppress noise waves. One of the domains is the frequency-wavenumber domain (F-K). In this domain interfering signals in the seismic data may have no interference at all and can be successfully removed from the data (Figure 15). When the filtering is done the data is transformed back into its standard domain (t,x) where the S/N ratio is improved (DECO, 2019).

This filter were only used on two of the lines in the data, as it was deemed not necessary on the rest of the survey. However, on the two lines it was applied to, noise was successfully removed and the data improved significantly. The filter is used by looking at a fraction of the data in the F-K plane and constructing a polygon to define a passing range for the filtering.

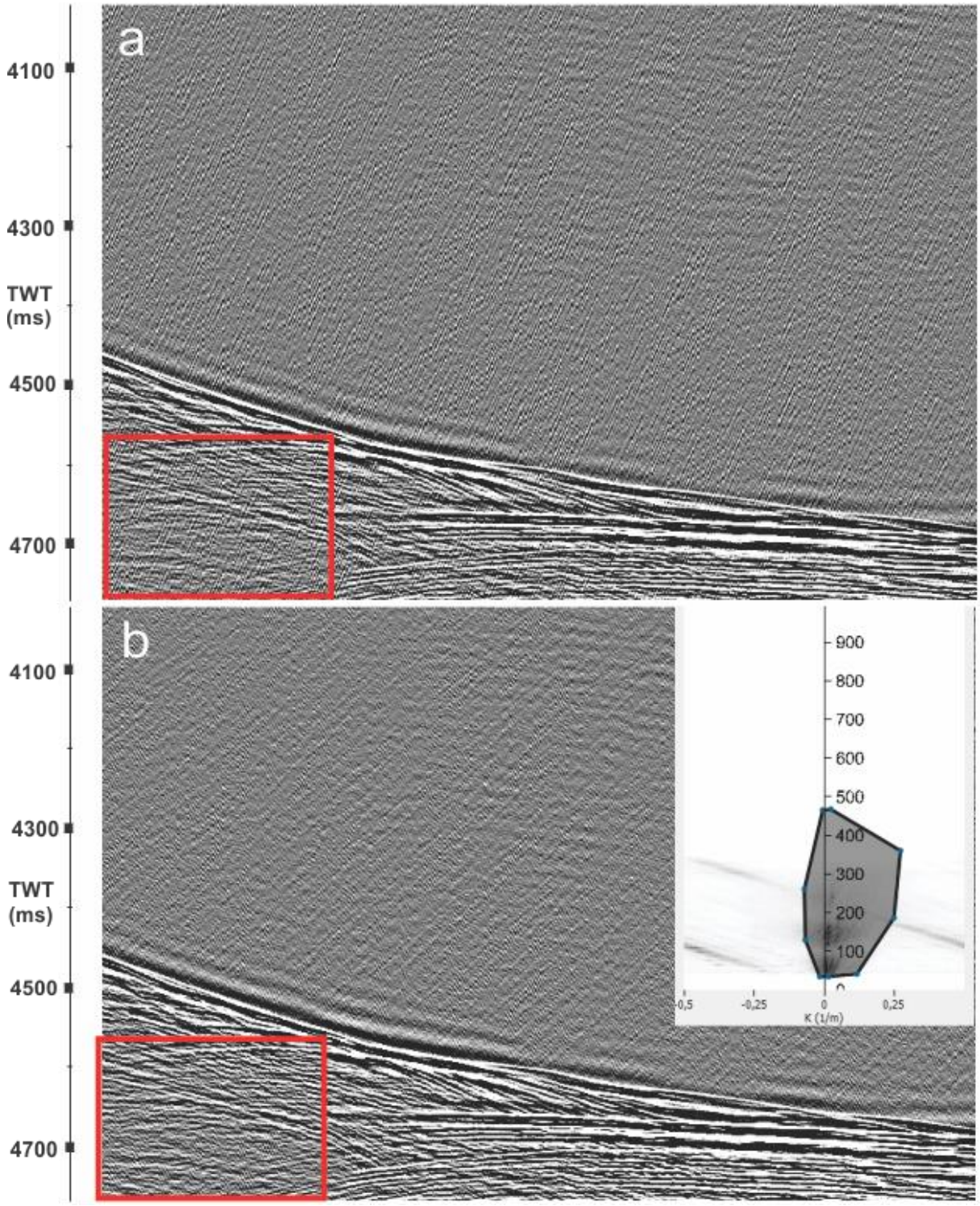

Figure 15 Comparison of seismic section before (a) and after (b) implementing F-K filter

2.3.7 Migration

A seismic receiver interprets the signal it receives as coming directly beneath the midpoint between the receiver and the source. This is true for horizontal reflectors but is not for dipping

reflectors. When imaging a dipping reflector, shifting of the reflection event from its true position occurs, both in vertical and horizontal direction, which in turn will decrease the imaged reflectors angle in comparison to its true angle (Alsadi, 2017).

Another type of distortion created by false imaging is diffractions caused by point reflectors or reflector terminations, which creates hyperbolas in the data. These are caused by channels receiving several reflections from the same point over time, causing a false reflection event that curves down from the actual point in both directions as a result of receiving a signal before and after the actual midpoint is passed. These hyperbolas interfere with real reflection events and can disturb interpretation of features such as faults where reflector terminations occur.

Distortion caused by dipping and termination of reflectors can both be corrected for by migration. Migration is an inverse process that transforms the seismic image into more true display of the geological structures that gave of distortions. This is given that the input migration parameters are appropriate for this section. Several parameters are influencing the result of migration, if too aggressive parameters are set, the whole profile can be overmigrated and give a false image (Yilmaz, 2001).

There are two ways to migrate, either pre or post stack. Migration is the reverse process of seismic forward modeling, which transforms the observed energy back to its subsurface reflector (Sun, 2002). To perform migration on seismic data, a basic knowledge of the seismic velocity of the material that are surveyed must be known. The data processed in this thesis were migrated using the Kirchoff migration, post stack. This type of migration involves the summation of amplitudes along diffraction hyperbolas, which are functions of the seismic velocity (Yilmaz, 2001). For Kirchoff migration the most important parameters are the aperture width and the maximum dip to migrate (Yilmaz, 2001). A low velocity hyperbola will have narrower aperture than a high velocity hyperbola, which means more migration is needed for higher velocities. Migration aperture is the spatial extent of the summation path span and is measured in number of traces that are included to collapse the hyperbola back to its original point (Yilmaz, 2001).

Because of the difference in hyperbolas shape in relation to velocity and the fact that velocities in most cases will increase with depth, this has to be corrected for. Even though the

seismic waves travel through salt water first, the depth of the seafloor varies greatly throughout the survey. This are corrected for by implementing a velocity table, which divides the seismic section up according to depth of the seafloor. Table 1 show line 1's migration velocity table and are divided into sections of CDP numbers. Line 1 starts with CDP 625 where the depth of the seafloor is around 2000 ms. The section gets shallower as the section continues and at the last section of the seafloor depth is around 500 ms.

Table 1 Velocity model for Line 1 used in Kirchoff migration. Velocity 1.49 km/s were used for salt water.

CDP	TWT interval (ms) : Velocity (km/s)
625	0-2000:1.49, 2001-3000:1.5
5125	0-1500:1.49, 1501-3000:1.5
10125	0-1000:1.49, 1001-1500:1.5
13125	0-700:1.49, 701-1500:1.5
14625	0-500:1.49, 501-1000:1.5

If the velocity is correct than the hyperbolas that are created from a terminated reflector will collapse into its original point and dipping reflectors will be corrected into its true angle.

2.3.8 Migration results

Results of the post stack Kirchoff time migration are seen in figure 16. There were considerable challenges on getting the aperture right for the entire survey as high aperture was needed for some of the lines to successfully collapse diffraction hyperbolas and to display faults in the data. Different parameters for aperture were used in consideration of depth of reflections, amount of dip angle on reflections and extent of diffractions. The migration process was considered successful for the purpose of reprocessing.

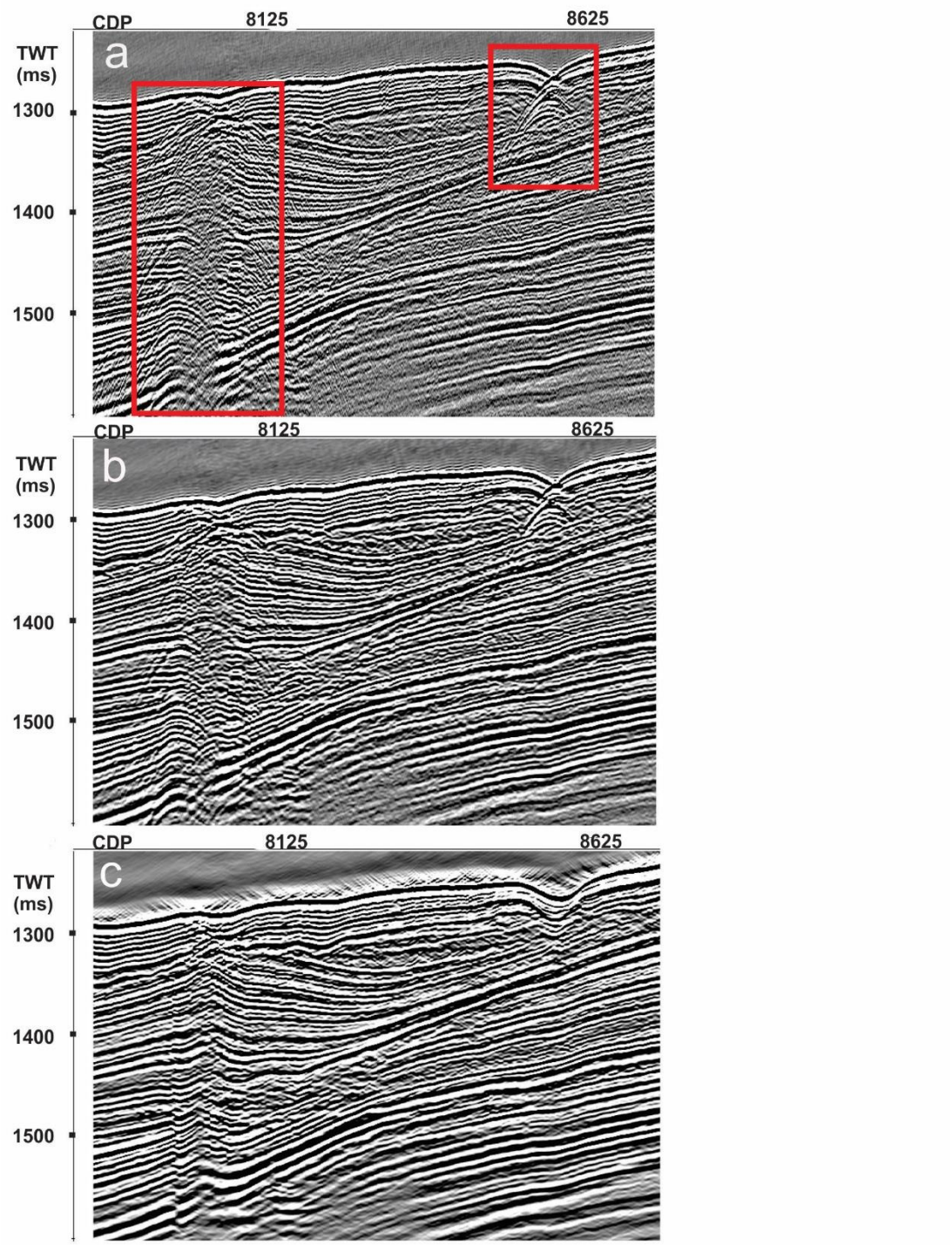

Figure 16 a) seismic section before migration which show several hyperbolas. b) Krichoff migration with conservative aperture. Hyperbolas are reduced, but are still visible and effecting the data. c)Hyperbolas are successfully collapsed with high aperture Kirchoff Migration.

On the top right of the seismic section a depression is observable on the seafloor with diffraction hyperbolaes coming out the lowest point (Figure 16). To the left of the profile a series of hyperbolas are stacked on top of each other in a vertical matter. When unmigrated

(Figure 16a) it is hard to tell what both of these features are displaying. Figure 16b show a migrated version with low aperture and it is visible that the improvement is not satisfactory. This aperture parameter were used successfully on other lines, but for this line a higher aperture were needed. Figure 16c show a migrated version with higher aperture and the hyperbolas are now successfully collapsed and the features are now visible and more correctly representing the actual subsurface. The depression can now be described as a synclinal that reaches down several layers instead of two reflections truncating at on another in a downward matter. The feature on the left is now interpretable with visible data that are not destructively interfered by diffractions. It can now be described as an abrupt displacement in the layer packaging.

2.4 Correlation and seismic database

The seismic data reprocessed in this thesis along with the other seismic surveys in the study area were imported to the interpretation software Petrel 2019 delivered by Schlumberger. The software is used for visualizing the data and correlating seismic horizons though the study area. From the interpreted horizons surface maps of the horizons were made along with time-thickness maps between the surfaces and the seafloor. The data used in seismic interpretation and correlation of stratigraphy are 2D seismic data from both multichannel and single channel surveys. In total there are 15 different surveys put together in the database, which includes the survey reprocessed in this thesis (Figure 17)(Table 2).

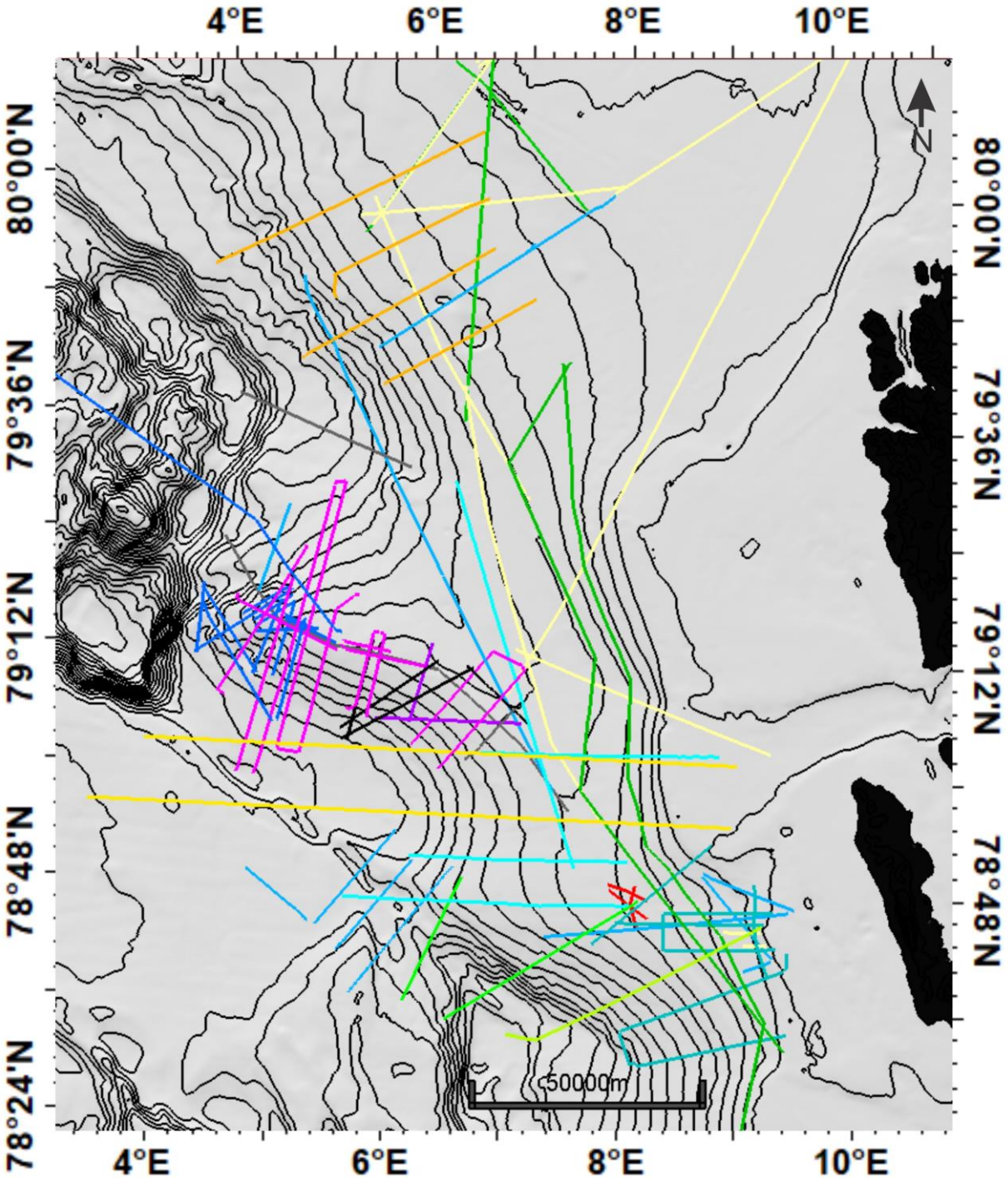

Figure 17 Overview of all seismic surveys and their associated lines. Color of line represent which survey they belong to where the same are used in table 2.

Table 2 Overview of all seismic surveys and the sources used for all surveys. Color of the survey name relate to Figure 17.

Survey name	Source	Length of streamer [m]	Number of receivers	Distance between receivers [m]
Cage 19-1	2 mini-GI (15/15 in3) & (30/30 in3)	100	32	3,125
Cage 18-4	2 mini-GI (15/15 in3) & (30/30 in3)	100	32	3,125
Cage 17-3	2 mini-GI (15/15 in3) & (30/30 in3)	100	32	3,125
Cage 17-5	2 mini-GI (15/15 in3) & (30/30 in3)	100	32	3,125
Cage 16-6	2 mini-GI (15/15 in3) & (30/30 in3) & GI (45/105 in3)	100	32	3,125
Cage 15-6	2 mini-GI (15/15 in3) & (30/30 in3) & 2 GI (45/45 in3) & (105/105 in3)	100	32	3,125
Cage 14-5	2 mini-GI (15/15 in3) & (30/30 in3)	100	32	3,125
Cage 14-1	2 mini-GI (15/15 in3) & (30/30 in3)	100	32	3,125
Cage 13-5	2 GI (45/45 in3) & (45/105 in3)	100	32	3,125
10JM GlaciBar	2 GI (45/45 in3) & (45/105 in3)	6	1	-
09KA-JM001	2 GI (45/45 in3) & (45/105 in3)	6	1	-
Svalex	6 G gun array (1416 in3)	3000	240	12,5
KP94	Bolt gun 80 in3	10	1	-
JM07VSTNSA	2 GI (45/105 in3) & (45/45 in3)	6	1	-
09JM_GEO3144	2 GI (45/105 in3) & (45/45 in3)	6	1	-

2.4.1 Cosine of Phase

In areas where the reflection strength is insufficient to successfully follow the seismic with the correlation, a certain attribute was used to increase the perceived strength of the reflections. Cosine of Phase is similar to Automatic Gain Control, which reduces the contrast of amplitudes independent of depth. Cosine of phase removes all amplitude contrasts, which allows for visualizing extremely weak reflections with small amplitudes (Barnes, 2006). This improves the reflection continuity and enhances seismic lateral variations, faults and seismic facies variations (Sarhan, 2017). The attribute is only used for correlation purposes where

reflection strength is too weak to interpret from original seismic data. As Figure 18 display, any significant amplitude features are lost in the extracted attribute.

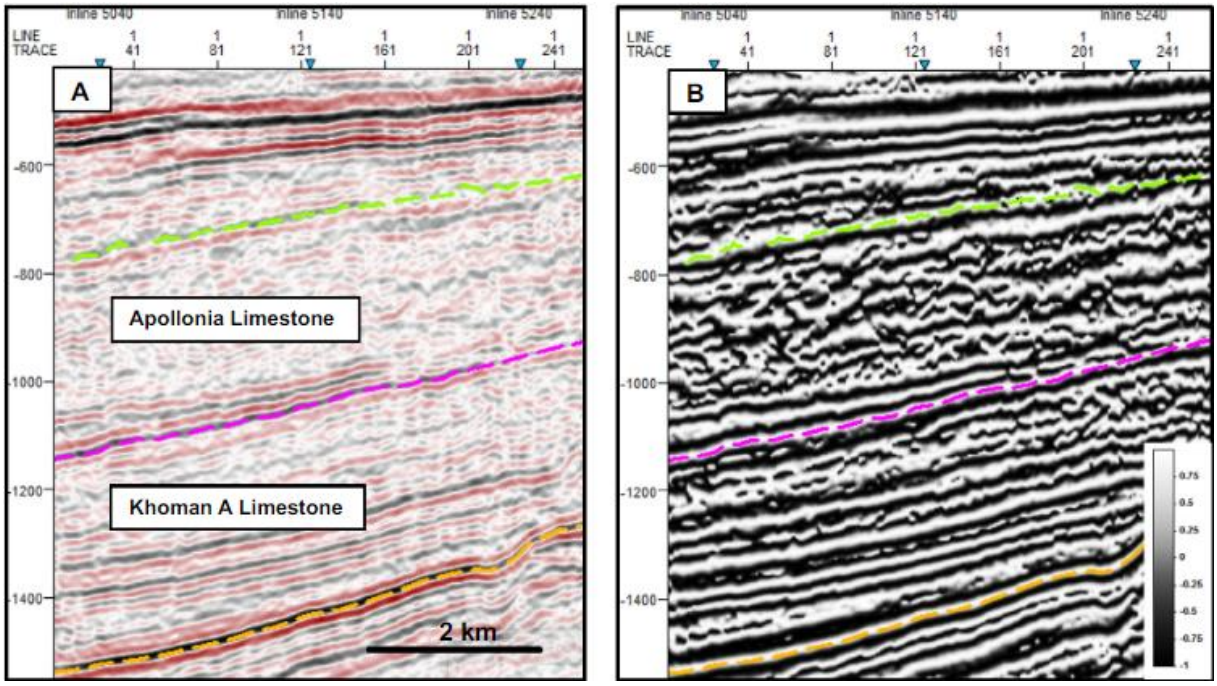

Figure 18 Comparison between original seismic section (A) and the extracted Cosine of Phase attribute (B). Figure from Sarhan (2017)

3 Seismic Interpretation

The aim of the interpretations is to get a better understanding of the sedimentary development and deposition of contourites on the western Svalbard margin with particular focus on the deep-sea environment >1000 m water depth. Neotectonic structures in the region will be interpreted on seismic and bathymetric data to assess how tectonic forces have influenced the sedimentary processes. Other features such as submarine landslides and free gas systems will be looked closer into in relevance to tectonic and sedimentary processes.

The stratigraphic framework presented by (Mattingsdal et al., 2014) is mainly formed for the Yermak Plateu. There is little prior work done on correlation of this stratigraphy further south along the WSM. The two most interesting reflectors on the Yermak Plateu is 1.5 Ma and 2.7 Ma. These have not been correlated further south. In interest of the intensification of glaciation in the region it is interesting to observe the glacial input and the development of contour deposits further south to the Knipovich ridge and west to Vestnesa and how the tectonics have influenced this development the last 11 Ma.

3.1 Stratigraphy

Mattingsdal et al. (2014) provided a 6 My stratigraphic framework for the western Svalbard margin (Figure 7). The main focus of this interpretation was to correlate this stratigraphy further south along the WSM and down into the deep-seated where major depocenters occur in massive drift deposits. The 1.5Ma and 2.7Ma events were the targeted horizons to correlate. This is based on the importance of the 2.7 Ma reflection as it corresponds to the YP 2 / YP 3 boundary (Eiken and Hinz, 1993) and marks the change of depositional setting from mainly along-slope currents and contourite deposition to have significant input of glacial sediments. The 1.5 Ma reflection is important as it marks the onset of glacial erosion. 2.7 Ma and 1.5 Ma both mark a change in depositional environment on WSM and Fram Strait and to correlate the horizons south is interesting in relation to how the deposition may have changed further south and in the deep sea (Chapter 1.3.3).

The interpretation of 1.5 and 2.78 Ma reflector, which originates from the seismic lines connected to ODP holes 911A, 910C and 912A is correlated approximately 240 km south until it terminates against Isfjorden Through Mouth Fan (TMF) and a multiple in the dataset (Figure 29). It covers a distance of 85 km in the east west direction from the Svalbard continental margin to the edge of Vestnesa ridge (Figure 19). The correlation is also taken to the western slope north of Vestnesa (Figure 20 and 21) to target sediments closer to the Molloy Transform Fault, but the horizons are truncated by slide scars from the Fram Slide Complex (Figure 20)(Chapter 1.3.4).

On the western part of Vestnesa the 2.78 Ma horizon were too deep to correlate through the original seismic so the attribute *Cosine of Phase* were extracted to successfully correlate to the edge of Vestnesa (Figure 19b)

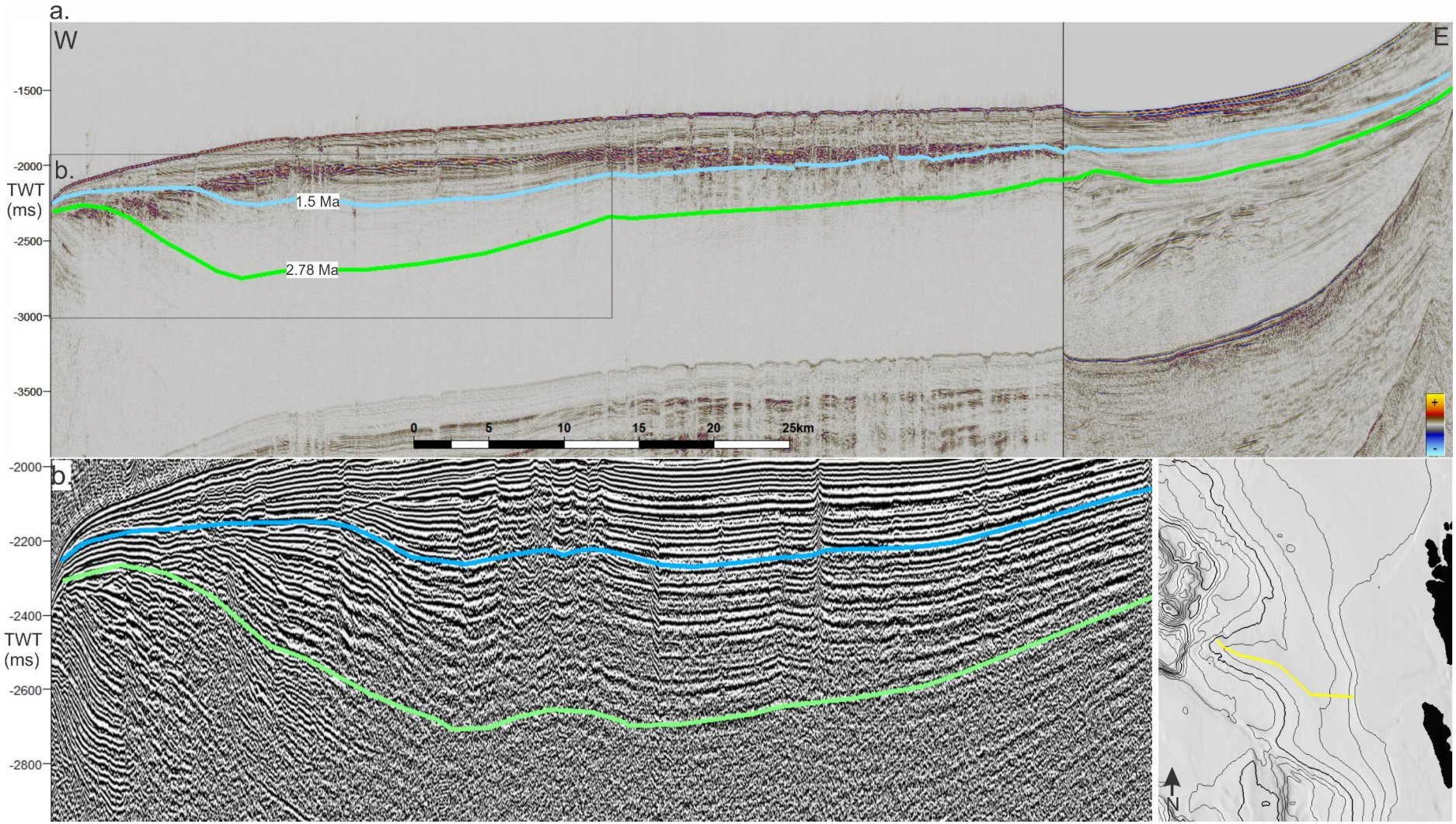

Figure 19 a) Composite line of line 5 from CAGE 13-5 and Svalex 11 over the crest of Vestnesa. b) Cosine of Phase attribute extracted from line 5

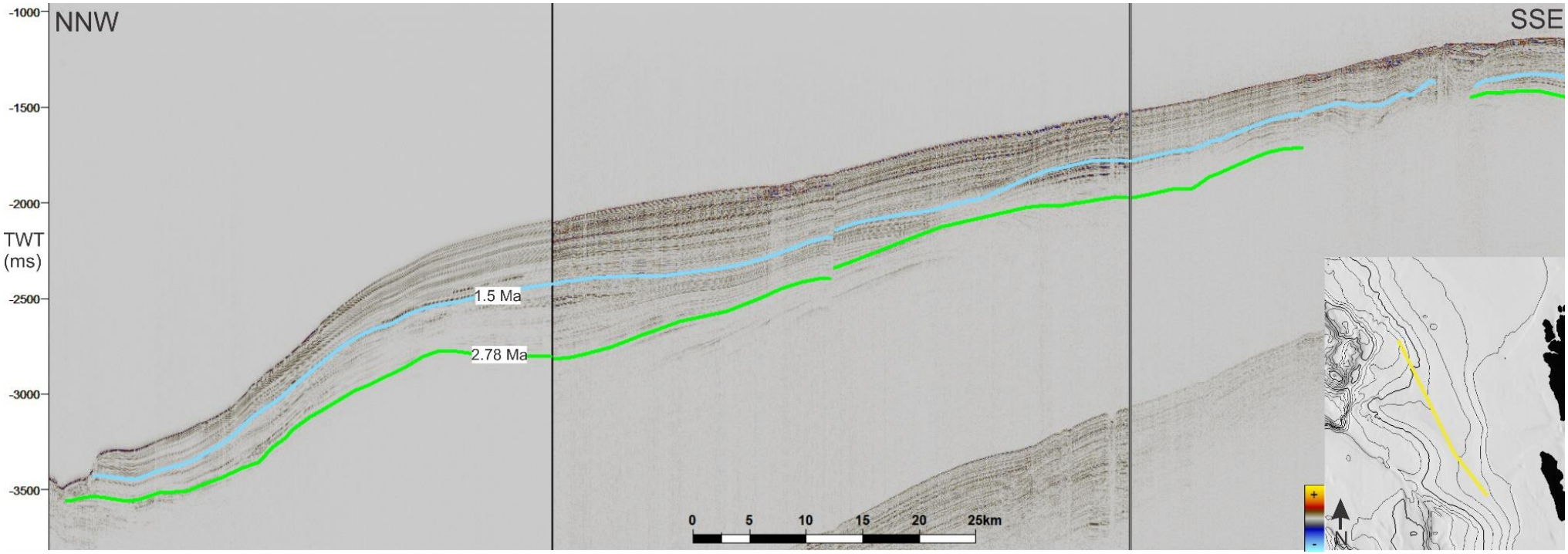

Figure 20 Composite line of line 5, 6 and 7 from Cage 14-5.

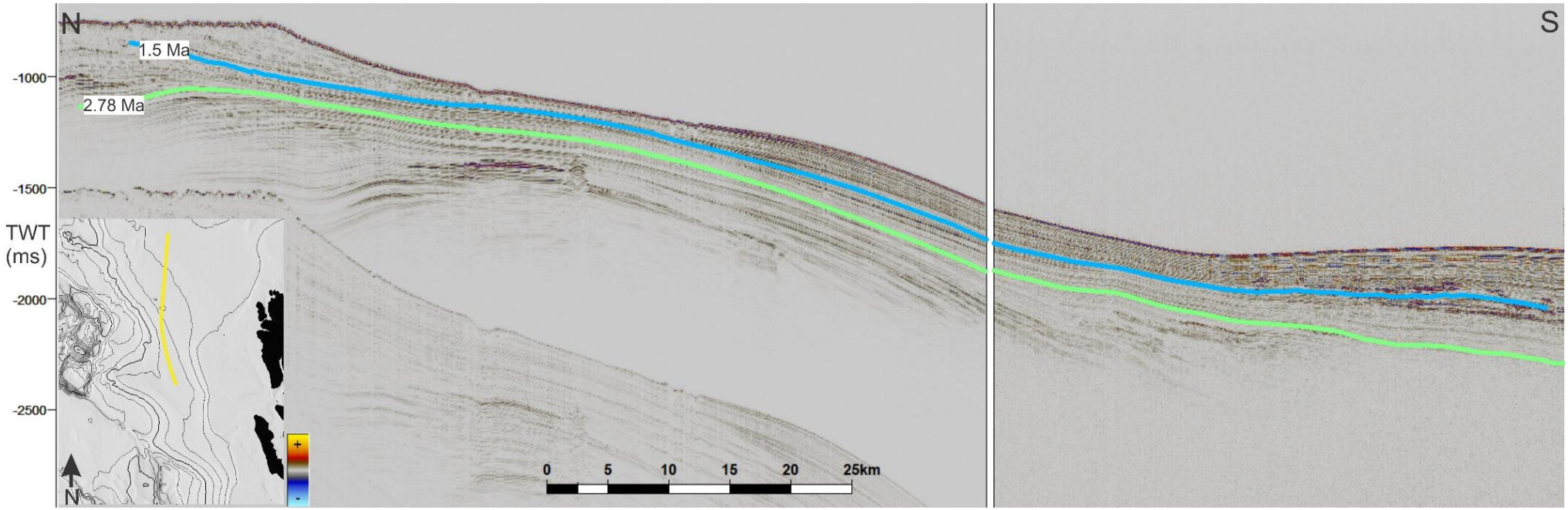

Figure 21 Composite line from 10JM GlaciBar survey

Figure 22 show all the seismic lines for which the 2.78 and 1.5 Ma horizons were interpreted from. These seismic lines are the base of interpretations and will together with bathymetry and surface maps make up the stratigraphic interpretations in this thesis.

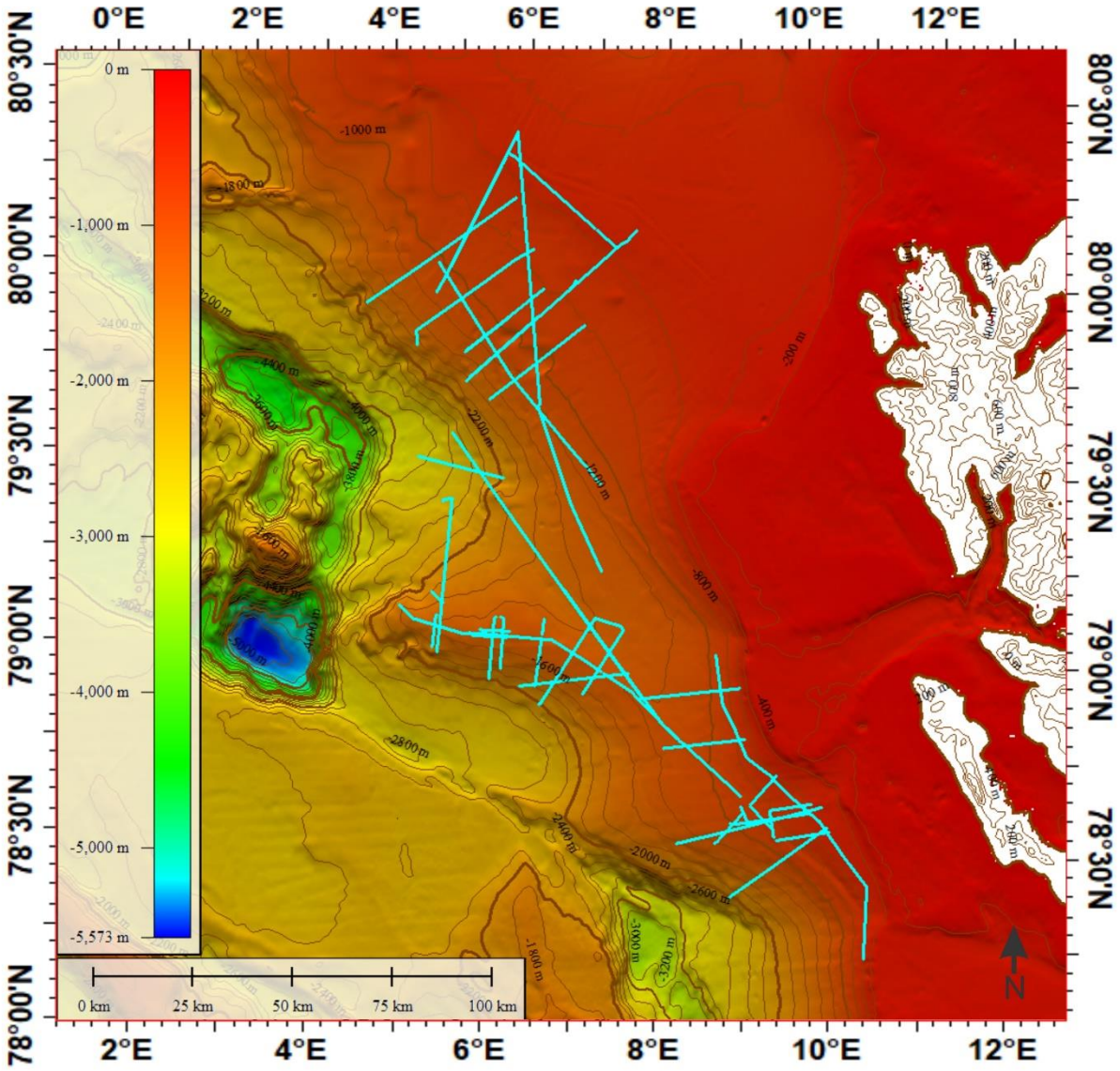

Figure 22 Overview of the interpreted 1.5 Ma and 2.78 Ma horizon

3.1.1 Distribution of sediments

The surface maps interpolated from the 1.5 Ma horizon show a similar topography as the seafloor with elevations on the Vestnesa ridge in the east and gradually rising dip towards the east towards the Yermak Plateu and the coast of Svalbard (Figure 23). 2.78 Ma horizon has different topography than 1.5 Ma and the seafloor at Vestnesa. It dips down northwards earlier in the middle and have lower topography at the center than the rest of Vestnesa.

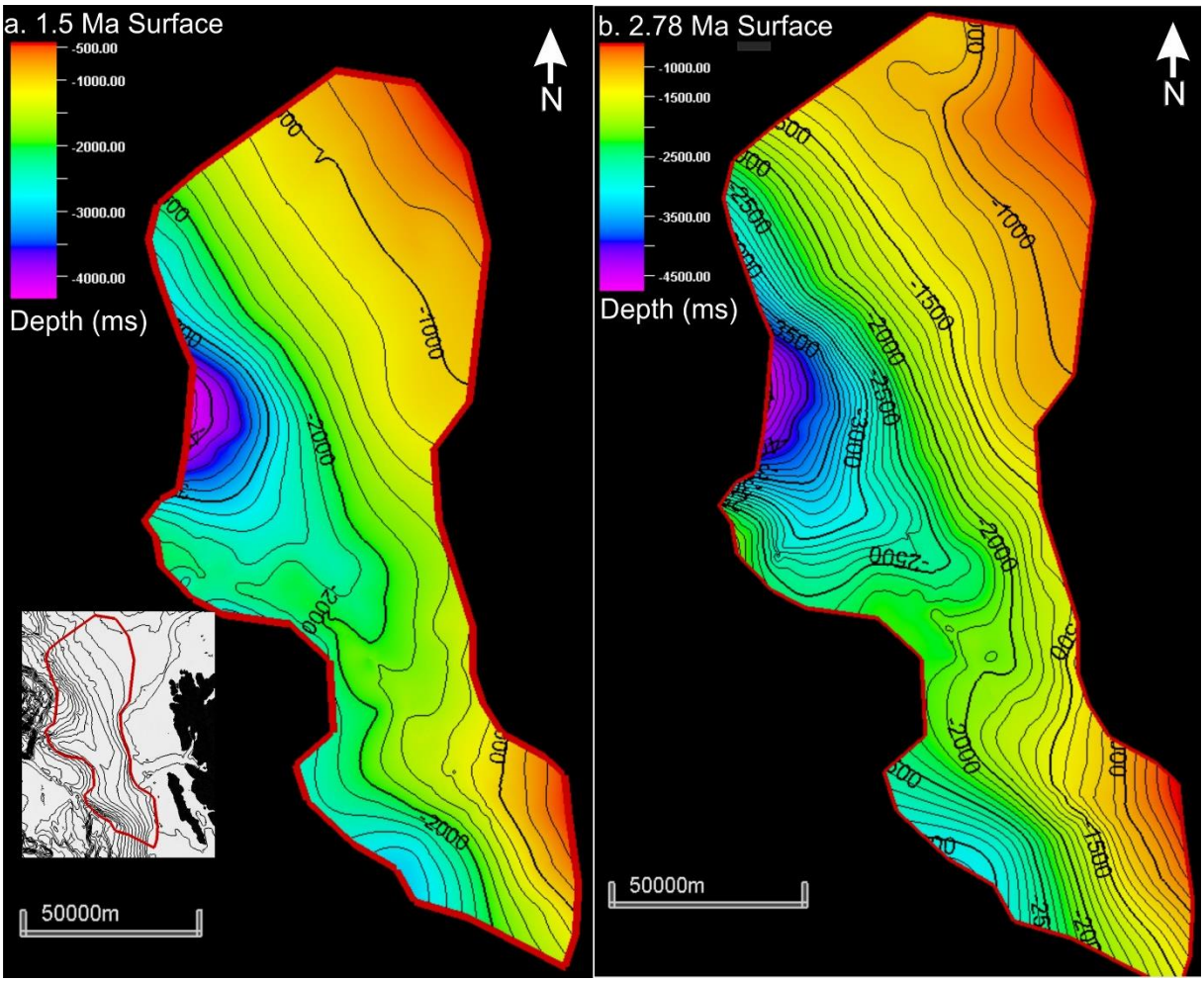

Figure 23 a) Surface map interpolated from the interpreted 1.5 Ma horizon. b) Surface map interpolated from the 2.78 Ma horizon.

From the surface maps made from the 1.5 Ma and 2.78 Ma horizons and the seafloor (Figure 23), thickness maps were made (Figure 24). The thickness maps show the distributions of sediments between the 1.5 Ma, 2.78 Ma and present day over the study area. There are in general thicker sediment packages to the south of Vestnesa compared to the north. However, the thickest sediment packages is located on Vestnesa Ridge where we see a significant increase in thickness in both intervals.

.

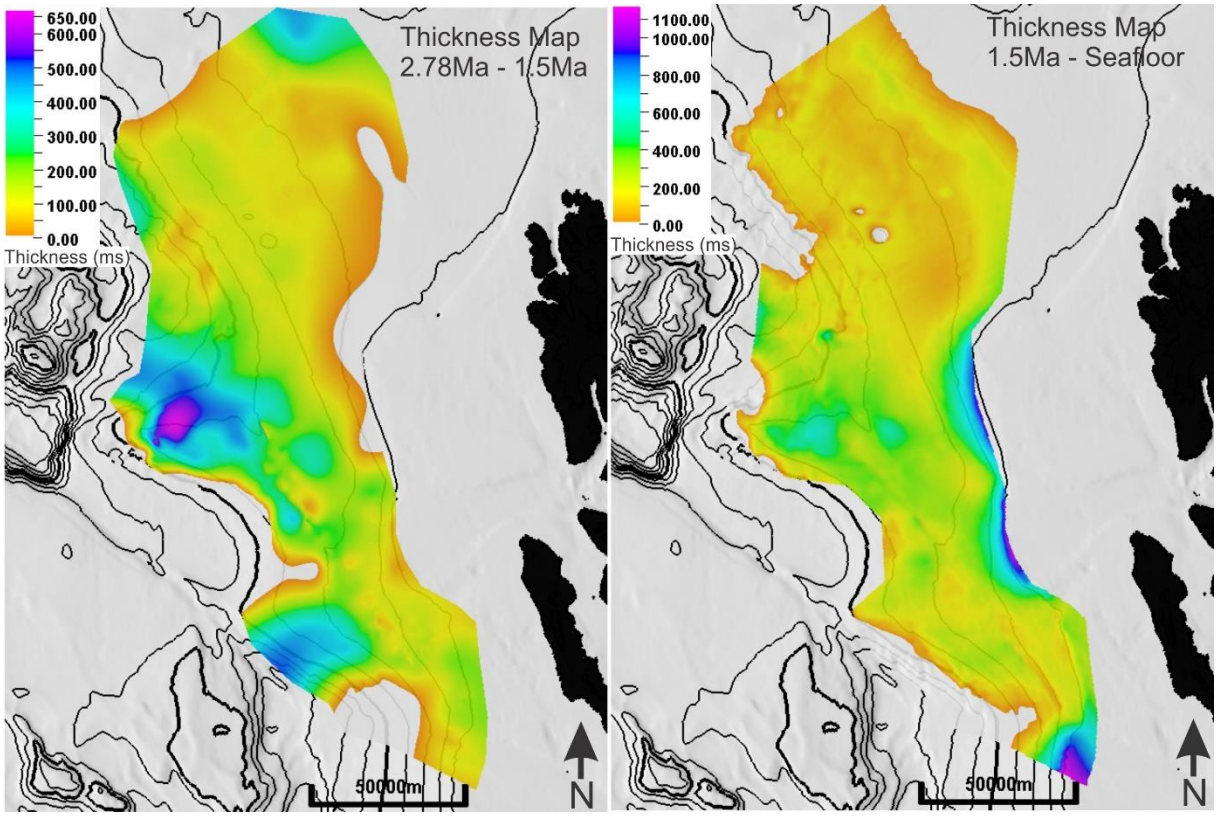

Figure 24 Thickness map made from surface 2.78 Ma - 1.5 Ma and 1.5 Ma to the seafloor.

3.1.2 Seismic stratigraphy North of Vestnesa

The thickness map (Figure 24) show a trend of thinner sediment packages north of Vestenesa with a general trend of approximately 200 ms thickness between 1.5 Ma and 2.78 Ma. It thins westwards as the surfaces dip down towards the Molly Transform Fault, as well as thinning towards the east towards the coastline of Svalbard. The seismic stratigraphy can be characterized by parallel and continuous reflection patterns with sporadic bright spots in the seismic (Figure 25).

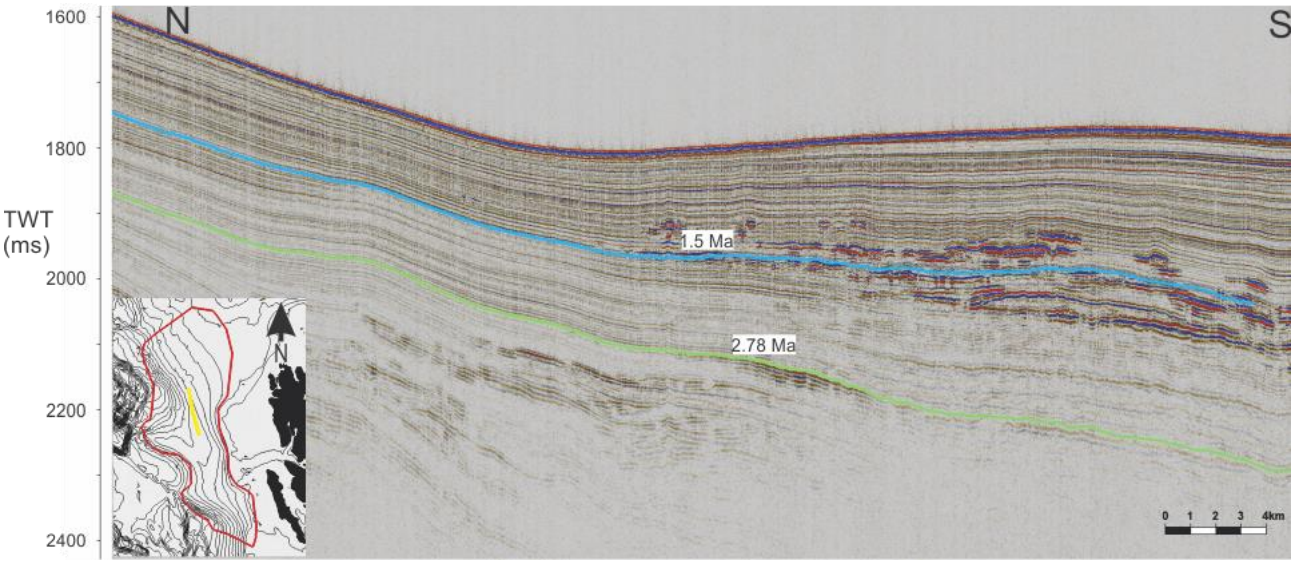

Figure 25 Seismic line 21 from 10Jm-GlaciBar

The seismic facie of the northern part of the study area changes from parallel and continuous to wavy and subparallel reflection pattern in the deeper parts of the slope (Figure 26). The change is abrupt and happens when the slope steepens towards the Molloy Deep. The characteristic of the seismic reflections downslope resembles the moat-levee type structure stacked in an upslope migration.

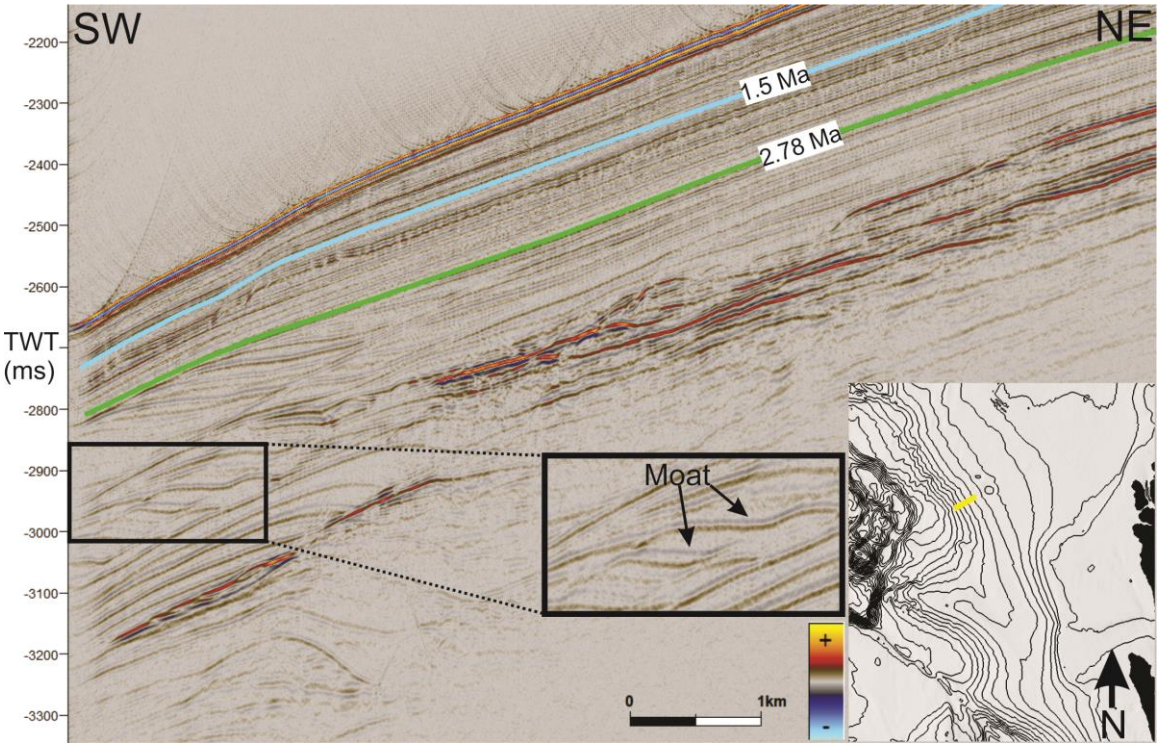

Figure 26 Seismic line 4 from CAGE 15-6

3.1.3 Seismic Stratigraphy on Vestnesa

The thickest sediment packages are found on Vestnesa where the greatest thickness between 1.5 Ma and 2.78 Ma are found. At the most it measures 650 ms which is three times the thickness of the same interval north of Vestnesa. The general thickness on Vestnesa, between 1.5 and 2.78, varies around 300-500 ms with a depocenter on the edge as seen on the thickness map (Figure 24) and the seismic (Figure 28). Along the highest point of Vestnesa Ridge several circular depressions are visible on the bathymetry (Figure 27). These are interpreted to be pockmarks and are also visible as depressions connected to other hydrocarbon indicators such as bright spots and acoustic masking (Bünz et al., 2012) (Figure 28).

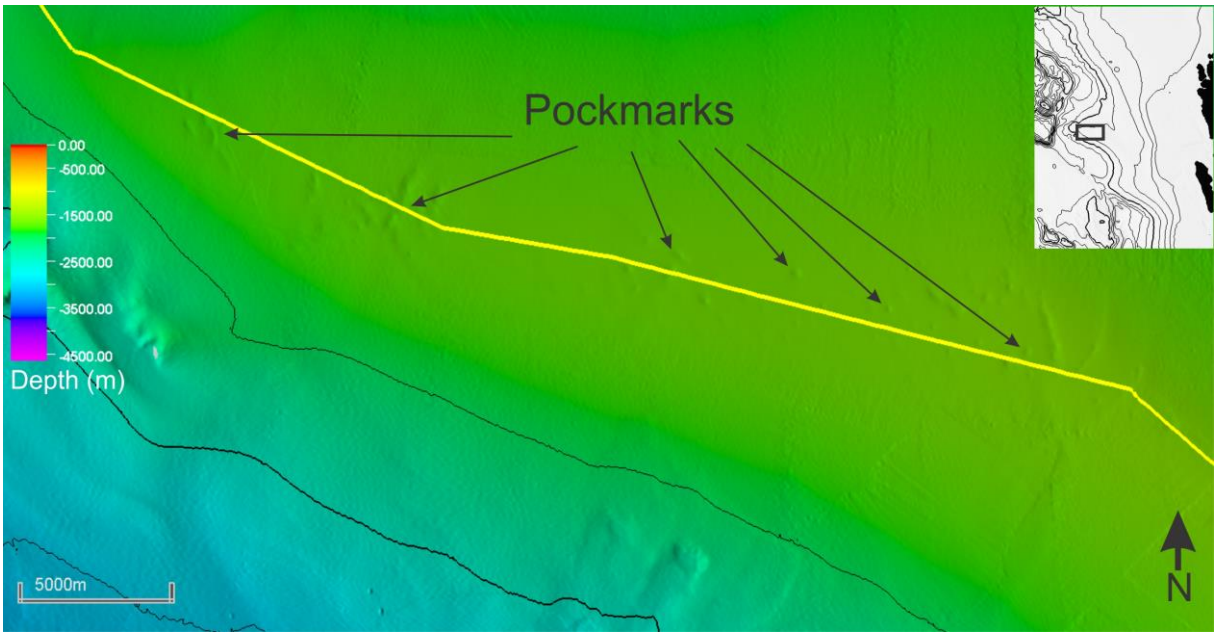

Figure 27 Bathymetry from Vestnesa displaying pockmarks on the seafloor. Yellow line is seismic line from Figure 28

The seismic stratigraphy can be characterized as parallel with a significant amount of disruptive features causing the reflections to be interrupted. These features can be seen as high amplitude reflections, or bright spots, which covers most of the profile on Vestnesa. These higher amplitude features are related to the accumulation and migration of free gas in the area. This is supported by the presence of the Bottom Simulating Reflector (BSR), pockmarks, acoustic masking and what appears to be gas chimneys (Vogt et al., 1994) (Bünz et al., 2012).

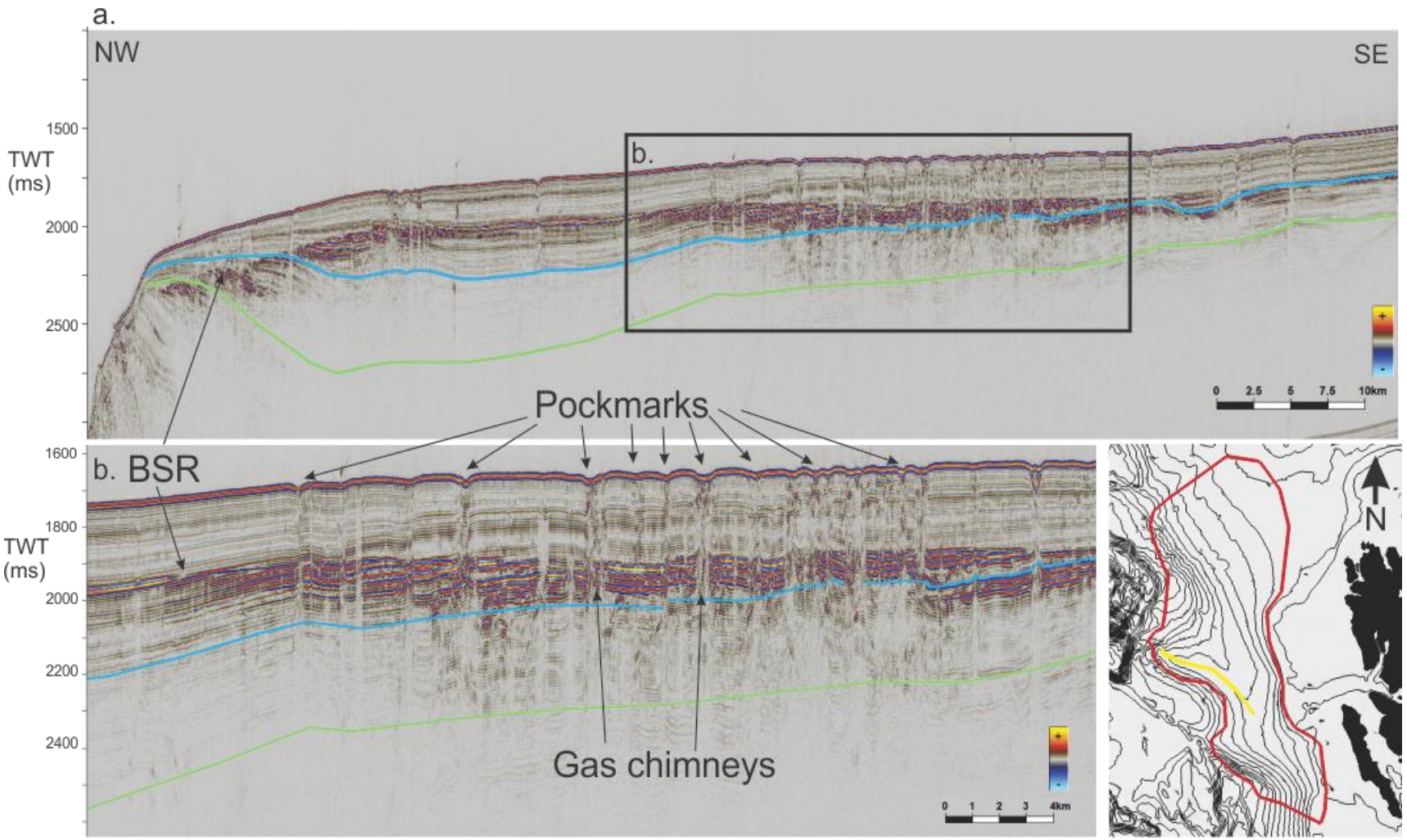

Figure 28 a) Seismic line 5 from CAGE 13-5. b) Zoomed in section of line 5.

3.1.4 Seismic stratigraphy south of Vestnesa

The sediment packaging between 1.5 Ma and 2.7 Ma are in general thicker south of Vestnesa compared to the North (Figure 24). The thickness is varying between 200 and 300 ms, but the thickness between the horizons and the seafloor have greater variance as the area is subject to the influence by the Kongsfjorden TMF and Isfjorden TMF (Figure 29). The input of sediments from the TMF's have buried parts of the YP units to the point where the YP units are not interpretable because of the depth and the consequential multiple terminating the reflections.

The seismic of the YP packages is characterised by continous parallel strata with variable reflection strength due to the changes in depth through out the profile (Figure 29). Kongsfjorden TMF has strong and partly continous reflection patterns with subparallel strata. In the northern part of the TMF there is more chaotic reflections than in the southern part. The gap between the continous reflections are much wider in the TMF and have stronger reflections than in the YP sequences.

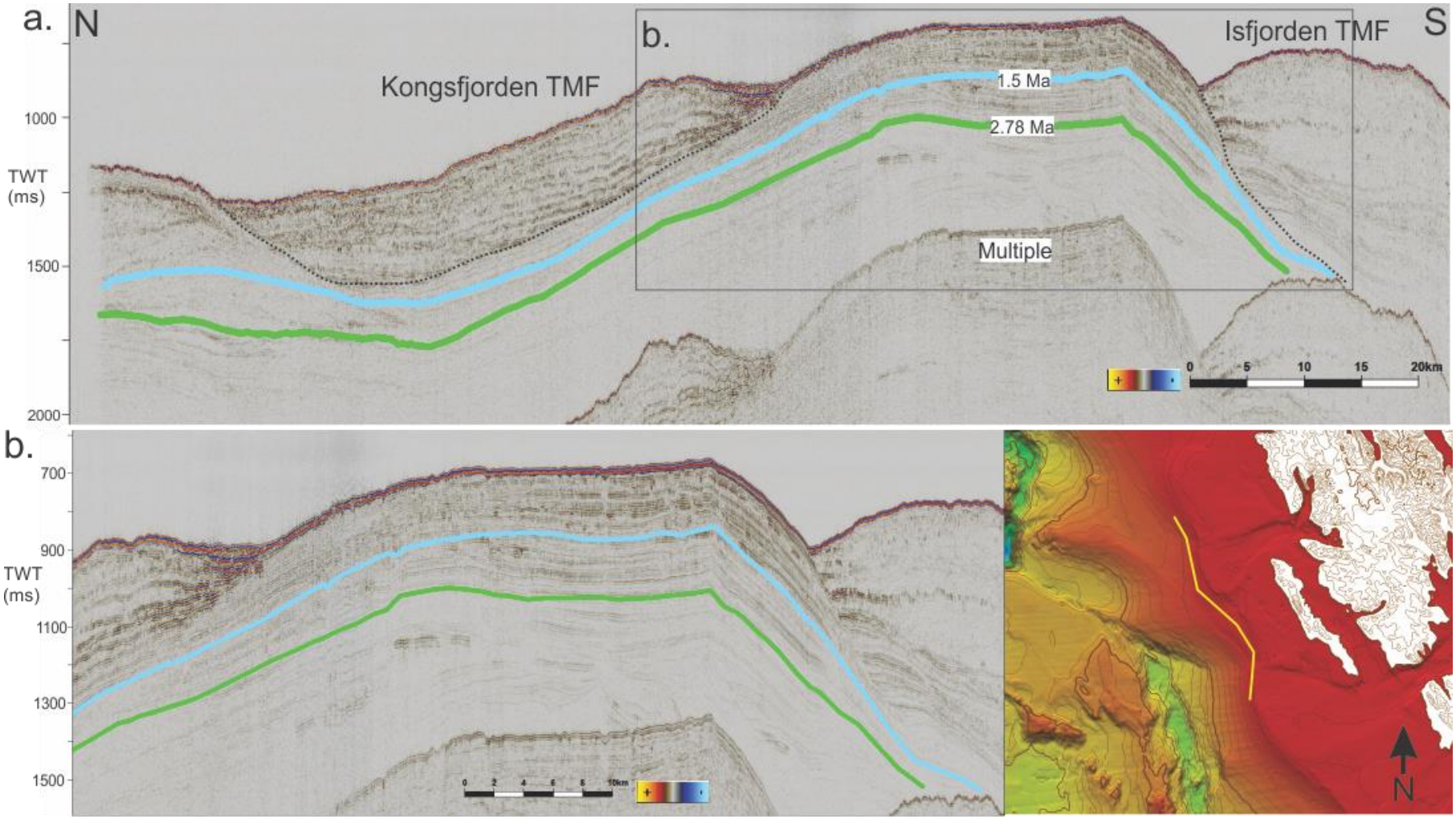

Figure 29 a) Seismic line 128 from survey 09KA-JM. b) Zoomed in section of the elevation between Kongsfjorden TMF and Isfjorden TMF

3.1.5 Drift features of unknown age

West of Vestnesa a sediment drift of unknown stratigraphic age are observed on the seismic, significantly deeper than Vestnesa (Figure 30). The drift is characterized by wavy, parallel reflection pattern and indicates a prograding drift structure as the crest has moved eastward over time. The structure is interpreted to be an elongated drift structure with the crest being the levee of the current and the bottom being the moat. It is deposited against the basement outcrop and the reflections from the drift dip upwards against the basement outcrop.

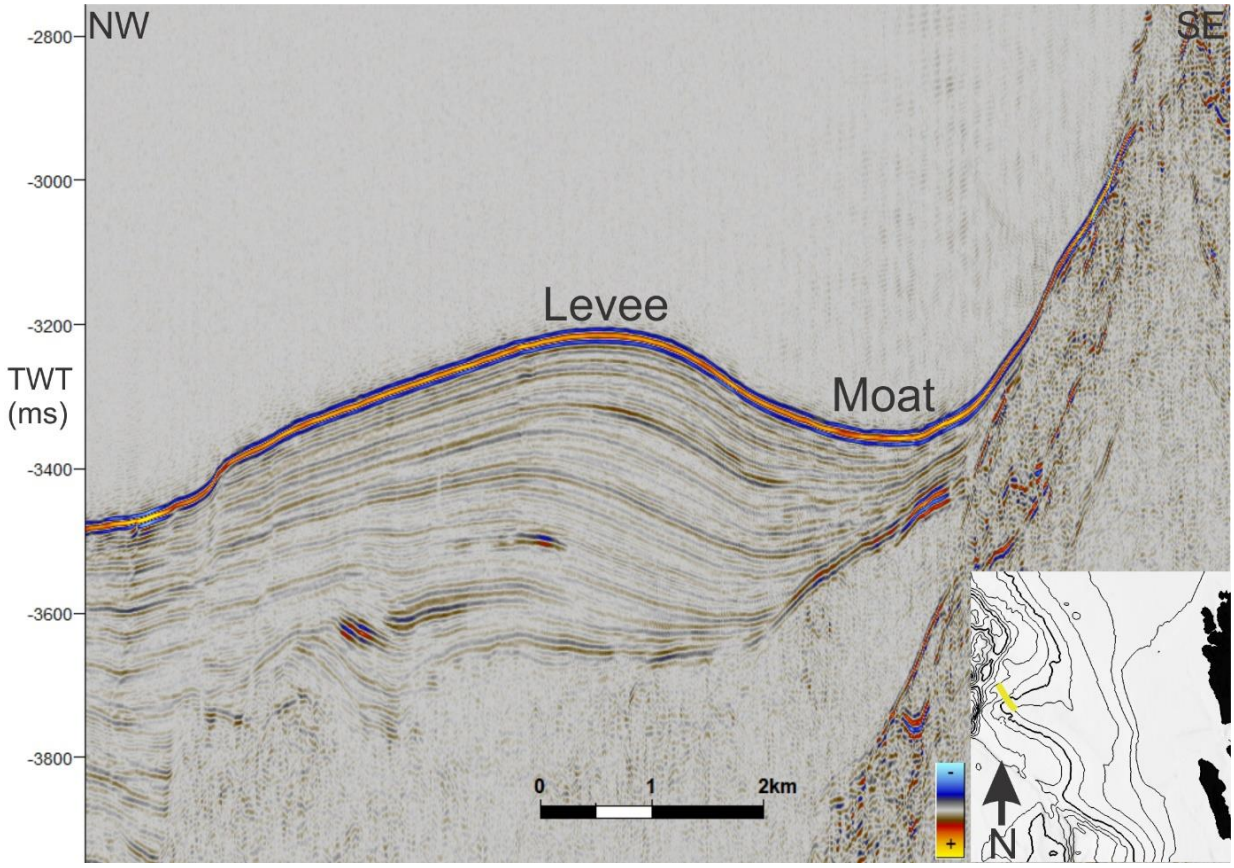

Figure 30 Drift deposit west of Vestnesa on seismic line 5 of CAGE 13-5

North of Vestnesa in the western slope of the study area similar features are found in the deeper areas east of the Molloy Deep. Figure 31a show drift features along the bottom of the slope with crest development towards the slope in eastern direction. Sediment packages are 150 ms thick and are characterized by subparallel and wavy strong reflection patterns. The drift feature on Figure 32b show same features with levee and moat and same type of crest

development. The drift is located on the slope and is a single drift feature compared to the first, which has at least two crests that are somewhat connected.

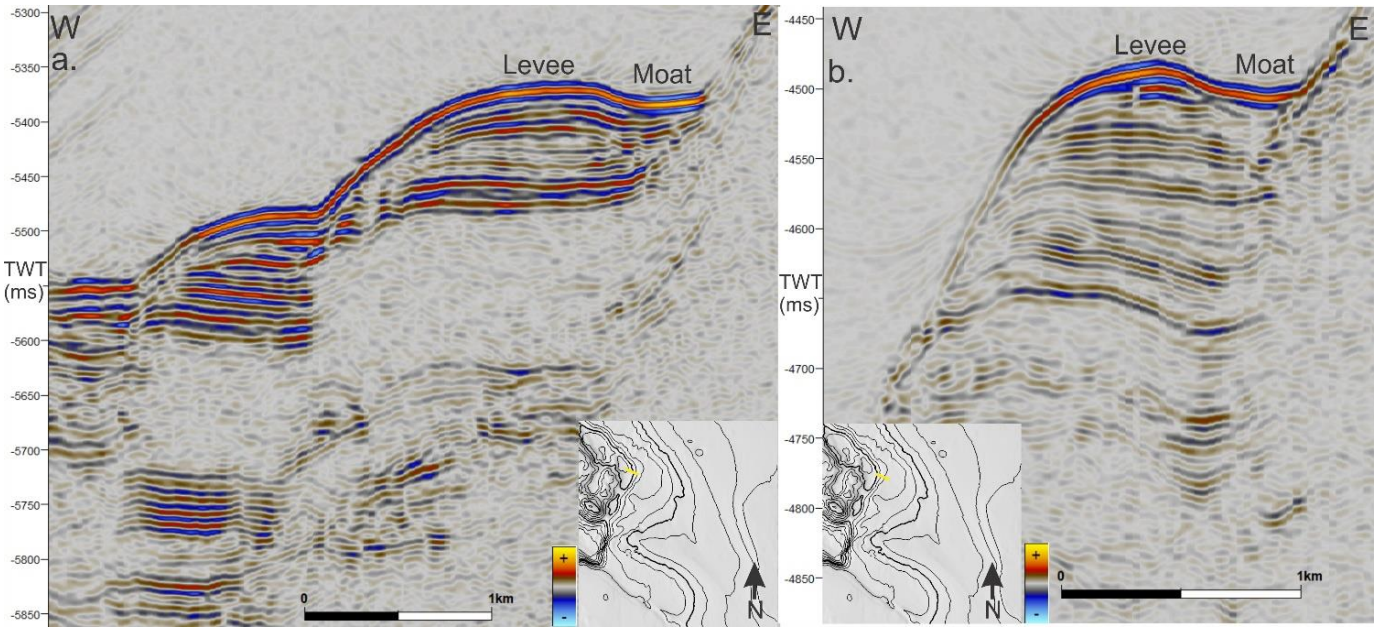

Figure 31 a) Drift structures at the base of the slope north of Vestnesa. Seismic line 7 from CAGE 13-5. b) Drift structure 2 km upslope from a).

3.2 Tectonic

To get a better understanding of the neotectonics in the study area, mapping tectonic features in the seismic and bathymetry is important. The study area is in close proximity to a spreading ridge with complex structure and tectonic setting with oceanic crust and fault development. In this subchapter there will be a focus on relating the tectonic features observed on bathymetry with seismic profiles to achieve a better understanding of the tectonic processes and its effects on the depositional environments in the study area.

3.2.1 Faults north of Vestnesa

At the slope north of Vestnesa Ridge several faults has been observed on the bathymetry (Figure 32) and seismic (Figure 33). The seismic line strikes perpendicular to the slope and Molloy Transform fault and parallel to the continued north western spreading ridge. Several faults are observed on the profile with significant displacement.

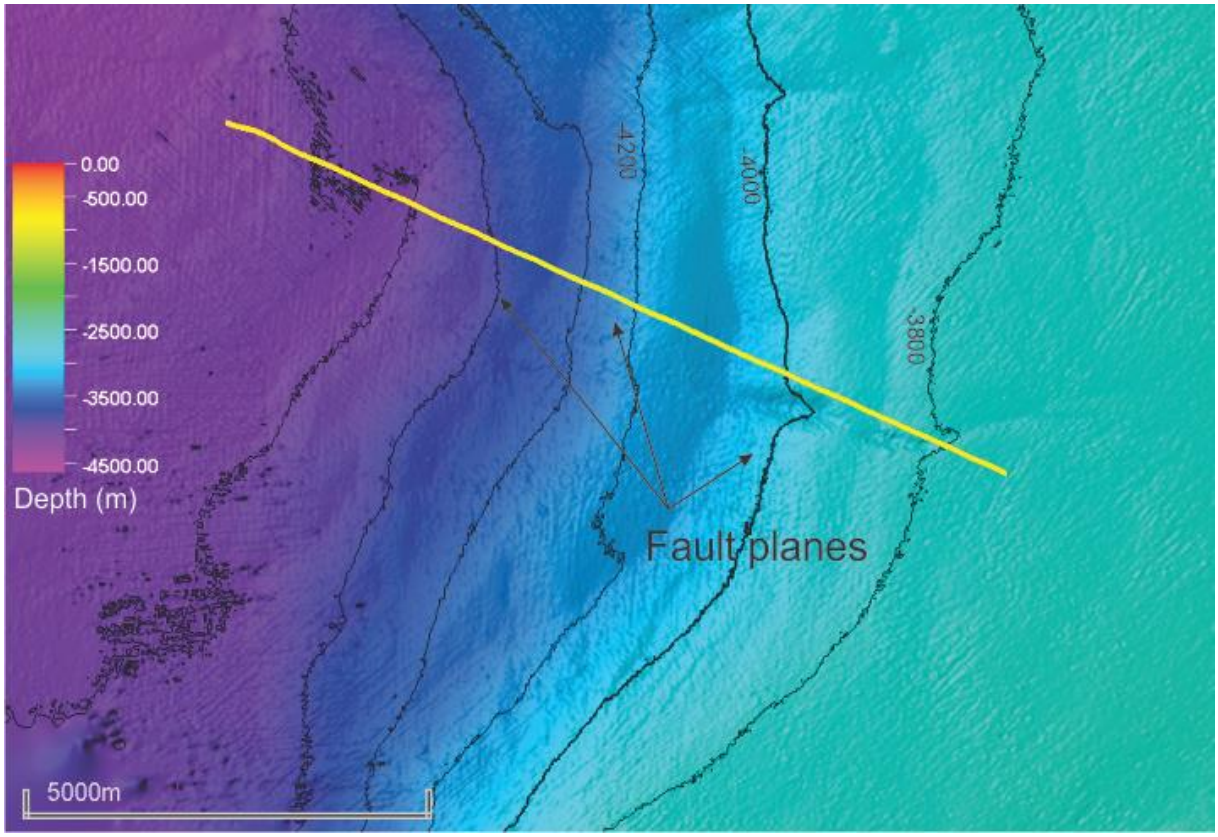

Figure 32 Bathymetry displaying the area surrounding line 7 from CAGE 13-5. Fault planes are visible and marked with arrows.

The faults have been interpreted to be normal faults and the downthrown fault blocks are facing westwards. However, the displacement of the faults vary considerably from the uppermost faults to the lower faults. The two downthrown blocks on the slope have a vertical displacement of up to 500 ms and the displacement on the bottom is approximately 100 ms. Observed in the figure there is a sediment package that has been recorded in the seismic data that is characterized by wavy parallel reflection patterns with strong amplitudes (Chapter 3.1.5). They are discontinuous by termination against the faults, but the seismic pattern is similar throughout the profile for the top 200 ms of the subsurface.

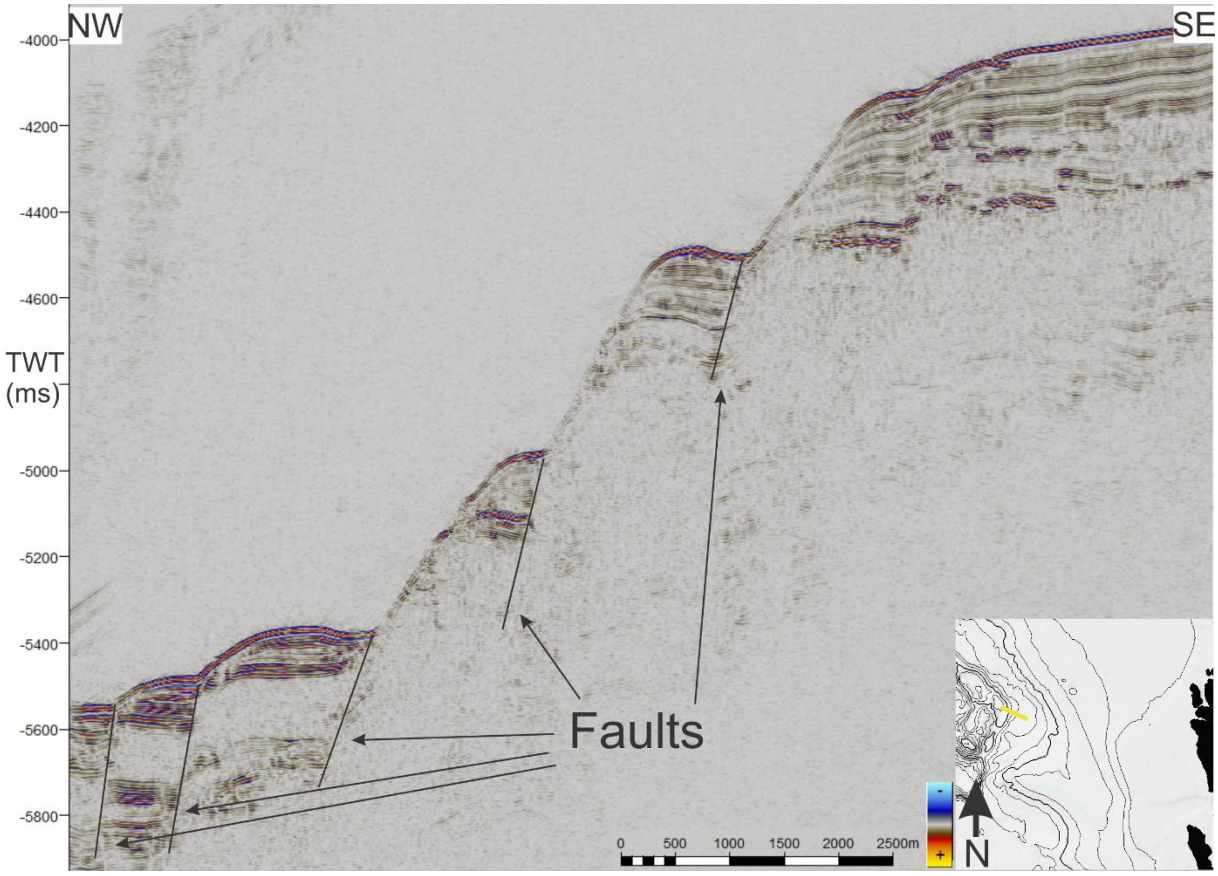

Figure 33 Seismic line 7 from CAGE 13-5 displaying the fault planes observed in Figure 32. The sedimentary features located on the fault blocks are presented in chapter 3.1.5

The bottom faults have a lower displacement than the faults at the slope indicating that they have formed more recently, which is also consistent with their proximity to the mid-ocean ridge axis. As the sediment thickness does not vary greatly on the visible seismic reflections, the sedimentation rate have not been significantly different in the different parts of the area.

3.2.2 Faults south of Vestnesa

South of Vestnesa a series of line features with North-South direction is observed on the seafloor and seismic (Figure 34). The seismic profile confirms that these are normal faults with lower displacements. The bathymetry show the faults in a wavy pattern instead of more linear as was observed north of Vestnesa. Below the seafloor a section can be divided for 300 ms which is characterized by parallel and continuous reflection patterns with lower reflection strength. Under this section the reflection strength increases and the reflection pattern is

characterized as wavy and subparallel. The sudden increase in reflection have been interpreted as a BSR in the area (Dumke et al., 2016).

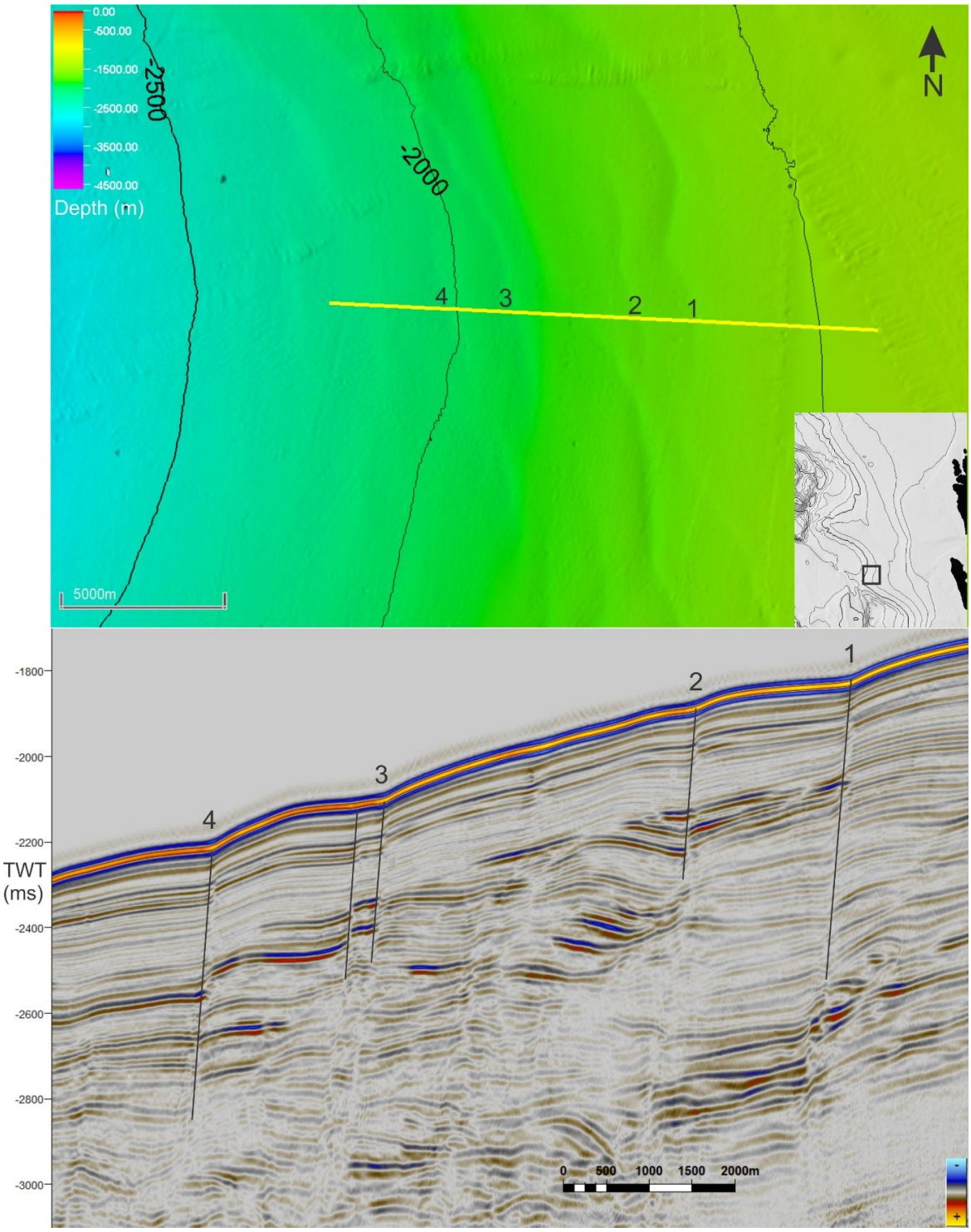

Figure 34 Bathymetry and seismic line Svalex 12 displaying observed faults south of Vestnesa.

The faults observed on Figure 34 can be traced as they propagate north and shift direction from north-south to northwest-southeast as they follow the slope along Vestnesa. The same seismic characteristic is observed; wavy and subparallel reflection patterns indicating moat-levee structure with vertical displacement of the seismic (Figure 35).

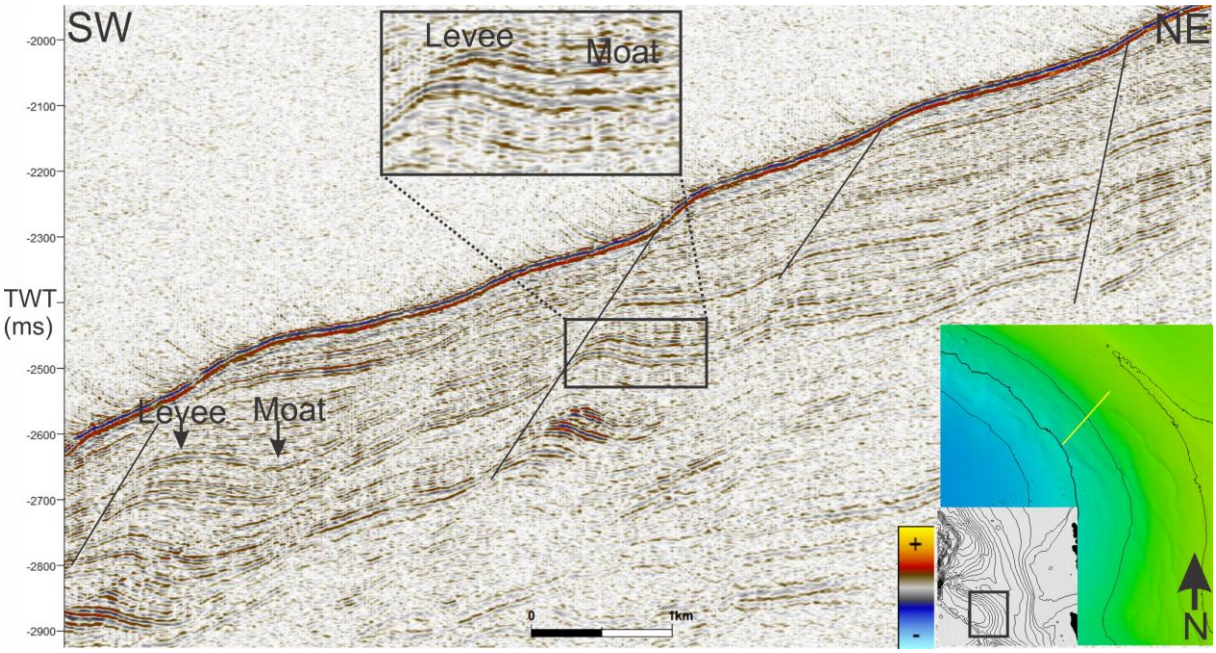

Figure 35 Seismic line 60 from JM07VSTNSA.

3.2.3 Basement Outcrop on Vestnesa

Features terminating all reflections including the seafloor were observed on the seismic (Figure 36). They are characterized as steep dipping and have a chaotic reflection pattern and are interpreted as basement outcrops of oceanic crust. These outcrops are found around the edge of Vestnesa and marks the edge of the seismic stratigraphy correlated in the study area. The outcrop is visible on several areas on the bathymetric data and have previously been mapped and interpreted as basement outcrops (Hustoft et al., 2009). As seen on Figure 36 the correlation of reflections have terminated here and is not taken further as no link between the sediments adjacent to the outcrop has been sustained that is observed on the seismic.

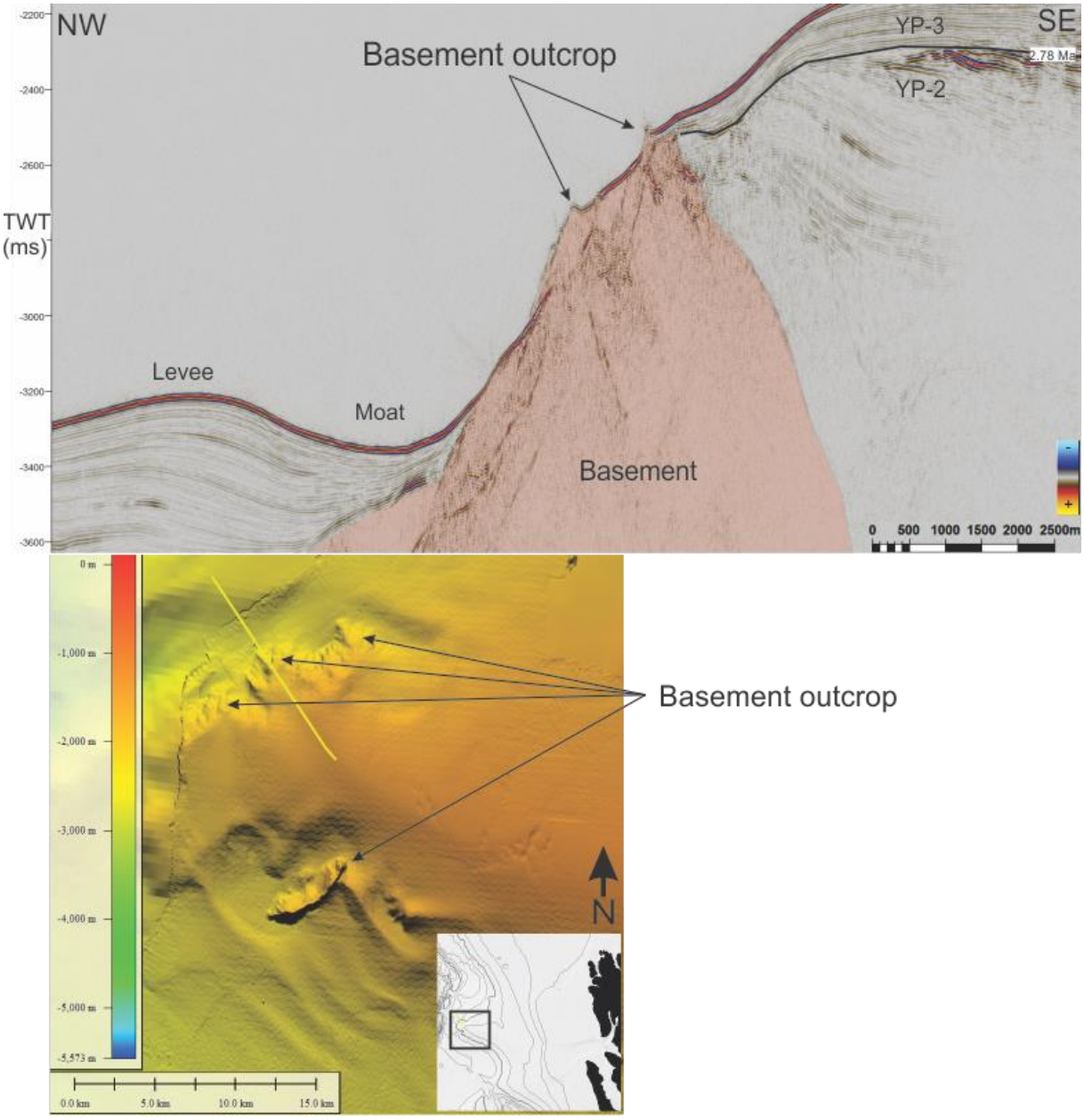

Figure 36 Seismic line 5 from CAGE 13-5 and bathymetry showing the basement outcrop observed on the edge of Vestnesa.

3.3 Submarine landslides

North of Vestnesa several landslides are observed on both bathymetric data and seismic data (Figure 37). Several slidescars are visible on the bathymetric data, which is identified on the seismic. Slide scar 1 and 2 are assumed to be different events and is referred to as slide 1 and 2. Slidescar 3 and 4 are from the same event and will be referred to as slide 3. Northwest of slide 3 a strong reflection is observed ca. 200-260 ms below the seafloor which seems to cut

across weaker reflections and is interpreted as a BSR which is product of gas hydrates formed in the area (Elger et al., 2017). The seismic under the seafloor where the landslides have gone can be characterized by parallel and continuous reflection patterns with varying reflection strength. Under the BSR there is acoustic masking causing low reflection amplitudes. Below slide 3 the BSR is less obvious and seems to be shallower than the adjacent observations of the BSR, here the amplitude strength of reflections below the BSR is higher. South East of slide 3 the BSR is somewhat deeper at 300-330 ms below the seabed.

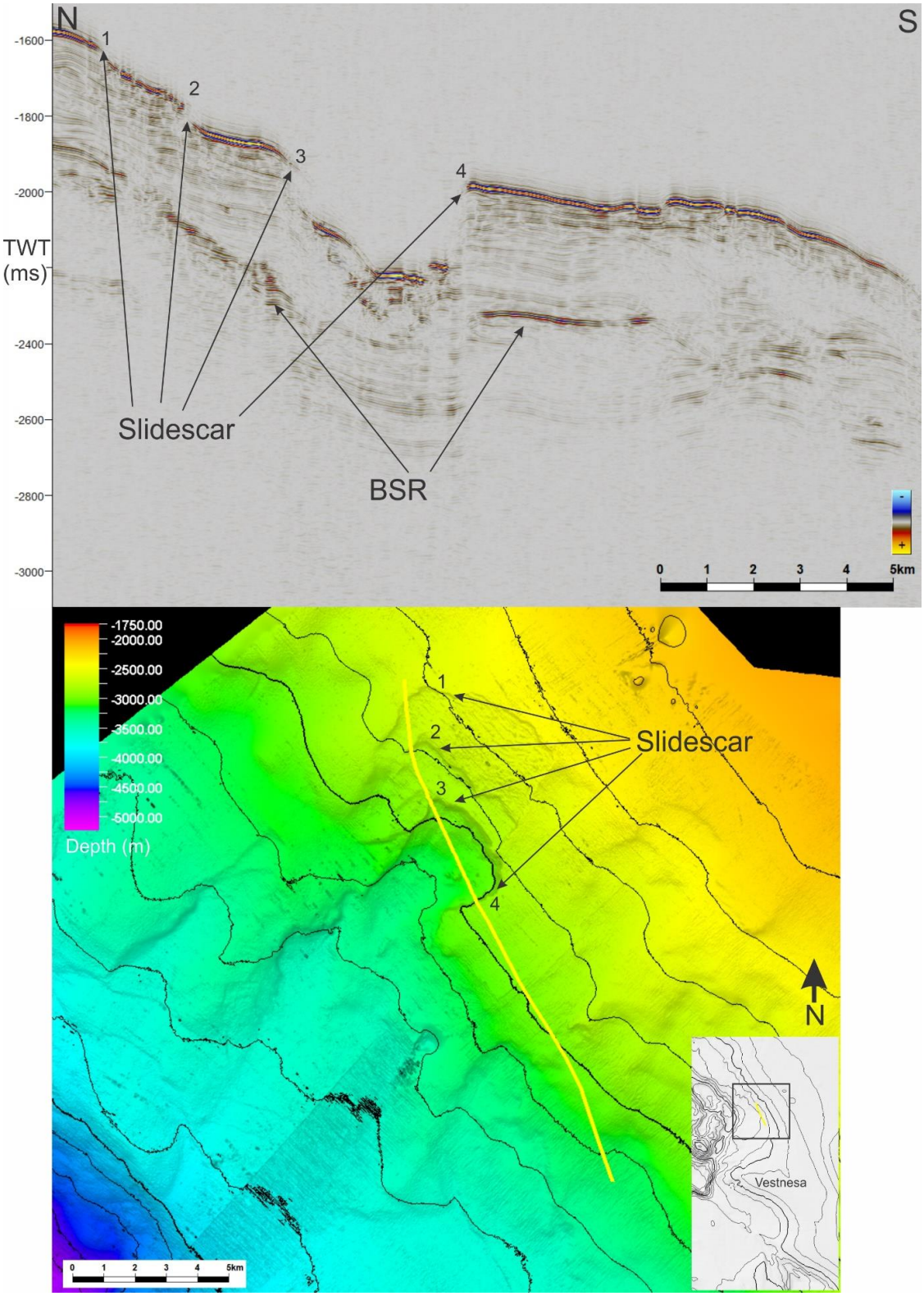

Figure 37 Seismic line 7 from CAGE 14-5 and bathymetry displaying slidescars observed north of Vestnesa at the western slope.

Approximately 20m km south south-east of the three slidescars another is observed stretching from south-west to north-east (Figure 38). This slidescar covers a greater area than the previous and is a part of larger slide complex which encompasses the previously observed slide scars. This complex is known as the Fram Strait Slide Complex (FSSC) and covers the entire area seen on the bathymetry (Elger et al., 2017). There is no observed BSR or other indications of gas hydrates or free gas in this area. However, this is far down the slope and it is unlikely that the slides were triggered in this area, which is most likely around the highest point of the slide scar.

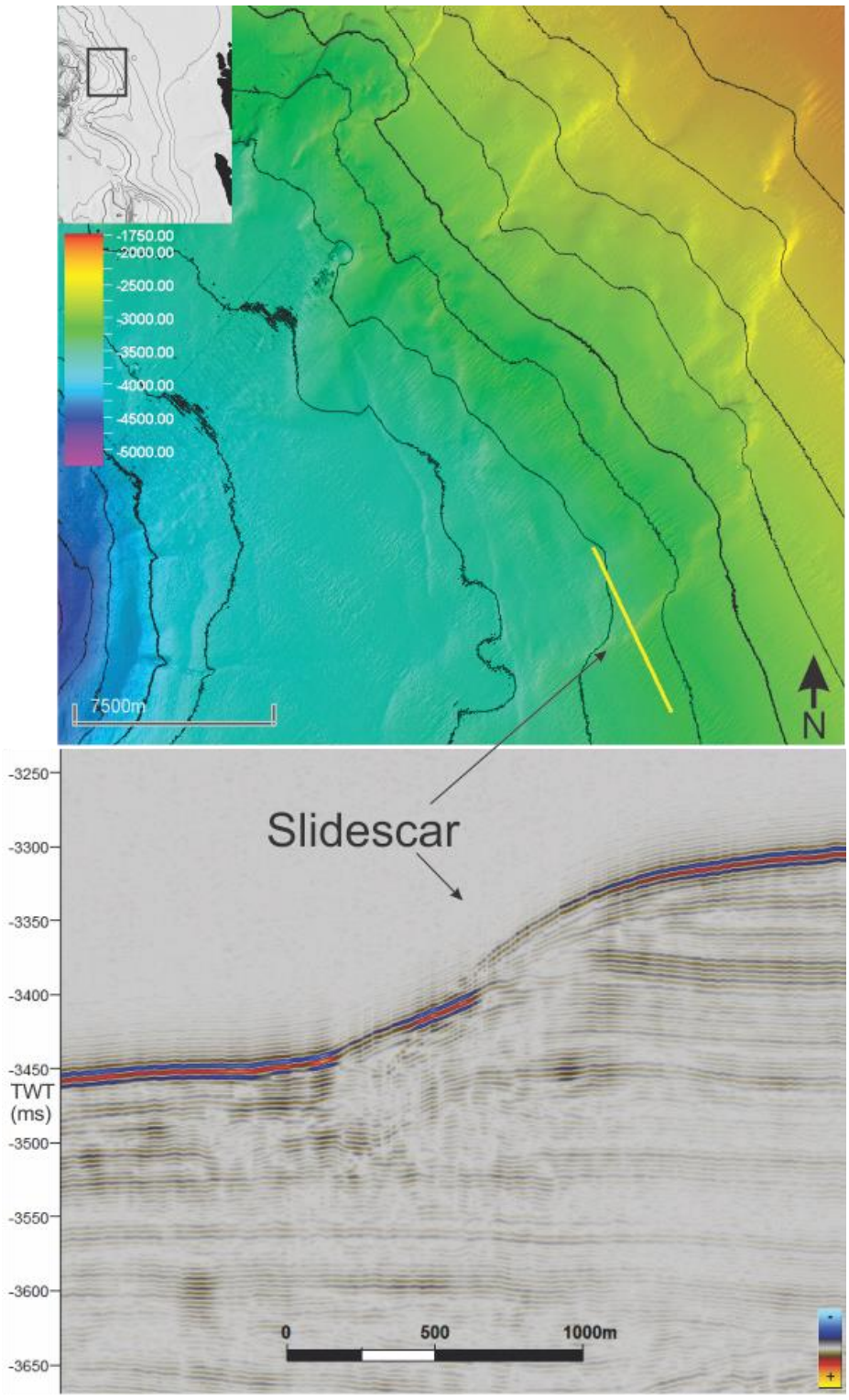

Figure 38 Seismic line 7 CAGE 14-5 and bathymetry displaying sidewalls

At the southern slope of Vestnesa smaller slide scars were observed on the bathymetry and seismic (Figure 39). They are smaller in extent but are in similarity to the northern FSSC observed as several events and the upper one is quite small in vertical extent and is consequentially harder to observe on the bathymetry. The two other slide scars are further down the slope and have a larger vertical extent but does not extend as far laterally on the bathymetry as the upper one. The BSR is, as it was in the FSSC, present under slidescar 2 and 3 cutting through the seismic reflection pattern, which is characterized by subparallel and wavy reflection patterns.

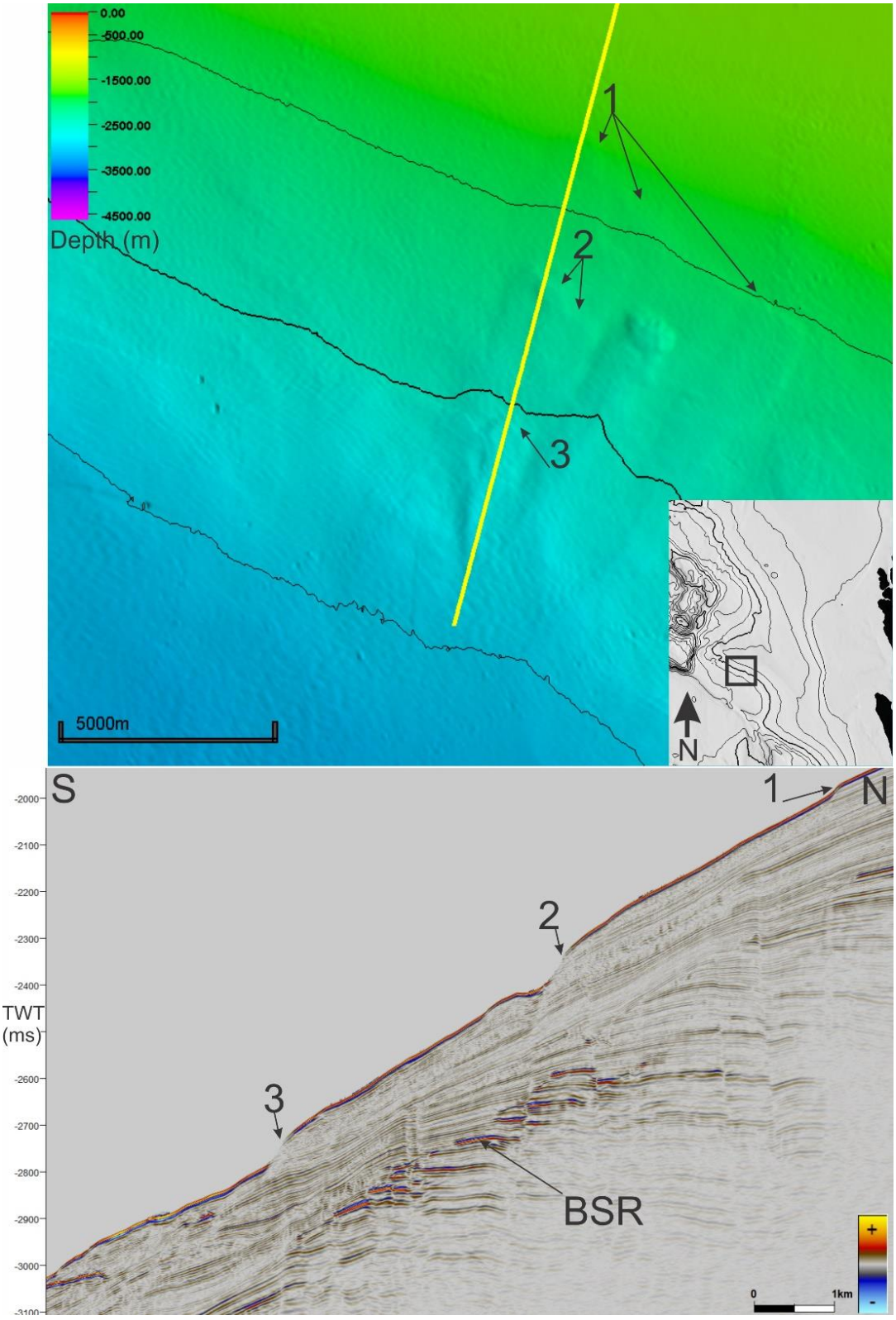

Figure 39 Seismic line 54 of CAGE 19-1 and bathymetry displaying three separate headwalls on the southern slope of Vestnesa.

4 Discussion

The primary goals for this thesis was the reprocessing and interpretation of 2D seismic lines in the Fram Strait and West Svalbard Margin. The reprocessed lines were acquired by CAGE over multiple years prior to 2016 and were integrated in a seismic database with a number of newer seismic surveys (Figure 17) in the study area to make up a regional database. This database together with bathymetry collected in the area made up the basis of interpretations, which focused on stratigraphic development of the WSM and Fram Strait in relation to contourite drift development, glacial sediments, neotectonic setting and processes of submarine landslides in the area. This chapter will discuss the progress made with the reprocessing, as well as the relation between sedimentary and tectonic processes and how they affect the depositional environment in the study area.

4.1 Reprocessing Results

A significant improvement has been achieved to the seismic profiles of the 14-5 CAGE survey through the reprocessing flow presented in chapter 2 (Figure 9). The signal to noise ratio has increased by executing processing steps that had not previously been done and a different type of migration.

One of the major differences in the processing was the migration. In this thesis I used Kirchoff migration as opposed to previous processing sequences that used Stolt Migration, which uses simpler methods to migrate the seismic profile (Chapter 2.3.7). The difference in the two methods is that for Stolt migration it is not possible to use a velocity model in intervals or manually change the aperture width (DECO, 2019). This means only one velocity is used to migrate the whole profile, which could cause the migration to be insufficient for certain seismic profiles with more complex geology. This is especially the case for profiles with great depth variations.

Figure 40a show several bursts that have not been removed by past processing. By using an aggressive BNR filter for this seismic line, the bursts were successfully removed and the main signal was preserved consequently increasing the S/R ratio (Figure 40b). The other significant

difference here is the migration, which can be observed to have not been successful in collapsing the diffraction hyperbolas in this setting. By migrating this profile with high aperture, the hyperbolas have collapsed into their original point of origin. Figure 40b show the migration with low aperture, which in this case was not satisfactory. On Figure 40c the seafloor reflection which was displayed as a reflection dipping downwards to the depression is now displayed as a reflection terminated by a slidescar (Chapter 3.3).

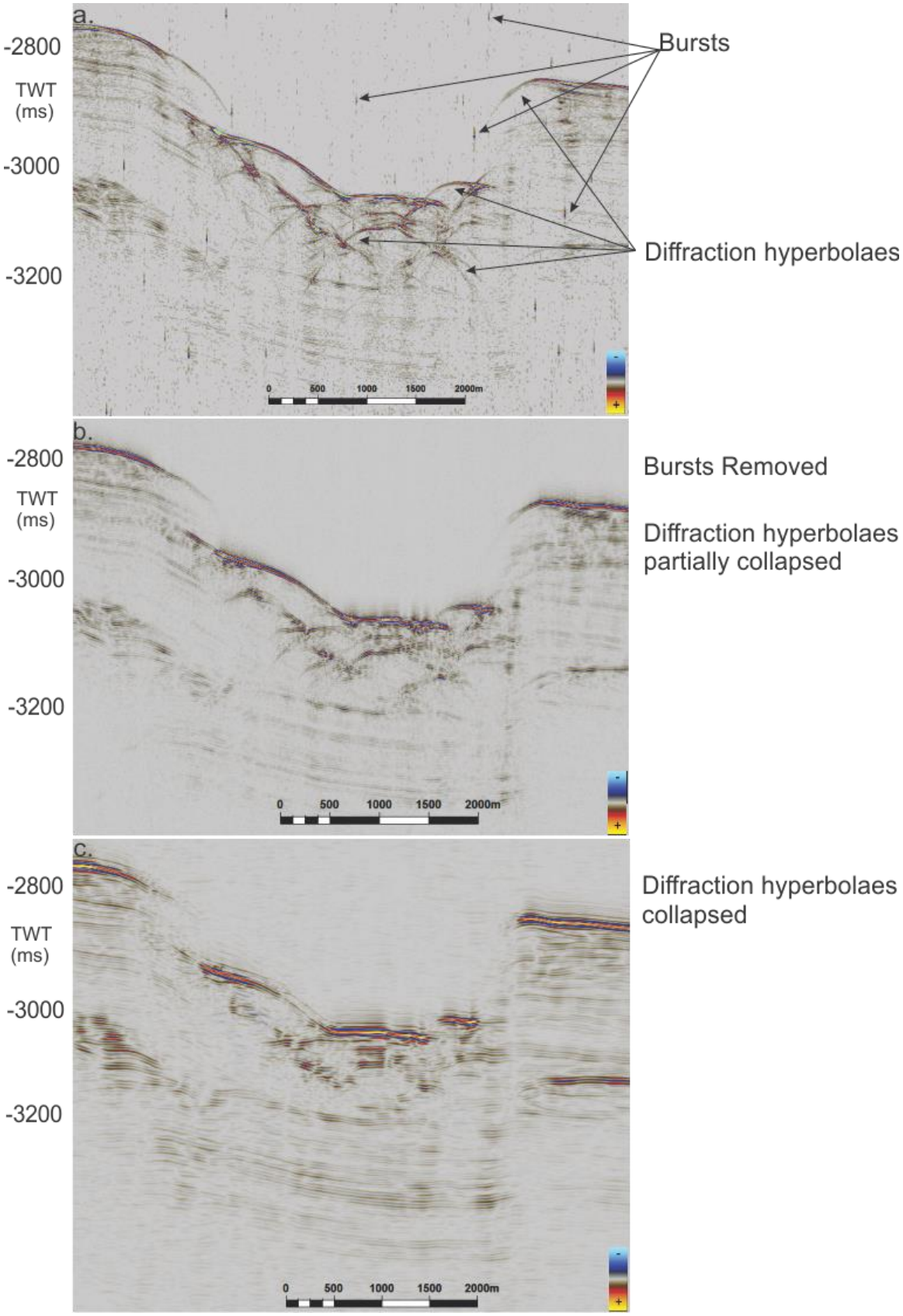
a.
-2800
TWT
(ms)
-3000
-3200
Bursts
Diffraction hyperbolaes
0
500
1000
1500
2000m
b.
-2800
TWT
(ms)
-3000
-3200
Bursts Removed
Diffraction hyperbolaes
partially collapsed
0
500
1000
1500
2000m
c.
-2800
TWT
(ms)
-3000
-3200
Diffraction hyperbolaes
collapsed
0
500
1000
1500
2000m

Figure 40 a) Old processed line 7 of CAGE 14-5 with significant amount of bursts and hyperbolas. b) Conservative aperture Kirchoff migration displaying the partially collapsed hyperbolas and successfully removed bursts. c) High aperture Kirchoff migration displaying successfully removed hyperbolas.

A frequent consequence of the Stolt migration was reversed hyperbolas at the seafloor and some reflections near the seafloor. Hyperbolas as a consequence of using a higher velocity model for the entire profile resulting in distortions of the main signal appear in most of the old processed lines (Figure 41a). By implementing an accurate velocity model for the different depth intervals in the seismic profile, hyperbolas were successfully collapsed (Figure 41b).

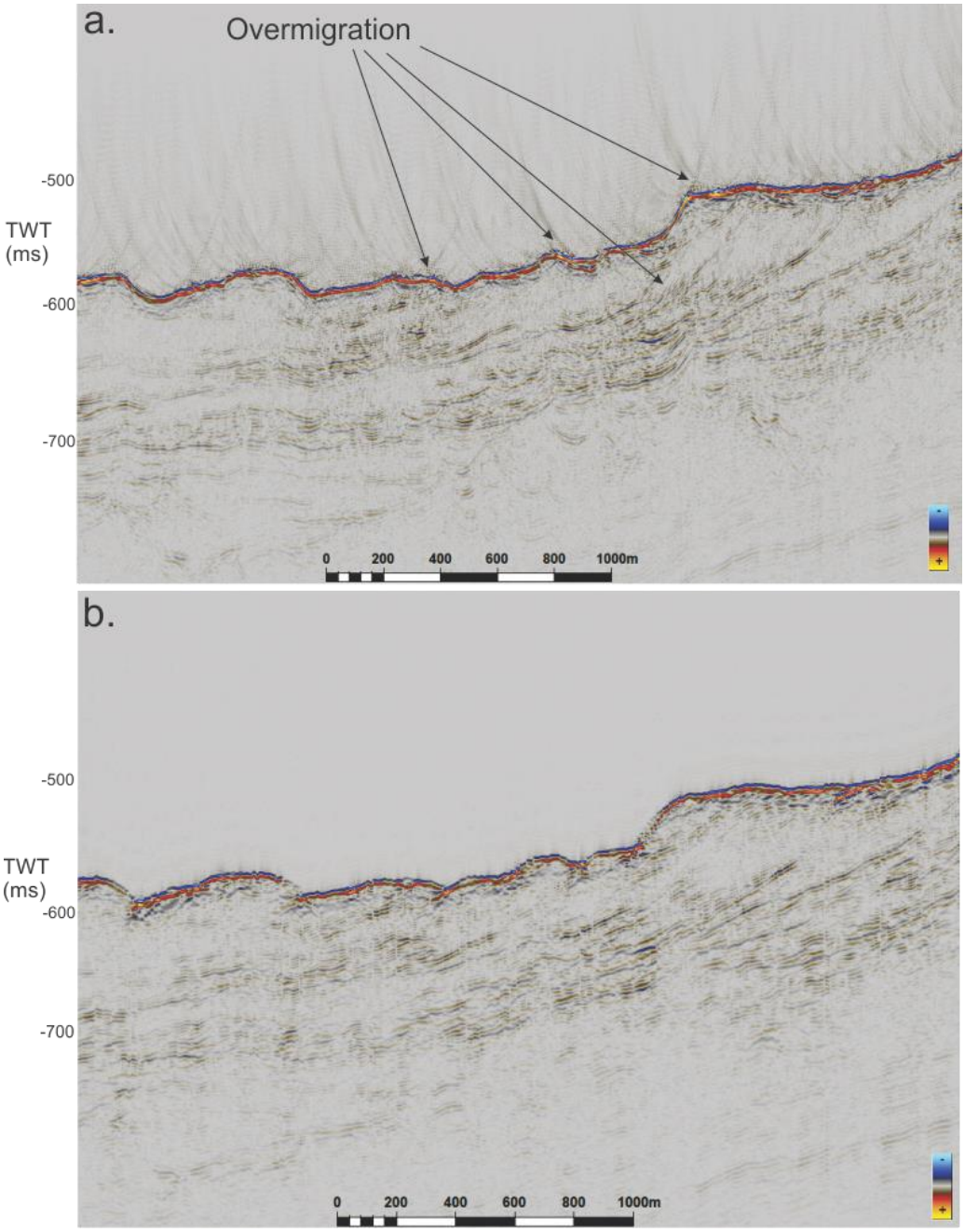

Figure 41 a) Old processed line 2 from CAGE 14-5 displaying reversed hyperbolas as a result of overmigration. b) Seismic line 2 reprocessed in this thesis.

Figure 42a show the same type of "overmigration" as figure 41a. Here, the data has become grainy under the seafloor and proper coherent reflections can hardly be recognized. In Figure 42b hyperbolas have collapsed and beneath the seafloor several individual reflections can be observed; although they are highly discontinuous and chaotic, they are less so than the original processed line.

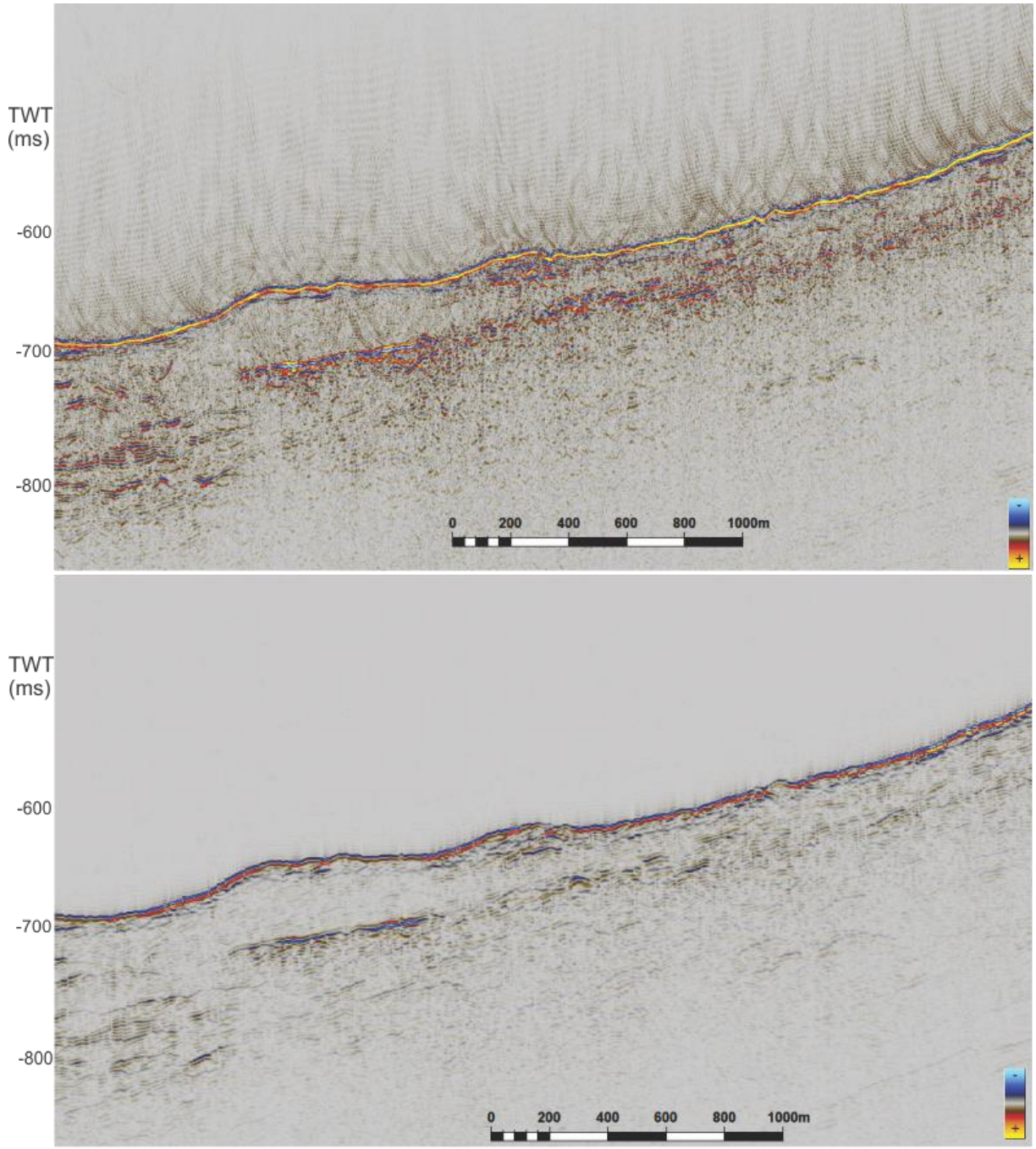

Figure 42 a) Old processed seismic line 4 from CAGE 14-5. b) Seismic line 2 reprocessed in this thesis.

There were several other examples of grainy, noisy seismic data. In figure 43a noise in the presence of acoustic masking were present and was fixed in the reprocessing steps. The top left square highlights an area of chaotic signals in Figure 43a, after the reprocessing this noise was filtered out and there is in its place now indications of the continuation of the reflection

that was truncated by the noise and acoustic masking (Figure 43b). This seismic profile was one of the FK-Filtered profiles. It may have helped the noise reduction in this example.

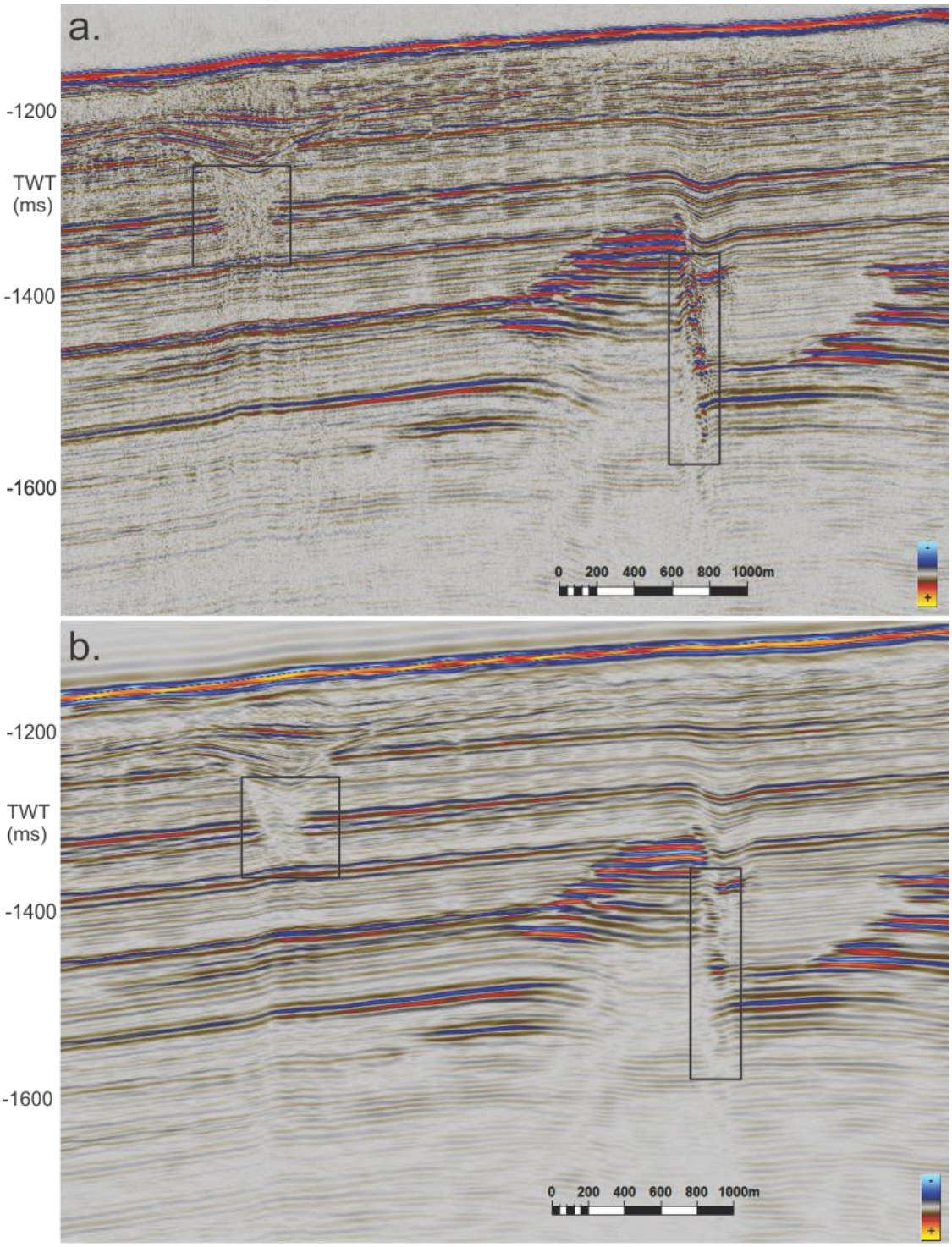

Figure 43 a) Old seismic line 10 from CAGE 14-5. b) Reprocessed seismic line 10.

In seismic sections where seafloor topography have steep dips in relation to a shelf break, basement outcrop or other geological features reflection were often obscured or not visible at all. This problem is also a case of migration that is not satisfactory, and it is observed on Figure 44a that the seafloor reflection is not visible and its energy is scattered into hyperbolas. Figure 44b displays the same seismic section only with Kirchoff migration and the steep dipping seafloor is now visible and without any distortions from diffraction hyperbolas.

.

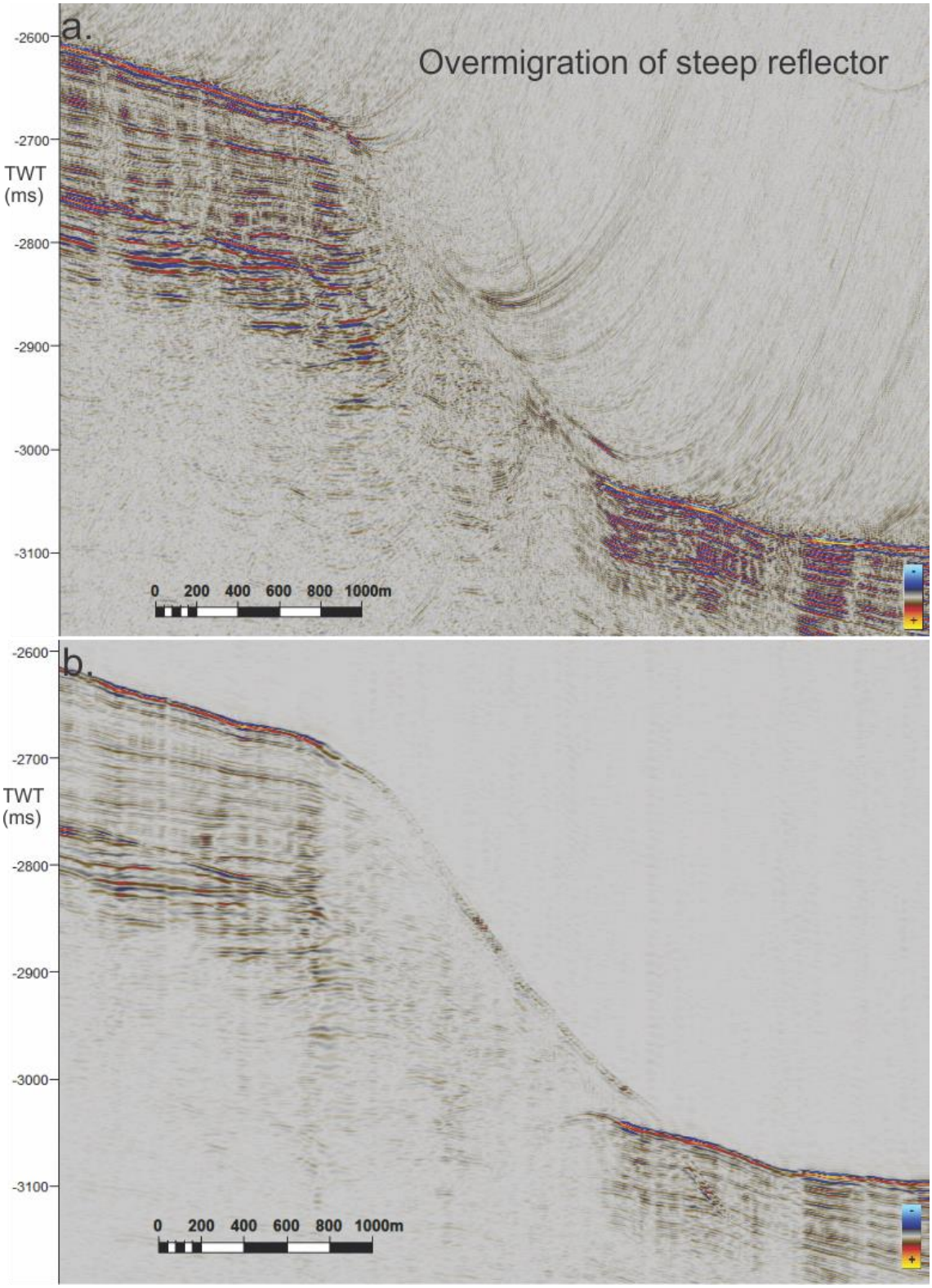

Figure 44 a) Old processed seismic line 17 from CAGE 14-5. Steep dipping reflection is not visible in the seismic. b) Seismic line 17 reprocessed in this thesis. Seafloor is now visible.

4.2 Improvement of the seismic data

The reprocessed 2D seismic data proved successful and had several examples of improved data quality compared to the originally processed data. Burst noise removal was in particular useful to reduce noise while preserving the data and was used on multiple lines where certain channels spawned sporadic bursts on the profile. It was often the case that only the last two streamers had channels with bursts. The BNR filter was then implemented to only target the specified channels to avoid potential signal loss in channels without bursts. The Kirchoff migration improved the data by collapsing hyperbolas in areas heavily affected by diffractions. This was especially the case in the northern part of the study area where slide scars had terminated the reflections. The Kirchhoff migration was able to transform the diffracted signal back to its true shape and the slide scars were visualized as sediments cut off by a sliding event (Figure 40).

The main difference in processing when comparing is the two migration methods that were used. Kirchoff migration proved to have more room for implementing more parameters such as aperture and an interval based velocity model. This proved helpful within a study of varying depth and steeply dipping reflections.

4.3 Stratigraphy on the WSM

The stratigraphic correlation in the study area was based on the stratigraphic framework made from ODP sites 911A, 910C and 912A (Mattingsdal et al., 2014). The correlation is limited in the south at the Isfjorden TMF (Figure 29) and to the west at the edge of Vestnesa (Figure 28). The seismic in the study area is predominantly characterized by parallel and continuous reflection patterns in the eastern gentler sloped areas near the coast of Svalbard (Figure 20 and 21) and wavy subparallel reflection patterns in the western parts where the slopes are steeper and at greater depths (Figure 26). Near the coast of Svalbard glacial through mouth fans are present that have influenced the nearby stratigraphy (Figure 29). The eastern part of the Fram Strait and the slope of West Svalbard Margin is heavily influenced by contourite development which is supported by the seismic data and ODP sites (Eiken & Hinz, 1993; Mattingsdal et al., 2014). The subparallel wavy reflection pattern found in the deeper parts are

related to elongated drift developments formed parallel to the bottom currents flowing through the study area.

The change in thickness of the sediment drifts between 2.78 Ma, 1.5 Ma and the seafloor (Figure 24) is observed to be relatively similar in the study area in spite of shifts in sedimentary setting at 1.5 Ma. However, the thickness varies in the study area from slightly thicker sediment drifts south along the WSM than north, indicating a higher sedimentation rate along the southern part of the study area.

The thickest sediment packages were observed on Vestnesa Ridge where a depocenter of sediment drifts were observed (Figure 28). A significantly higher sedimentation rate in this area may indicate conditions favoring sediment deposition more than erosion and reworking of the sediments.

4.4 Contourite drifts

Several contourite features have been mapped in the study area and different features are located at different areas (Chapter 3.1.5, 3.1.2 and 3.2.2). Moats and levee features are mostly present at the slopes and the western parts of the study area while at gentler sloped areas at the middle and eastern part of the WSM the seismic show more parallel and continuous deposition indicating sheeted drifts in non-confined environments and/or hemipelagic settling. The whole sediment deposition of Vestnesa is considered to be deposited by the WCS and is considered a major drift deposition.

4.4.1 Effect of faults on contourite drift deposition

Faults were observed at the bottom of the slope below the FSC, North of Vestnesa (Figure 33). Moat-levee structures were observed in between the fault planes stacked on top of each other with crest development upslope (Chapter 3.1.5). As the sediment thickness does not vary greatly on the visible seismic reflections, the sedimentation rate may not have been significantly different in the different parts of this area. Because the displacement is different, it results in two different sedimentary processes related to faults forming two different drift features. Where sedimentation rate is higher than the displacement, the fault are affecting the sedimentation resulting in a fault controlled drift. Where the displacement is larger than the

sedimentation rate, it terminates the sedimentary layers against the fault plane and confining the current that deposits the drift. This results in a type of confined contourite drift formation or a drift formation against faults (Figure 45).

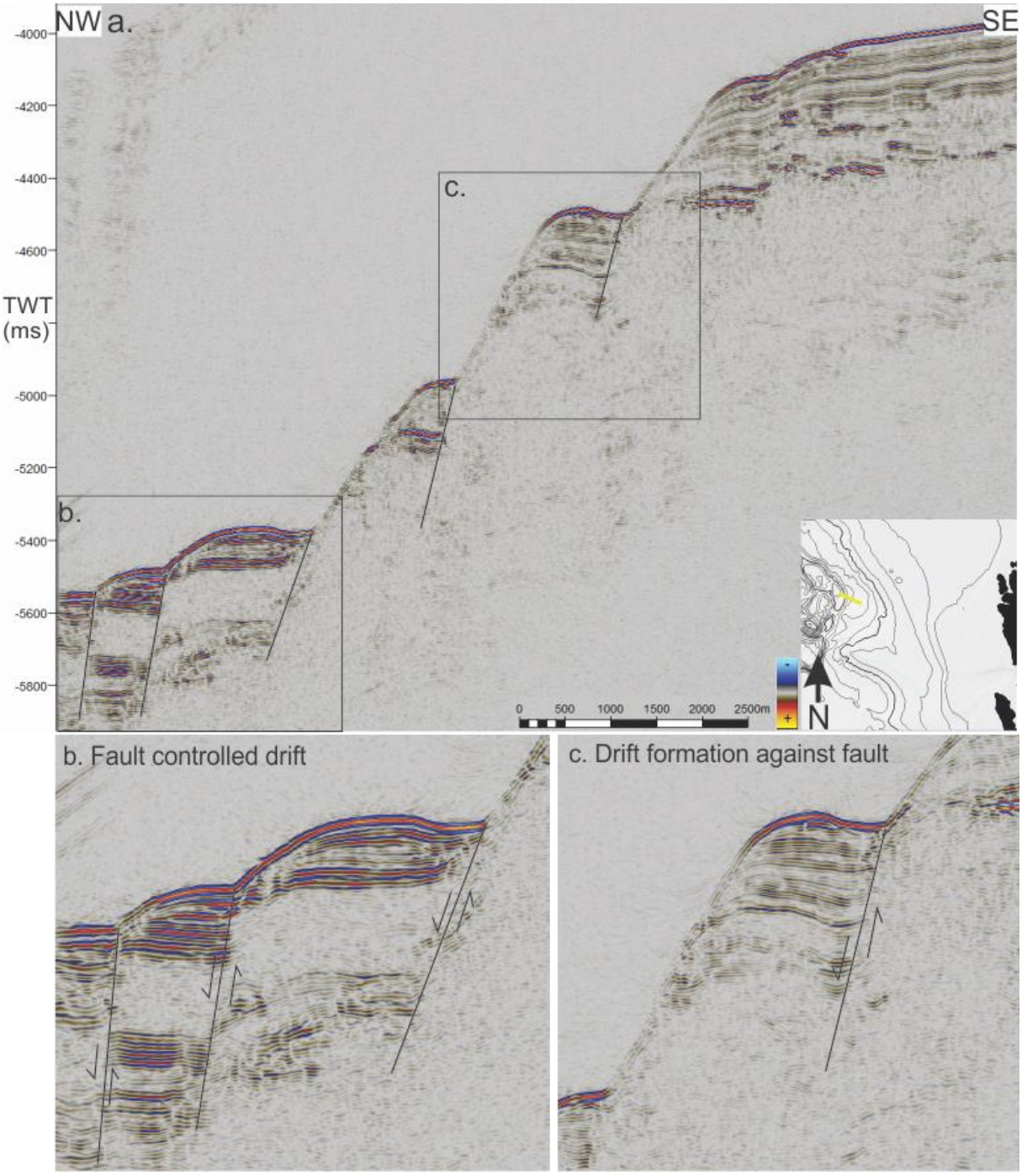

Figure 45 Seismic line 7 from CAGE 13-5 as displayed in Figure 31 and 33.

The faults in the study area are affecting the deposition of drifts in various degrees. As observed it depends on the rate of displacement of the faults and the sedimentation rate of drifts in how the deposits are classified. With the normal faults in the study area it is either Fault controlled drifts or drift formation against fault where the first one has deposition rate > displacement rate and the latter have sedimentation rate < displacement rate.

These features are in very close proximity to the Molloy Ridge, which is part of a spreading ridge. The type of faults observed in the seismic are interpreted to be normal faults, which are results of extensional regimes consistent with the spreading regime of the mid-ocean ridge system. The uppermost fault blocks are observed to have approximately the same sediment thickness as the bottom fault, and even smaller sediment drift structures. These fault blocks are furthest away from the Molloy Ridge and should have larger and thicker sediment drifts developed because they are older, if we assume a constant sediment supply and current. It indicates that even though the uppermost fault blocks were probably present before the bottom fault blocks, sedimentation and drift development mat not have been initiated before all the fault blocks observed were well developed. These drifts are also at a significant great depth of more than 3000m below sea level, which is quite unusual considering the current velocity needed for drift development. This may be related to the changes in topography and its influence on contour currents along the WSM.

4.4.2 Contourite drifts confined by basement outcrop

East of the basement outcrop (Chapter 3.2.3) a sediment drift of unknown age are observed on the seismic in the deeper part of the slope west of the Vestnesa edge. The drift is characterized by wavy, parallel reflection pattern and indicates a prograding drift structure as the crest has moved eastward over time (Figure 36). The structure is interpreted to be an elongated drift structure with the crest being the levee of the current and the bottom being the moat. It is produced by along slope currents and is deposited against the basement outcrop. The reflections from the drift dip upwards from the moat against the basement outcrop indicating that sedimentation have been affected by the outcrop. The drift can be interpreted as a confined elongated contourite drift and indicate relatively stronger along slope currents.

Similar to the drifts discussed in the previous subchapter (Chapter 4.4.1) this drift is also located at great depth. The reflections of the drift dip upwards against the basement structure indicating that the drift were deposited onto the basement structure. This indicates that the drift development were affected by the outcrop making it likely the drift is relatively young. As discussed in the previous chapter, drifts at this depth is uncommon because of the current velocity needed. The development of the Vestnesa Ridge may have posed as an obstacle for northward flowing currents such as the WCS. This obstacle may have redirected the flow westwards and around Vestnesa where the space for current flow is smaller, creating a gap for currents to flow through. As the flow is redirected through a narrow gap the current velocity increases and may have facilitated the drift development.

4.4.3 Drift development on the West Svalbard Margin

All major drifts formed as typical moat-levee structures were exclusively observed at the deepest parts of the slope independent of where in the study area they were located. South of Vestnesa (Figure 34), western slope of Vestnesa (Figure 30) and north of Vestnesa (Figure 26 and 31) the moat-levee structures were stacked on top of each other indicating a strengthening of bottom currents at greater depths. The same observations were made by (Osti et al., 2019) at the FSC and seem to be the case for the deepest and steepest parts of the slope along the WSM within the study area.

Vestnesa has a significantly thicker sediment package compared to the rest of the study area (Figure 24), which indicates that Vestnesa has conditions favoring deposition of sediments in this particular area. The presence of major basement outcrop in positive structures at the edge of Vestnesa may have served as obstacles for any deep current flowing through the WSM. Together with the opening of the Fram Strait, which left a deep rift valley, it may have affected the sedimentations along WSM and served as factors favoring sediment deposition on Vestnesa.

4.5 Submarine Landslides

Several landslides are present both North West in the study area and south of Vestnesa (Chapter 3.3). The FSC encompasses several landslides over multiple events and large portion of the slope north of Vestnesa (Figure 37). There are many possible triggering factors for a

submarine landslide in this area. In glaciated regions such as the WSM the overloading of glacial sediments on top of finer sediment depositions such as hemipelagic and pelagic settling or contourite drifts may cause excess porepressure in the sediments consequently reducing the effective stress and makes the slope prone to failure. This has been observed in many cases along the Norwegian Margin and West Barents Sea Margin (Bryn et al., 2005) (Laberg & Camerlenghi, 2008).

A trigger for this situation might be an earthquake, which in result will further increase the pore pressure and liquefaction of the sediments triggering the slope failure. As this area is just upslope from the Molloy Ridge it is in close proximity to a highly active tectonic area where earthquakes have been documented in the last century (Läderach et al., 2011).

Toe erosion of the slope is another factor of instability in favor of slope failure. Normal faults of significant displacement have been observed in bottom of the slope (Chapter 3.2.1). Though this is not considered erosion it serves the same effect as the faults undercut the bottom of the slope and in return reduces its stability.

Bottom Simulating Reflectors have been observed on several locations in the study area (Figure 28, 34, 37 and 39). A gas hydrate related BSR indicates free gas trapped under an impermeable gas hydrated sediments within the GHSZ. Previous studies have suggested that free gas will increase the pore pressure in sediments and that the occurrence of gas hydrates along arctic margins have contributed to slope instability (Mienert et al., 1998) (Bryn et al., 2005). However, as long as gas hydrates are in the stability zone they do not directly contribute to excess pore pressure as they are trapped under the BSR. The conditions need to either get warmer or less pressurized so gas hydrates will melt and freeing the gas to migrate into unstable sediments increasing the pore pressure. However, (Osti et al., 2019) found no evidence of fluid controlled triggers to slope failure within the FSC, based on the observations of no active venting on the seafloor or indications of dissociations of gas hydrates in proximity to headwalls.

The FSC is not in very close proximity of a TMF and may present a case along the West Svalbard Margin where glacial sediments causing excess pore pressure is not the main cause or preconditioning or slope failure. There is evidence of significant build-up of contourite drifts in the form of sediment waves on the deepest part of the slope. Osti et al. (2019) proposed that the onset of contourite drifts in its wavy pattern allowed for the development of shear planes along the surfaces of condensed sedimentary successions. And through toe erosion and steepening of the slope controlled by normal faults made the preconditioning factors for slope failure.

A similar setting is observed on the southern slope of Vestnesa (Figure 39). The slope has evidence of an upper headwall companied by sidewalls both observed on seismic and bathymetry. Within the slope failure smaller headwalls were observed, which in similarity to the FSC points to evidence of multiple events of slope failure. Normal faults where sediment drift structures make up the fault blocks have been observed south-east of the slope failures propagating along the WSM and following the slope of Vestnesa (Figure 34 and 35). The build-up of the faults bare resemblance of the faults on the bottom of the slope of FSC (Figure 45), where the fault planes are located between the build up of several contourite drifts. This type of contourite drift development combined with a steep slope and fault development, may have produced gravity induced slump/creeps along the fault planes. These types of slow moving mass wasting processes will create the same type of patterns as normal faults, which was interpreted south of Vestnesa (Figure 34 and 35). As the slump/creep moved from south of Vestnesa northwards and shifting westwards to the southern slope of Vestnesa the slope gets steeper and the conditions for a landslide have increased. As well as serving as weak planes for slope failure, the vertical displacement of sediments along the fault planes undercuts the slope and results in toe erosion for the slope reducing the slope stability.

Combining these conditions with the fact that the area have been affected by multiple earthquakes the last century (Läderach et al., 2011) it may have served as the main factors for the slope failure events on the southern slope of Vestnesa.

4.6 Overview

All observation and interpretations of the WSM have been presented in Figure 46, which serves as an overview of the resulting tectonic and depositional environment affected by sedimentary and tectonic processes affecting the area. The stratigraphy north of Vestnesa is dominated by parallel and continuous reflection patterns indicative of sheeted drifts and the sediment packages are in general thinner than the rest of the study area. However, eastward and downslope the seismic characteristic changes to wavy and subparallel reflection patterns (Chapter 4.3). This part of the slope is influenced by landslides on multiple events of different magnitudes that cover a large portion of the slope (Chapter 3.3). The bottom part of the slope is affected by faulting and have been affected by the deposition of contourites and the resulting deposition is fault controlled drifts and drift formation against faults (Chapter 4.4.1).

Vestnesa is heavily influenced by oceanic crust development in basement outcrops (Figure 36). The BSR observed in the area is present along the whole ridge of Vestnesa, which indicates the presence of free gas accumulations and migrations, which has resulted in pockmarks on the seafloor (Bünz et al., 2012). The southern slope of Vestnesa has in similarity to the northern part of the study area been affected by landslides, but in a smaller scale and number (Chapter 4.5). Further south along the shelf large fault patterns are present on the seafloor, which stretches in a north-south direction until they follow the slope of Vestnesa in east-west direction, and is interpreted to be normal faults as a result of the northward migrating Knipovich Ridge (Crane et al., 2001).

The seismic characteristics on the WSM can generally be categorized by two different reflection patterns. 1) Parallel and horizontal 2) wavy and subparallel (Figure 46). They represent different deposition environments as 1) are found along the gentler sloped and shallow regions closer to the coast of Svalbard. 2) are found along the steeper slopes at greater depths. Landslides observed in the study area are limited to areas where reflection pattern 2 are located and have served as conditions for slope failure (Figure 46).

The basement outcrops may have influenced the deposition of Vestnesa funneling the northward bottom currents along the steeper parts of Vestnesa into the Molloy Ridge where it turned northwards around the western edge of Vestnesa, depositing moat-levee drift deposits

on its way as a result of increased bottom currents. The Molloy Ridge provides a narrow deep water gate for currents to flow through with increased velocity.

Drift deposits in stacked moat-levee structure may have contributed to slope instability along the slopes of WSM as observed at FSC and southern slope of Vestnesa. This makes the northward flowing bottom current a great influence on the possibility of slope failures and the development of contourite drifts along the whole slope of WSM.

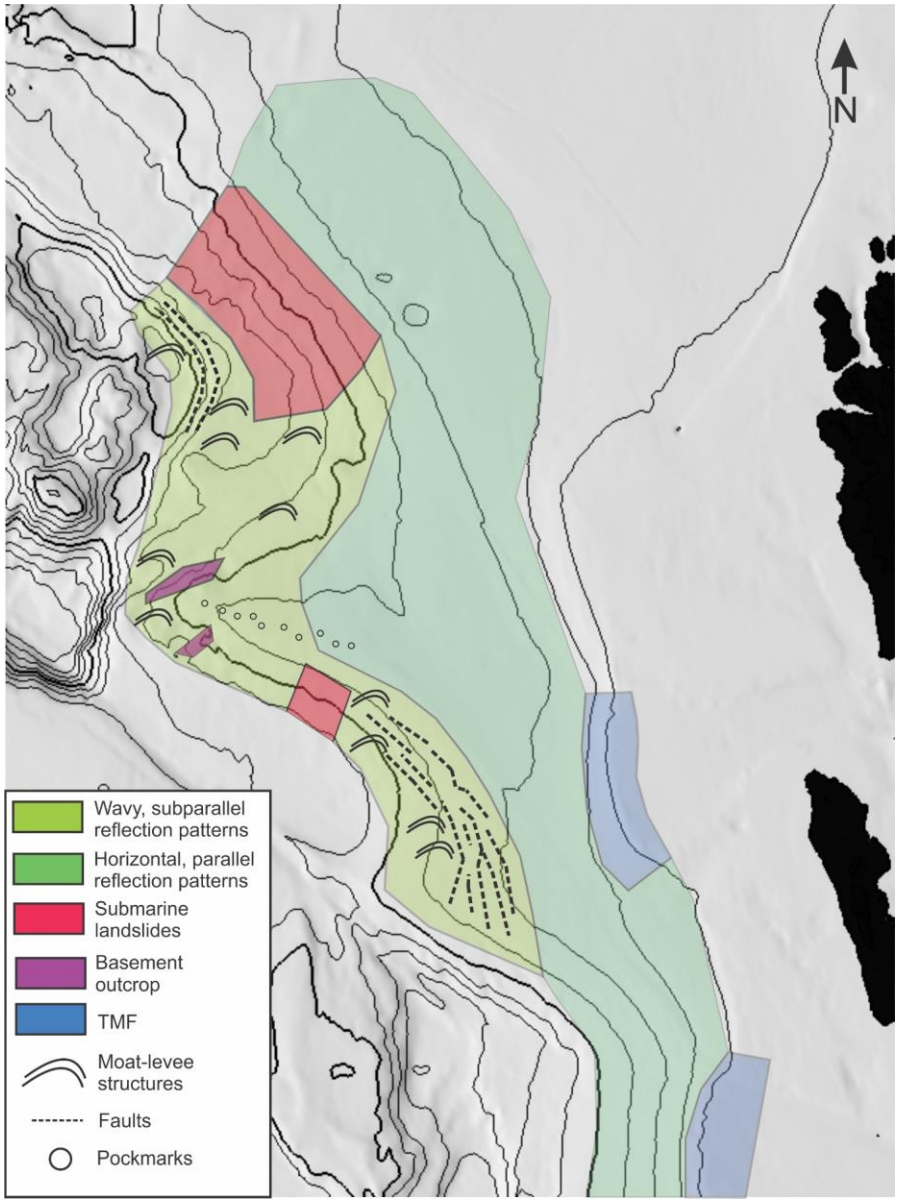

Figure 46 Overview of the geological features, seismic reflection patterns and sedimentary settings interpreted in the results and discussion.

5 Conclusions

2D seismic data of multiple years of data acquisition in CAGE have been reprocessed and integrated with several other seismic and bathymetric surveys into a regional database encompassing the WSM. Using this database, seismic interpretation focused primarily on the deep-water area of the WSM and its huge drift deposits, where stratigraphic correlation so far has been poor. This correlation allows a better understanding of deep-water contourite drift development and its relation to neotectonic setting and submarine landslides.

The reprocessing proved to be successful as several geological features such as slidescars and steep dipping reflections were imaged accurately. The signal to noise ratio of the seismic data improved significantly especially by applying Kirchoff Migration and Burst Noise Removal revealing reflections previously obscured by noise.

The stratigraphic correlation of 1.5 Ma and 2.78 Ma horizons from ODP boreholes on the Yermak Plateau and existing stratigraphic information were taken as far south as the Isfjorden Through Mouth Fan and as far west as the edge of Vestnesa. The difference in thicknesses between the horizons revealed an increased sedimentation rate for the Vestnesa drift during the past 2.7 Ma. The correlation also indicated slightly thicker sediment packages in the south of the WSM than in the north.

Drift development with moat-levee structures were exclusively observed along the western part of the study area at the deeper and steeper parts of the slope. Such drifts were observed deeper than 3000m indicating strong bottom currents at great depths. The spreading of Molloy Ridge and development of Vestnesa Ridge may have given the conditions for such currents to be funneled into smaller spaces effectively increasing the current velocity.

Observed headwalls and sidewalls on the southern slope of Vestnesa have been interpreted to be landslide events. Similar to FSC they are found in areas of wavy subparallel reflection patterns indicative of moat-levee structures of sediment drifts. These type of structures are related to development of shear planes and contribute to slope instability. Normal faults have been observed at the bottom of the slope below the FSC and south of Vestnesa which may

have undercut the slope and contributed to toe erosion. These condition contributing to slope failure, combined with an earthquake from the active seismic region of Molloy Ridge

References

Alsadi, H. N. (2017). Processing of Seismic Reflection Data. In *Seismic Hydrocarbon Exploration* (pp. 245-290): Springer.

Amundsen, I. M. H., Blinova, M., Hjelstuen, B. O., Mjelde, R., & Haflidason, H. (2011). The Cenozoic western Svalbard margin: sediment geometry and sedimentary processes in an area of ultraslow oceanic spreading. *Marine Geophysical Research, 32*(4), 441-453.

Barnes, A. (2006). Too many seismic attributes. *CSEG Recorder, 31*(3), 40-45.

Beszczynska-Möller, A., Fahrbach, E., Schauer, U., & Hansen, E. (2012). Variability in Atlantic water temperature and transport at the entrance to the Arctic Ocean, 1997–2010. *ICES Journal of Marine Science, 69*(5), 852-863.

Brown, A. R. (2011). *Interpretation of Three-Dimensional Seismic Data: AAPG Memoir 42, /SEG Investigation in Geophysics, No. 9* (Vol. 42): AAPG.

Bryn, P., Berg, K., Forsberg, C. F., Solheim, A., & Kvalstad, T. J. (2005). Explaining the Storegga slide. *Marine and Petroleum Geology, 22*(1-2), 11-19.

Bünz, S., Polyanov, S., Vadakkepuliyambatta, S., Consolaro, C., & Mienert, J. (2012). Active gas venting through hydrate-bearing sediments on the Vestnesa Ridge, offshore W-Svalbard. *Marine Geology, 332*, 189-197.

Cofaigh, C. Ó., Taylor, J., Dowdeswell, J. A., & Pudsey, C. J. (2003). Palaeo‐ice streams, trough mouth fans and high‐latitude continental slope sedimentation. *Boreas, 32*(1), 37-55.

Condie, K. C. (2013). *Plate tectonics & crustal evolution*: Elsevier.

Crane, K., Doss, H., Vogt, P., Sundvor, E., Cherkashov, G., Poroshina, I., & Joseph, D. (2001). The role of the Spitsbergen shear zone in determining morphology, segmentation and evolution of the Knipovich Ridge. *Marine Geophysical Researches, 22*(3), 153-205.

Crane, K., Sundvor, E., Buck, R., & Martinez, F. (1991). Rifting in the northern Norwegian-Greenland Sea: Thermal tests of asymmetric spreading. *Journal of Geophysical Research: Solid Earth, 96*(B9), 14529-14550. doi:10.1029/91jb01231

DECO. (2019). RadExPro 2019.1 User Manual.

Dott Jr, R. (1963). Dynamics of subaqueous gravity depositional processes. *AAPG Bulletin, 47*(1), 104-128.

Dumke, I., Burwicz, E. B., Berndt, C., Klaeschen, D., Feseker, T., Geissler, W. H., & Sarkar, S. (2016). Gas hydrate distribution and hydrocarbon maturation north of the Knipovich Ridge, western Svalbard margin. *Journal of Geophysical Research: Solid Earth, 121*(3), 1405-1424.

Eiken, O., & Hinz, K. (1993). Contourites in the Fram Strait. *Sedimentary Geology, 82*(1), 15 - 32. doi:https://doi.org/10.1016/0037-0738(93)90110-Q

Elger, J., Berndt, C., Krastel, S., Piper, D. J., Gross, F., & Geissler, W. H. (2017). Chronology of the Fram Slide Complex offshore NW Svalbard and its implications for local and regional slope stability. *Marine Geology, 393*, 141-155.

Engen, Ø., Faleide, J. I., & Dyreng, T. K. (2008). Opening of the Fram Strait gateway: A review of plate tectonic constraints. *Tectonophysics, 450*(1), 51-69. doi:https://doi.org/10.1016/j.tecto.2008.01.002

Faugères, J.-C., Stow, D. A. V., Imbert, P., & Viana, A. (1999). Seismic features diagnostic of contourite drifts. *Marine Geology, 162*(1), 1-38. doi:https://doi.org/10.1016/S0025-3227(99)00068-7

Faugères, J. C., & Stow, D. A. V. (2008). Chapter 14 Contourite Drifts: Nature, Evolution and Controls. In M. Rebesco & A. Camerlenghi (Eds.), *Developments in sedimentology* (Vol. 60, pp. 257-288): Elsevier.

Geissler, W. H., & Jokat, W. (2004). A geophysical study of the northern Svalbard continental margin. *Geophysical Journal International, 158*(1), 50-66. doi:10.1111/j.1365-246X.2004.02315.x

Hjulstrom, F. (1935). Studies of the morphological activity of rivers as illustrated by the River Fyris, Bulletin. *Geological Institute Upsalsa, 25*, 221-527.

Hustoft, S., Bünz, S., Mienert, J., & Chand, S. (2009). Gas hydrate reservoir and active methane-venting province in sediments on< 20 Ma young oceanic crust in the Fram Strait, offshore NW-Svalbard. *Earth and Planetary Science Letters, 284*(1-2), 12-24.

Kandilarov, A., Landa, H., Mjelde, R., Pedersen, R., Okino, K., & Murai, Y. (2010). Crustal structure of the ultra-slow spreading Knipovich Ridge, North Atlantic, along a presumed ridge segment center. *Marine Geophysical Researches, 31*. doi:10.1007/s11001-010-9095-8

Kearey, P., Brooks, M., & Hill, I. (2013). *An introduction to geophysical exploration*: John Wiley & Sons.

Kearey, P., Klepeis, K. A., & Vine, F. J. (2009). *Global tectonics*: John Wiley & Sons.

Knies, J., Matthiessen, J., Vogt, C., Laberg, J. S., Hjelstuen, B. O., Smelror, M., . . . Vorren, T. O. (2009). The Plio-Pleistocene glaciation of the Barents Sea–Svalbard region: a new model based on revised chronostratigraphy. *Quaternary Science Reviews, 28*(9), 812-829. doi:https://doi.org/10.1016/j.quascirev.2008.12.002

Kvenvolden, K. A., & McMenamin, M. A. (1980). Hydrates of natural gas: a review of their geologic occurrence.

Laberg, J., & Camerlenghi, A. (2008). The significance of contourites for submarine slope stability. *Developments in sedimentology, 60*, 537-556.

Laberg, J., & Vorren, T. (1996). The middle and late Pleistocence evolution and the Bear Island trough mouth fan. *Global and Planetary Change, 12*(1-4), 309-330.

Lundin, E., & Doré, A. G. (2002). Mid-Cenozoic post-breakup deformation in the 'passive' margins bordering the Norwegian–Greenland Sea. *Marine and Petroleum Geology, 19*(1), 79-93. doi:https://doi.org/10.1016/S0264-8172(01)00046-0

Läderach, C., Schlindwein, V., Schenke, H.-W., & Jokat, W. (2011). Seismicity and active tectonic processes in the ultra-slow spreading Lena Trough, Arctic Ocean. *Geophysical Journal International, 184*(3), 1354-1370. doi:10.1111/j.1365-246X.2010.04926.x

Makogon, I. U. r. F. (1981). *Hydrates of natural gas*: PennWell Books Tulsa, Oklahoma.

Mattingsdal, R., Knies, J., Andreassen, K., Fabian, K., Husum, K., Grøsfjeld, K., & De Schepper, S. (2014). A new 6 Myr stratigraphic framework for the Atlantic–Arctic Gateway. *Quaternary Science Reviews, 92*, 170-178.

Meiburg, E., & Kneller, B. (2010). Turbidity currents and their deposits. *Annual Review of Fluid Mechanics, 42*, 135-156.
Mienert, J., Posewang, J., & Baumann, M. (1998). Gas hydrates along the northeastern Atlantic margin: possible hydrate-bound margin instabilities and possible release of methane. *Geological Society, London, Special Publications, 137*(1), 275-291.
Osti, G., Waghorn, K. A., Waage, M., Plaza-Faverola, A., & Ferré, B. (2019). Evolution of contourite drifts in regions of slope failures at eastern Fram Strait. *arktos, 5*(2), 105-120.
Plaza-Faverola, A., & Keiding, M. (2019). Correlation between tectonic stress regimes and methane seepage on the western Svalbard margin.
Rebesco, M., & Camerlenghi, A. (2008). *Contourites*: Elsevier.
Rebesco, M., Hernández-Molina, F. J., Van Rooij, D., & Wåhlin, A. (2014). Contourites and associated sediments controlled by deep-water circulation processes: State-of-the-art and future considerations. *Marine Geology, 352*, 111-154. doi:https://doi.org/10.1016/j.margeo.2014.03.011
Rebesco, M., & Stow, D. (2001). Seismic expression of contourites and related deposits: A preface. *Marine Geophysical Researches, 22*, 303-308. doi:10.1023/A:1016316913639
Sarhan, M. A. (2017). The efficiency of seismic attributes to differentiate between massive and non-massive carbonate successions for hydrocarbon exploration activity. *NRIAG Journal of Astronomy and Geophysics, 6*(2), 311-325.
Stow, D. A. V., Hunter, S., Wilkinson, D., & Hernández-Molina, F. J. (2008). Chapter 9 The Nature of Contourite Deposition. In M. Rebesco & A. Camerlenghi (Eds.), *Developments in sedimentology* (Vol. 60, pp. 143-156): Elsevier.
Sun, H. (2002). Wavepath migration for depth imaging and velocity analysis.
Thiede, J., Myhre, A., & Firth, J. (1995). *Cenozoic northern hemisphere polar and subpolar ocean paleoenvironments (summary of ODP Leg 151 drilling results).* Paper presented at the Proceedings of the Ocean Drilling Program. Initial reports.
Vogt, P. R., Crane, K., Sundvor, E., Max, M. D., & Pfirman, S. L. (1994). Methane-generated (?) pockmarks on young, thickly sedimented oceanic crust in the Arctic: Vestnesa ridge, Fram strait. *Geology, 22*(3), 255-258.
Yilmaz, Ö. (2001). *Seismic data analysis: Processing, inversion, and interpretation of seismic data*: Society of exploration geophysicists.